

THE DEFORMATION CHARACTERISTICS  
OF ZINC AND CADMIUM

by

NEIL REESOR RISEBROUGH

B.A.Sc., University of Toronto, 1960  
M.A.Sc., University of Toronto, 1961

A THESIS SUBMITTED IN PARTIAL FULFILMENT OF  
THE REQUIREMENTS FOR THE DEGREE OF  
DOCTOR OF PHILOSOPHY

in the Department

of

METALLURGY

We accept this thesis as conforming to the  
required standard

THE UNIVERSITY OF BRITISH COLUMBIA

December, 1965

In presenting this thesis in partial fulfilment of the requirements for an advanced degree at the University of British Columbia, I agree that the Library shall make it freely available for reference and study. I further agree that permission for extensive copying of this thesis for scholarly purposes may be granted by the Head of my Department or by his representatives. It is understood that copying or publication of this thesis for financial gain shall not be allowed without my written permission.

Department of Metallurgy

The University of British Columbia,  
Vancouver 8, Canada

Date February 15th, 1966

The University of British Columbia

FACULTY OF GRADUATE STUDIES

PROGRAMME OF THE

FINAL ORAL EXAMINATION

FOR THE DEGREE OF

DOCTOR OF PHILOSOPHY

of

NEIL REESOR RISEBROUGH

B.A.Sc., University of Toronto, 1960

M.A.Sc., University of Toronto, 1961

TUESDAY, FEBRUARY 15, 1966 AT 2:30 P.M.

IN ROOM 210 METALLURGY BUILDING

COMMITTEE IN CHARGE

Chairman: J. Ross MacKay

W. M. Armstrong

J. A. Lund

C. A. Brockley

E. Teghtsoonian

L. G. Harrison

D. Tromans

D. L. Williams

External Examiner: J. E. Dorn

Professor of Materials Science

Lawrence Radiation Laboratory

Berkeley, California.

# THE DEFORMATION CHARACTERISTICS OF ZINC AND CADMIUM

## ABSTRACT

This work was undertaken to study the nature of the deformation mechanisms in polycrystalline zinc and cadmium over a temperature range from 77°K to 300°K.

It has been observed that the only non basal slip system which is observed under normal light microscopy is that of second order pyramidal  $\{11\bar{2}2\}$   $\langle 11\bar{2}3 \rangle$ . At temperatures above  $T_H = \frac{T}{M} = .4$ , the amount

of non basal slip is greater in zinc than in cadmium. The amount of twinning, substructure formation and grain boundary migration is comparable in both systems. Negative work hardening beyond the U.T.S. at temperatures above  $T_H = .4$  is associated with re-crystallization.

In both systems at temperatures below  $T_H = .26$  a region of temperature and strain rate independent linear work hardening occurs. The extent of linear hardening increases with decreasing temperature below  $T_H = .26$ . Above  $T_H = .26$ , polycrystalline hardening in both systems is parabolic from yield on and the rate of hardening at a given value of strain decreases with increasing temperature. Cadmium single crystals showed a similar trend in that below .26 both  $\theta_I$  and  $\theta_{II}$  remained constant. However, above .26 there was a steady decrease in the shear hardening rates.

It was observed that the Cottrell-Stokes law is obeyed only in the linear hardening regions of polycrystals and in Stage II hardening of single crystals below .26. When dynamic recovery occurs  $\frac{\Delta\sigma}{\sigma}$  increases with increasing strain.

It has been observed that below .26 the linear hardening rate in cadmium decreased with increasing grain size (constant specimen dimensions) so that

$$\theta = \theta_0 + kd^{-\frac{1}{2}}$$

The value of  $\theta_0$  was shown to correspond to the tensile hardening rate during Stage II single crystal deformation. The tensile hardening rate was used because of the extensive twinning found to be associated with Stage II hardening. The grain size dependence of  $\theta$  has been interpreted in terms of a grain size dependence of the extent of  $\{11\bar{2}2\} \langle 11\bar{2}3 \rangle$  slip.

It was found that during linear hardening in both zinc and cadmium the difference in flow stress at two different temperatures is a reversible difference implying that the dislocation configurations produced with increasing strain do not vary in nature or extent with temperature. Under such conditions it is possible to formulate a mechanical equation of state.

Extensive rate theory measurements have been made in both systems in order to attempt an evaluation of the rate controlling mechanisms both during linear hardening and during dynamic recovery. The former has tentatively been associated with intersection. Dynamic recovery on the other hand has been linked to the loop annealing observations of Price.

#### GRADUATE STUDIES

Field of Study: Metallurgy

|                               |                 |
|-------------------------------|-----------------|
| Metallurgical Thermodynamics  | C. S. Samis     |
| Metallurgical Kinetics        | E. Peters       |
| Hydrometallurgy               | E. Peters       |
| Structure of Metals III       | E. Teghtsoonian |
| Topics in Physical Metallurgy | J. A. Lund      |

Related Studies:

Statistical Mechanics

R. F. Snider

Elementary Quantum Mechanics

F. W. Dalby

Computer Programming

C. Froese

ABSTRACT

This work was undertaken to study the nature of the deformation mechanisms in polycrystalline zinc and cadmium over a temperature range from 77°K to 300°K.

It has been observed that the only non basal slip system which is observed under normal light microscopy is that of second order pyramidal  $\{11\bar{2}2\} \langle 11\bar{2}3 \rangle$ . At temperature above  $T_H = \frac{T}{T_M} = .4$ , the amount of non basal slip is greater in zinc than in cadmium. The amount of twinning, substructure formation and grain boundary migration is comparable in both systems. Negative work hardening beyond the U.T.S. at temperatures above  $T_H = .4$  is associated with recrystallization.

In both systems at temperatures below  $T_H = .26$  a region of temperature and strain rate independent linear work hardening occurs. The extent of linear hardening increases with decreasing temperature below  $T_H = .26$ . Above  $T_H = .26$ , polycrystalline hardening in both systems is parabolic from yield on and the rate of hardening at a given value of strain decreases with increasing temperature. Cadmium single crystals showed a similar trend in that below  $.26$  both  $\theta_I$  and  $\theta_{II}$  remained constant. However above  $.26$  there was a steady decrease in the shear hardening rates.

It was observed that the Cottrell-Stokes law is obeyed only in the linear hardening regions of polycrystals and in Stage II hardening of single crystals below  $.26$ . When dynamic recovery occurs  $\frac{\Delta\sigma}{\sigma}$  increases with increasing strain.

It has been observed that below  $.26$  the linear hardening rate

in cadmium decreased with increasing grain size ( constant specimen dimensions) so that

$$\theta = \theta_0 + kd^{-\frac{1}{2}}$$

The value of  $\theta_0$  was shown to correspond to the tensile hardening rate during Stage II single crystal deformation. The tensile hardening rate was used because of the extensive twinning found to be associated with Stage II hardening. The grain size dependence of  $\theta$  has been interpreted in terms of a grain size dependence of the extent of  $\{11\bar{2}2\}\langle 11\bar{2}3 \rangle$  slip.

It was found that during linear hardening in both zinc and cadmium the difference in flow stress at two different temperatures is a reversible difference implying that the dislocation configurations produced with increasing strain do not vary in nature or extent with temperature. Under such conditions it is possible to formulate a mechanical equation of state.

Extensive rate theory measurements have been made in both systems in order to attempt an evaluation of the rate controlling mechanisms both during linear hardening and during dynamic recovery. The former has tentatively been associated with intersection. Dynamic recovery on the other hand has been linked to the loop annealing observations of Price.

## ACKNOWLEDGEMENT

The author is grateful for the advice and encouragement given by his research director, Dr. E. Teghtsoonian, and for helpful discussions with fellow graduate students. Financial assistance was received in the form of an International Nickel Company of Canada Limited Fellowship.

## TABLE OF CONTENTS

|  | Page |
|--|------|
| 1. <u>DEFORMATION CHARACTERISTICS OF ZINC AND CADMIUM</u> .....          | 1    |
| 1.1. INTRODUCTION .....  | 1    |
| 1.2. EXPERIMENTAL PROCEDURE .....  | 3    |
| 1.2.1. Materials and Specimen Preparation .....                          | 3    |
| 1.2.2. Testing Procedure .....   | 6    |
| 1.3. STRESS-STRAIN RELATIONSHIPS .....                                   | 7    |
| 1.3.1. Nature of the Stress-Strain Curves .....                          | 7    |
| 1.3.2. Ductility .....   | 14   |
| a) Cadmium .....   | 14   |
| b) Zinc .....  | 16   |
| 1.3.3. Grain Boundary Effects .....                                      | 16   |
| 1.3.4. Recrystallization .....   | 25   |
| 1.3.5. Maximum Stress Variation with Temperature and<br>Strain Rate..... | 27   |
| 1.4. DEFORMATION MODES IN ZINC AND CADMIUM .....                         | 30   |
| 1.4.1. Slip .....  | 30   |
| a) Zinc .....  | 31   |
| b) Cadmium .....   | 37   |
| 1.4.2. Twinning .....  | 41   |
| 1.4.3. The Formation of Low Angle Boundaries during Deformation.         | 46   |
| 1.5. YIELD STRESS AND WORK HARDENING .....                               | 50   |
| 1.5.1. The Temperature Dependence of Yield .....                         | 50   |
| 1.5.2. Temperature Sensitivity of the Flow Stress .....                  | 53   |
| a) Cadmium .....   | 53   |
| b) Zinc .....  | 57   |

## TABLE OF CONTENTS (continued)

|  | Page |
|--|------|
| 1.5.3. Strain Rate Sensitivity of the Flow Stress .....          | 61   |
| 1.5.4. The Deformation of Cadmium Single Crystals .....          | 66   |
| 1.5.5. Temperature Dependence of Work Hardening .....            | 71   |
| 1.5.6. The Grain Size Dependence of Hardening at -196°C .....    | 71   |
| 2. <u>MECHANISMS OF HARDENING IN ZINC AND CADMIUM</u> .....      | 78   |
| 2.1. INTRODUCTION .....  | 78   |
| 2.2. TEMPERATURE CHANGE TESTS .....                              | 85   |
| 2.2.1. Procedure .....   | 85   |
| 2.2.2. Cottrell-Stokes Tests .....                               | 85   |
| 2.2.3. The Mechanical Equation of State.....                     | 88   |
| a) Cadmium .....   | 90   |
| b) Zinc .....  | 90   |
| 2.2.4. Equivalent States above $T_H = .26$ .....                 | 94   |
| 2.3. STRAIN RATE CHANGE TESTS .....                              | 98   |
| 2.3.1. Procedure .....   | 99   |
| 2.3.2. Cottrell-Stokes Behaviour in Cadmium at -196°C .....      | 99   |
| a) Single Crystals .....   | 99   |
| b) Polycrystals .....  | 101  |
| 2.3.3. The Effect of Temperature on Cottrell-Stokes Behaviour .. | 103  |
| 2.4. HARDENING AT -196°C IN CADMIUM .....                        | 107  |
| 2.4.1. Activation Volume .....                                   | 107  |
| 2.4.2. Activation Energy .....                                   | 111  |
| 2.5. HARDENING ABOVE -196°C IN ZINC AND CADMIUM .....            | 112  |
| 2.5.1. Yield Behaviour in Cadmium .....                          | 112  |

## TABLE OF CONTENTS (continued)

|   | Page |
|---|------|
| 2.5.2. The Variation of $\Delta H$ with Strain in 25 $\mu$ Cadmium .....    | 118  |
| 2.5.3. Yield behaviour in Zinc .....  | 119  |
| 3. <u>DISCUSSION</u> .....  | 123  |
| 3.1. LOOP FORMATION AND ANNEALING .....                                     | 123  |
| 3.2. DYNAMIC RECOVERY .....   | 128  |
| 3.2.2. Cross slip .....   | 129  |
| 3.2.3. Diffusion Controlled Processes .....                                 | 131  |
| 3.3. THE MECHANICAL EQUATION OF STATE .....                                 | 135  |
| 3.4. THE COTTRELL-STOKES LAW .....  | 136  |
| 3.4.1. Obeyance .....   | 137  |
| 3.4.2. Dynamic Recovery .....   | 138  |
| 3.5. RATE CONTROLLING PROCESSES BELOW $T_H = .26$ .....                     | 138  |
| 3.5.1. Peierls Stress .....   | 138  |
| 3.5.2. Cross Slip .....   | 139  |
| 3.5.3. The Non Conservative Motion of Jogs .....                            | 140  |
| 3.5.4. Intersection .....   | 141  |
| 4. <u>SUMMARY AND CONCLUSIONS</u> .....                                     | 143  |
| 5. <u>SUGGESTIONS FOR FUTURE WORK</u> .....                                 | 146  |
| 6. <u>APPENDICES</u> .....  | 147  |
| 6.1. RATE THEORY .....  | 147  |
| 6.2. UNLOADING YIELD POINTS IN CADMIUM .....                                | 154  |
| 6.3. THE DETERMINATION OF $\Delta\sigma$ FROM STRAIN RATE CHANGE TESTS .... | 160  |

TABLE OF CONTENTS (continued)

|                              | Page |
|------------------------------|------|
| 7. <u>BIBLIOGRAPHY</u> ..... | 164  |

## LIST OF FIGURES

| No. |   | Page |
|-----|---|------|
| 1.  | Polycrystalline specimen .....  | 8    |
| 2.  | Polycrystal testing apparatus .....   | 8    |
| 3.  | Single crystal testing apparatus .....  | 9    |
| 4.  | Stress-strain curves for 25 $\mu$ cadmium .....                                       | 10   |
| 5.  | Stress-strain curves for 400 $\mu$ cadmium .....                                      | 11   |
| 6.  | Stress-strain curves for 20 $\mu$ zinc .....  | 12   |
| 7.  | Stress-strain curves for 400 $\mu$ zinc .....   | 13   |
| 8.  | The effect of temperature on the ductility of 25 $\mu$ cadmium ....                   | 15   |
| 9.  | The effect of temperature on the ductility of 400 $\mu$ cadmium ...                   | 15   |
| 10. | The effect of grain size on the ductility of zinc .....                               | 17   |
| 11. | The effect of temperature on the ductility of 20 $\mu$ zinc .....                     | 18   |
| 12. | Grain boundaries in 25 $\mu$ cadmium before and after<br>7% deformation at 20°C.....  | 20   |
| 13. | Grain boundary motion in 400 $\mu$ zinc and cadmium .....                             | 21   |
| 14. | Grain boundary shear in 400 $\mu$ zinc and cadmium at +20°C .....                     | 22   |
| 15. | Recrystallization in 25 $\mu$ cadmium deformed 20% at +20°C .....                     | 26   |
| 16. | The temperature dependence of the maximum stress in cadmium ...                       | 28   |
| 17. | The temperature dependence of the maximum stress in zinc .....                        | 28   |
| 18. | The effect of strain rate on the maximum stress<br>in 25 $\mu$ cadmium .....          | 29   |
| 19. | The effect of strain rate on the maximum stress in 20 $\mu$ zinc ...                  | 29   |
| 20. | Pyramidal glide systems in zinc and cadmium (after Price) ....                        | 32   |
| 21. | {11 $\bar{2}$ 2} <11 $\bar{2}$ 3> slip in 400 $\mu$ zinc at various strains .....     | 35   |
| 22. | {11 $\bar{2}$ 2} <11 $\bar{2}$ 3> slip in 400 $\mu$ zinc at -196°C .....              | 39   |
| 23. | {11 $\bar{2}$ 2} <11 $\bar{2}$ 3> traces on 400 $\mu$ cadmium deformed 7% at -196°C.. | 40   |
| 24. | Microstructure of 400 $\mu$ cadmium deformed 7% at +20°C .....                        | 42   |

## LIST OF FIGURES (continued)

| No. |   | Page |
|-----|---|------|
| 25. | Microstructure of 400 $\mu$ cadmium deformed 7% at -196°C .....   | 43   |
| 26. | Lack of twinning in the presence of boundary migration .....  | 45   |
| 27. | Twin basal slip and twin nucleation .....   | 45   |
| 28. | Low angle boundaries in cadmium deformed 7% at -30°C .....  | 48   |
| 29. | The formation of non crystallographic boundaries in cadmium due to underlying small grains .....  | 48   |
| 30. | Crystallographic boundary formation in 400 $\mu$ zinc and cadmium .   | 49   |
| 31. | Flow stress-temperature relationships for 0.020 inch grain diameter cadmium as found by Stoloff .....   | 51   |
| 32. | Temperature dependence of the yield stress in polycrystalline zinc and cadmium .....  | 52   |
| 33. | The temperature dependence of the strain hardening parameter in polycrystalline copper as found by Russell .....                                | 54   |
| 34. | Flow stress-temperature relationships for 25 $\mu$ cadmium .....  | 55   |
| 35. | Flow stress-temperature relationships for 400 $\mu$ cadmium .....   | 56   |
| 36. | The variation with temperature of the work hardening parameter in 25 $\mu$ cadmium .....  | 58   |
| 37. | The variation with temperature of the work hardening parameter in 400 $\mu$ cadmium .....   | 59   |
| 38. | Flow stress-temperature relationships for 20 $\mu$ zinc .....   | 60   |
| 39. | The variation with temperature of the work hardening parameter in 20 $\mu$ zinc .....   | 60   |
| 40. | Linear hardening of polycrystalline zinc and cadmium below $T_H = .26$ .....  | 62   |
| 41. | The effect of strain rate on the flow stress of 20 $\mu$ zinc at +20°C .....  | 63   |
| 42. | The variation of the strain rate parameter $\frac{\Delta\sigma}{\Delta\ln\dot{\epsilon}}$ with temperature and strain in 25 $\mu$ cadmium ..... | 64   |
| 43. | The variation of the strain rate parameter $\frac{\Delta\sigma}{\Delta\ln\dot{\epsilon}}$ with temperature and strain in 20 $\mu$ zinc .....    | 65   |

## LIST OF FIGURES (continued)

x

| No. |   | Page |
|-----|---|------|
| 44. | Single crystal stress strain curve for cadmium at +20°C .....   | 68   |
| 45. | Stress-strain curves for cadmium single crystals<br>at various temperatures .....   | 69   |
| 46. | The temperature dependence of Stage I hardening in cadmium ...  | 74   |
| 47. | The temperature dependence of Stage II hardening in cadmium ..  | 74   |
| 48. | Temperature dependence of the rate of work hardening<br>during Stage I deformation .....  | 75   |
| 49. | Stress-strain curves for cadmium of various grain sizes<br>at -196°C .....  | 76   |
| 50. | The effect of grain size on the rate of linear hardening<br>at -196°C .....   | 77   |
| 51. | The temperature dependence of yield in terms of the stress<br>components .....  | 79   |
| 52. | The components of the total flow stress in f.c.c. crystals ...  | 80   |
| 53. | Components of the difference in flow stress when two<br>identical specimens are deformed at different temperatures ...                                      | 81   |
| 54. | The relationship between the change in flow stress per °K<br>and the resultant stress at -196°C obtained during the<br>temperature cycling of cadmium ..... | 87   |
| 55. | The effect of elevated temperature prestaining on the<br>stress strain curve of polycrystalline copper at 77°K .....  | 89   |
| 56. | Temperature cycling of 25 $\mu$ cadmium between -140°C and -196°C .   | 91   |
| 57. | The effect of prestraining at -95°C on the subsequent<br>deformation behaviour at -120°C in 20 $\mu$ zinc .....   | 92   |
| 58. | The effect of prestraining at -70°C on the subsequent<br>deformation behaviour at -120°C in 20 $\mu$ zinc .....   | 93   |
| 59. | Equivalent states at different strains .....  | 95   |
| 60. | Reversible temperature change tests at equivalent states<br>in polycrystalline copper .....   | 96   |
| 61. | The correlation of strains at different temperatures<br>in 20 $\mu$ zinc .....  | 97   |

## LIST OF FIGURES (continued)

| No. |   | Page |
|-----|---|------|
| 62. | The variation of the Cottrell-Stokes parameter during the deformation of cadmium single crystals at $-196^{\circ}\text{C}$ .....                      | 100  |
| 63. | The grain size dependence of $\frac{\Delta\sigma}{\sigma}$ at $-196^{\circ}\text{C}$ .....  | 102  |
| 64. | The variation with stress of $\frac{\Delta\sigma}{\sigma}$ obtained from $25\mu$ cadmium at different temperatures .....                              | 104  |
| 65. | The stress dependence of $\frac{\Delta\sigma}{\sigma}$ ( $400\mu$ cadmium) .....  | 105  |
| 66. | The failure of the Cottrell-Stokes law at $-50^{\circ}\text{C}$ .....   | 105  |
| 67. | The variation with stress of the Cottrell-Stokes parameter obtained from strain rate change tests on $20\mu$ zinc .....                               | 106  |
| 68. | The stress dependence of the activation volume (cadmium) .....  | 108  |
| 69. | Force-distance curves .....   | 115  |
| 70. | The variation of $\Delta G$ with temperature for $25\mu$ cadmium .....  | 116  |
| 71. | The variation of $\Delta H$ with strain and temperature in $25\mu$ cadmium .....  | 120  |
| 72. | The variation of $\Delta G$ with temperature for $20\mu$ zinc .....   | 122  |
| 73. | The formation of a prismatic dislocation loop by an edge dislocation which is held up at an obstacle .....  | 123  |
| 74. | The effect of jogs of various heights on screw dislocation motion .....   | 124  |
| 75. | Stages in the formation of an elongated loop on the basal plane by the cross glide of a $\{11\bar{2}2\}\langle 11\bar{2}3\rangle$ screw dislocation . | 126  |
| 76. | Dislocations in hexagonal close packed crystals .....   | 127  |
| 77. | The conservative climb of a basal dislocation loop .....  | 132  |
| 78. | Typical force-distance curve for a thermally activated deformation process .....  | 153  |
| 79. | Unloading yield point in polycrystalline cadmium .....  | 154  |
| 80. | Unloading yield point terminology .....   | 156  |
| 81. | The variation of $\sigma_b/\sigma_a$ with strain at $-196^{\circ}\text{C}$ .....  | 158  |

## LIST OF FIGURES (continued)

| No. |  | Page |
|-----|--|------|
| 82. | The decrease in flow stress due to static recovery during interrupted testing of 25 $\mu$ cadmium at -95°C ..... | 159  |
| 83. | The nature of the flow stress obtained during strain rate change tests in polycrystals .....                     | 161  |

## LIST OF TABLES

| No. |  | Page |
|-----|--|------|
| 1.  | Physical properties of hexagonal metals .....  | 4    |
| 2.  | Non basal slip systems observed in zinc .....  | 33   |
| 3.  | Non basal slip systems observed in cadmium .....   | 34   |
| 4.  | Slip systems in hexagonal metals .....   | 38   |
| 5.  | Upper temperature limits for linear hardening in<br>polycrystalline zinc and cadmium .....   | 61   |
| 6.  | Stress required for twin formation in cadmium single<br>crystals .....   | 70   |
| 7.  | Incubation strain required in polycrystalline copper prior<br>to the appearance of an irreversible component of the<br>difference in flow stress ..... | 89   |
| 8.  | Grain size dependence of Cottrell-Stokes behaviour .....   | 101  |
| 9.  | Grain size dependence of the activation volume at yield<br>in cadmium at $-196^{\circ}\text{C}$ .....  | 109  |
| 10. | Energy values at yield for cadmium deformed at $-196^{\circ}\text{C}$ .....  | 111  |
| 11. | Energy values at yield for $25\mu$ cadmium .....   | 113  |
| 12. | Rate parameters at yield in $20\mu$ zinc .....   | 121  |
| 13. | Loop formation in zinc and cadmium .....   | 127  |

## 1. DEFORMATION CHARACTERISTICS OF ZINC AND CADMIUM

### 1.1 INTRODUCTION

In the past, the major emphasis in the field of plastic deformation has been placed on face centered cubic metals. Much of this work has been restricted to the use of single crystals in an attempt to determine the dislocation mechanisms which control the work hardening processes. The study of single crystal behaviour has the advantage of avoiding the difficult problem of dealing with the constraining conditions imposed by grain boundaries during the deformation of polycrystalline aggregates. This simplicity, which enables one to obtain a better knowledge of shear stress conditions on particular slip planes has disadvantages due to the poor reproducibility of flow stress values of different single crystals because of the effects of slight changes in such factors as substructure, impurity concentration, orientation and initial dislocation density. The correlation of single crystal and polycrystalline data for face centred metals is a topic of some current interest<sup>1-5</sup> and should in the future provide a groundwork for the understanding of macroscopic deformation characteristics.

In the past few years the study of body centred cubic metals, notably iron, has been intensified. Conrad<sup>6-10</sup>, Gregory<sup>11</sup>, Basinski<sup>12</sup> and others have attempted to determine the rate controlling mechanism over a wide range of temperature. Much of this work involved the use of polycrystalline specimens.

The field of hexagonal metal deformation has been somewhat ignored due in most part to the anisotropic nature of the hexagonal system and the resultant difficulties encountered in mechanical working and engineering use. With possibly the exception of zinc and cadmium, the more prominent hexagonal metals including Ti, Be, Mg, Co, and Zr are associated with difficult metallurgical procedures during extraction and refining which tend to make them expensive and hence undesirable as engineering materials except in applications where definite advantages occur.

Of all the hexagonal metals, titanium and magnesium have been studied in the greatest detail because of their favourable strength to weight ratio. Because of gaseous embrittlement and difficulties encountered during mechanical forming, titanium has not become as widely used as once predicted. Magnesium is difficult to produce in wrought form due to embrittlement during cold working. Therefore the problem of determining the deformation mechanisms which control flow in magnesium has been a subject of considerable interest.<sup>13-22</sup>

On the other hand very little work has been done on zinc and cadmium since the classic works of Schmid and Boas in the early 1930's.<sup>23</sup> Recently considerable interest has been shown in the development of new wrought zinc alloys to compete commercially with some aluminum and copper alloys. Poor creep properties due to its high effective temperature at room temperature and reduced ductility because of cleavage fracture at reduced temperatures have so far limited its use. It is necessary therefore to have a more detailed knowledge of the deformation mechanisms to provide a ground work for future alloy development. Most investigations to date have been concerned with either the hardening

mechanisms during basal glide<sup>24-25</sup> or the nature of cleavage fracture.<sup>26-27</sup> Very little work has been done with polycrystalline zinc to determine such factors as the strain rate and temperature sensitivity of the flow stress, the mode and degree of non basal slip, the nature of dynamic recovery, the relevance of grain boundary effects etc.

Although similarities exist between zinc and cadmium as shown in Table I, the apparent deformation characteristics differ in that cadmium does not fail by cleavage fracture and maintains substantial ductility down to 4.2°K. However a quasi ductile-brittle transition involving a change in fracture mode from ductile shear to intergranular fracture has been reported by Stoloff<sup>28</sup> and Magnussen.<sup>29</sup> Therefore by comparing zinc and cadmium under standard conditions of purity, grain size, temperature, strain rate and specimen geometry it may be possible to obtain a more detailed knowledge of the flow and fracture mechanisms.

The first part of this thesis is concerned with the more macroscopic flow parameters whereas part two describes attempts to determine the rate controlling mechanisms by the use of rate theory.

## 1.2 EXPERIMENTAL PROCEDURE

### 1.2.1 Materials and Specimen Preparation

The zinc and cadmium used in the course of this work was of 99.999% purity and was supplied in the form of one-half inch rods by the Consolidated Mining and Smelting Company, Trail, B.C.

These rods were remelted in air and cast into graphite moulds to give ingots with dimensions 5" x 2 $\frac{1}{2}$ " x  $\frac{1}{2}$ ". These were then rolled into

TABLE I

Physical Properties of Hexagonal Metals

| Element                            | Zn     | Cd     | Mg    | Be    | Co    | Ti    | Zr    |
|------------------------------------|--------|--------|-------|-------|-------|-------|-------|
| Melting Temperature °C             | 420    | 320    | 650   | 1277  | 1495  | 1668  | 1852  |
| Density gms/c.c.                   | 7.14   | 8.65   | 1.74  | 1.85  | 8.9   | 4.51  | 6.49  |
| c/a ratio                          | 1.856  | 1.886  | 1.624 | 1.586 | 1.623 | 1.588 | 1.590 |
| Stacking Fault Energy <sup>A</sup> | medium | medium | high  | high  | low   | high  | high  |
| Periodic Group No.                 | 11B    | 11B    | 11A   | 11A   | VIII  | IVB   | IVB   |

<sup>A</sup> Stacking Fault Energies Low - under 25 ergs/cm<sup>2</sup>  
 Medium - 25-100 ergs/cm<sup>2</sup>  
 High - > 100 ergs/cm<sup>2</sup>

sheet. The initial rolling passes for zinc were carried out at 150°C in order to avoid cracking. The grain refinement which occurred during this hot rolling operation was such as to allow further reductions to be carried out at room temperature. Recrystallization during rolling readily occurred at room temperature because of the small grain size.

Cadmium was rolled at room temperature throughout the reduction process. In both cases reduction was carried out in .010 inch steps from .150 inches to the final sheet size of .031 inches. This treatment produced a very uniform and fine grained recrystallized sheet with a grain size of 20μ for zinc and 25μ for cadmium.

The grain size could be varied significantly by changing the amount of reduction in the final roll pass. For instance a final grain size of 50μ instead of 25μ could be obtained in cadmium by using a final reduction of 5% instead of 25%. For this reason all specimens were cut from the same sheet in order to eliminate small differences in grain size and preferred orientation.

Tensile specimens were punched to give a reduced gauge length of .8 inches with cross sectional dimensions of .200" x .031" (Fig.1). Since this procedure caused slight deformation around the specimen edges it was necessary to chemically polish the surface prior to testing. Approximately .0015 inches were removed to give a final specimen thickness of .0280 inches. The polishing solution used for both zinc and cadmium was as follows -

- 320 gms CrO<sub>3</sub>
- 20 gms Na<sub>2</sub> SO<sub>4</sub>
- 1000 mls H<sub>2</sub>O

This represents a slight modification of Gilman's solution<sup>30</sup>. Besides

polishing the surface, this treatment caused grain boundaries to become slightly grooved thereby facilitating metallographic examination after testing.

Large grained specimens were obtained by annealing punched specimens in air under the following conditions:

Cadmium - 2 hrs at 230°C  
Zinc - 2 hrs at 180°C

The specimens were then furnace cooled from temperature over a period of 1 hour. The resultant grain size in each case was  $400\mu \pm 25\mu$ . This produced specimens with only 1 to 2 grains across the specimen thickness. Because of this, the scatter in flow stress values was somewhat greater than for fine grained specimens. The purpose of producing such specimens was to facilitate metallographic observations and to provide an intermediate test specimen between the normal fine grained material and single crystals.

The single crystals used were grown by a modified Bridgman technique in evacuated 3mm diameter pyrex glass tubes. Extruded .100 inch lengths of cadmium were placed in the tubes which were subsequently lowered at the rate of 1" per hour through a 12" vertical tube furnace. Crystals up to 18 inches in length could be grown providing numerous samples of the same orientation.

#### 1.2.2 Testing Procedure

Specimens were deformed on a Floor Model Instron using strain rates that varied from  $4.0 \times 10^{-3} \text{sec}^{-1}$  to  $4.0 \times 10^{-5} \text{sec}^{-1}$ . Testing media included liquid nitrogen, cooled petroleum ether (-140 to +20°C), hot water (+20 to +100°C) and silicone oil (above 100°C). The bath temperature

in each case could be controlled to  $\pm 2^\circ\text{C}$ . Split jaw grips which produced a very rigid testing apparatus were used for the polycrystalline specimens. (Fig.2).

Single crystals were mounted in solder in aluminum grips and were deformed in a testing rig which allowed complete freedom of rotation (Fig.3). The distance between grips was between 30 and 35 mm giving a length to diameter ratio of 10/1.

In order to facilitate comparison with previous work all data on polycrystals is expressed in terms pounds per square inch (p.s.i.) whereas single crystal results are given in terms of c.g.s. units.

### 1.3 STRESS-STRAIN RELATIONSHIPS

#### 1.3.1 Nature of the Stress Strain Curves

True stress-true strain curves for both grain sizes in zinc and cadmium at a few selected temperatures are shown in Figures 4, 5, 6 and 7. The cadmium curves are qualitatively the same as those observed by Stoloff and Gensamer<sup>28</sup> for .020 inch grain size material. Specifically, work hardening in the early regions of strain is parabolic at high effective temperatures and tends to become more linear with decreasing temperature. (Effective temperature is given by  $T_H = \frac{T}{T_M}$  where  $T_M$  is the melting point). At temperatures above approximately  $T_H = .40$  there is a large amount of strain beyond the point of maximum stress which was not observed to be associated with necking. It was also observed that this effect is greatly reduced in the 400 $\mu$  material.

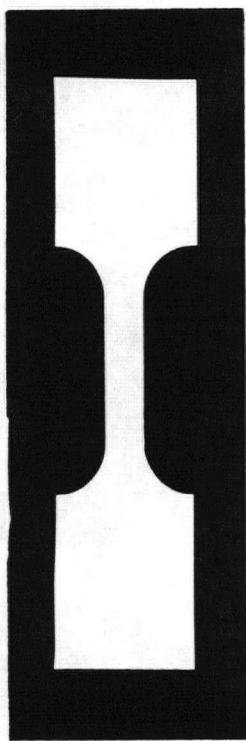


Fig. 1 Polycrystalline specimen (true size)

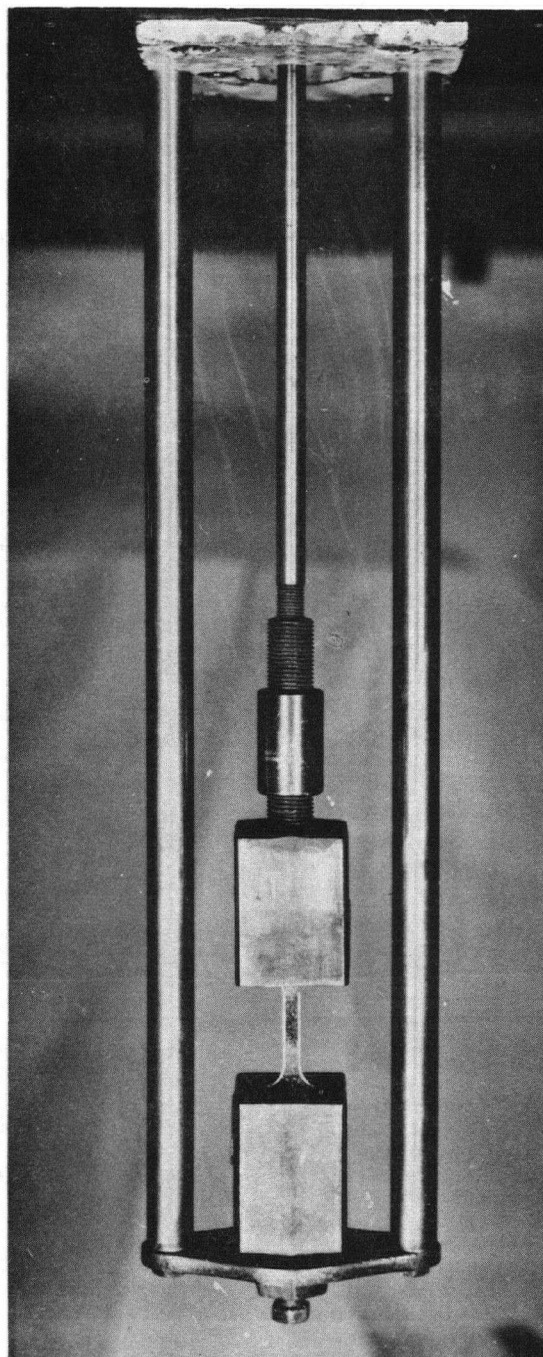


Fig. 2 Polycrystal testing apparatus.

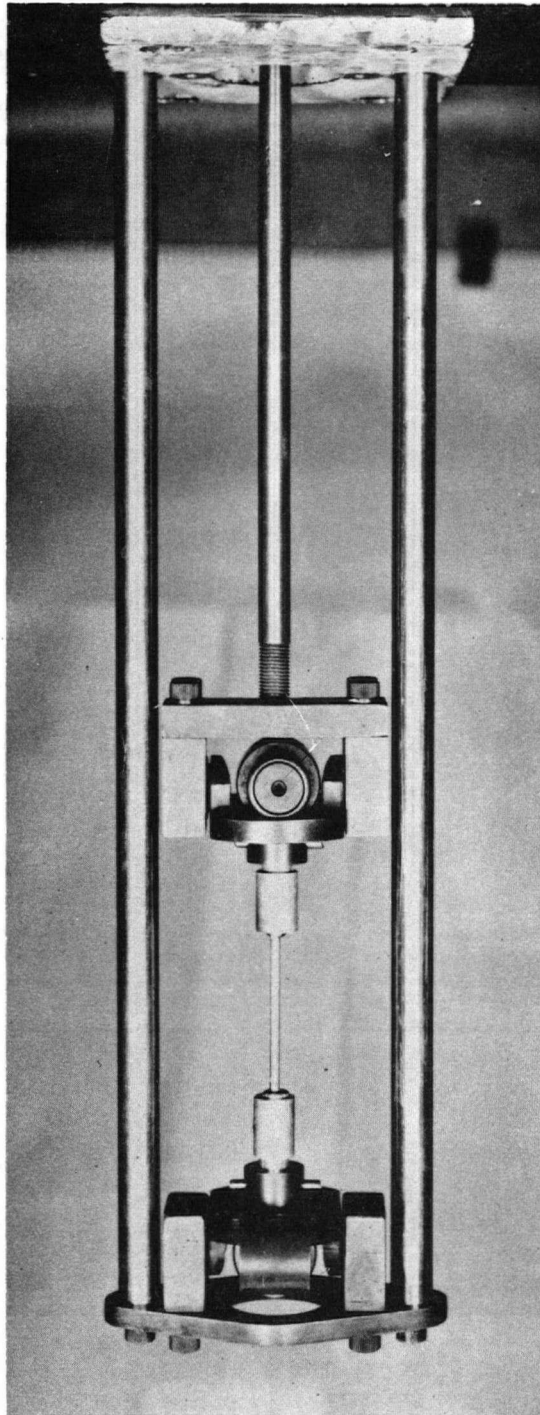


Fig. 3 Single crystal testing apparatus.

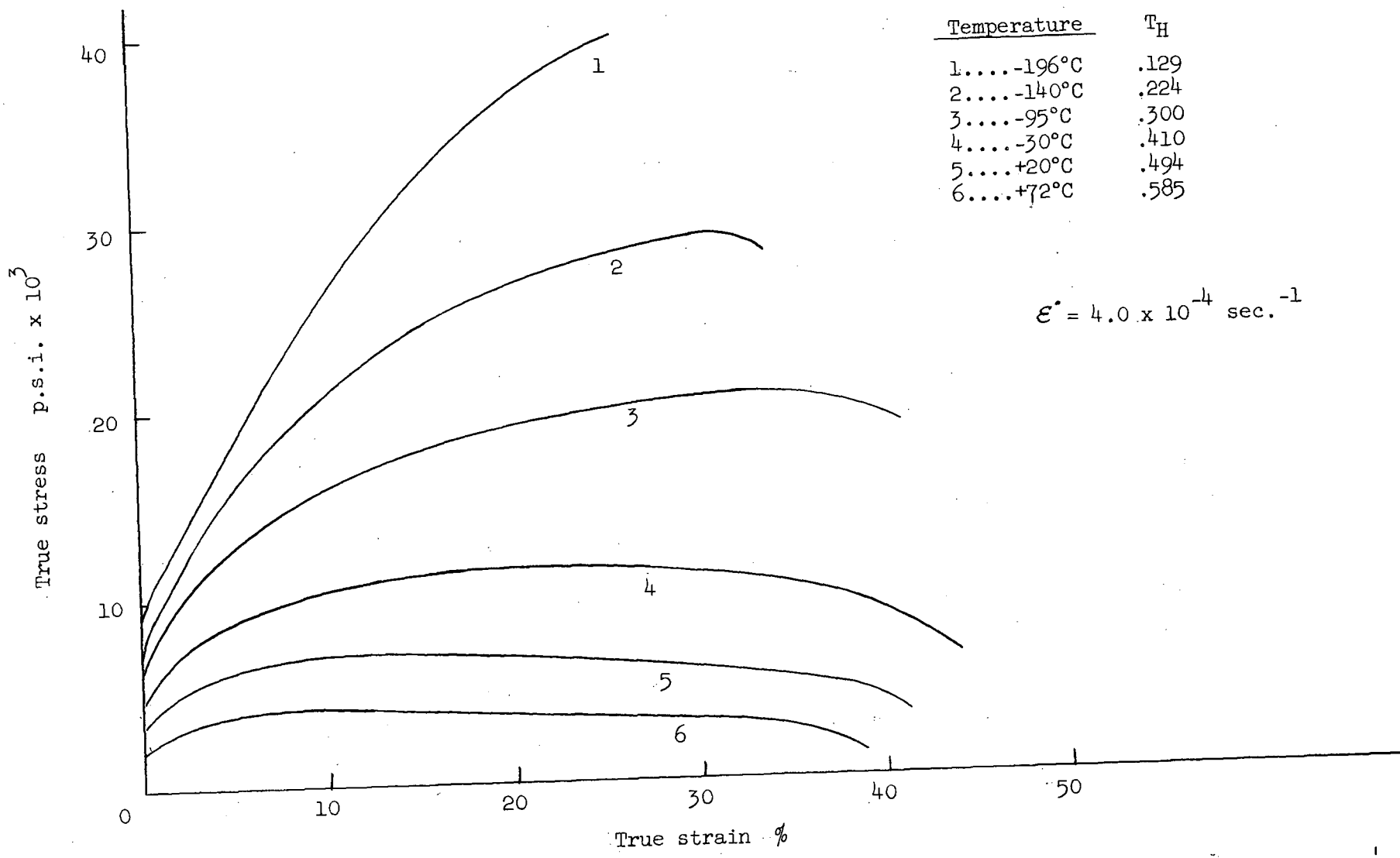


Fig. 4. Stress - strain curves for 25μ cadmium.

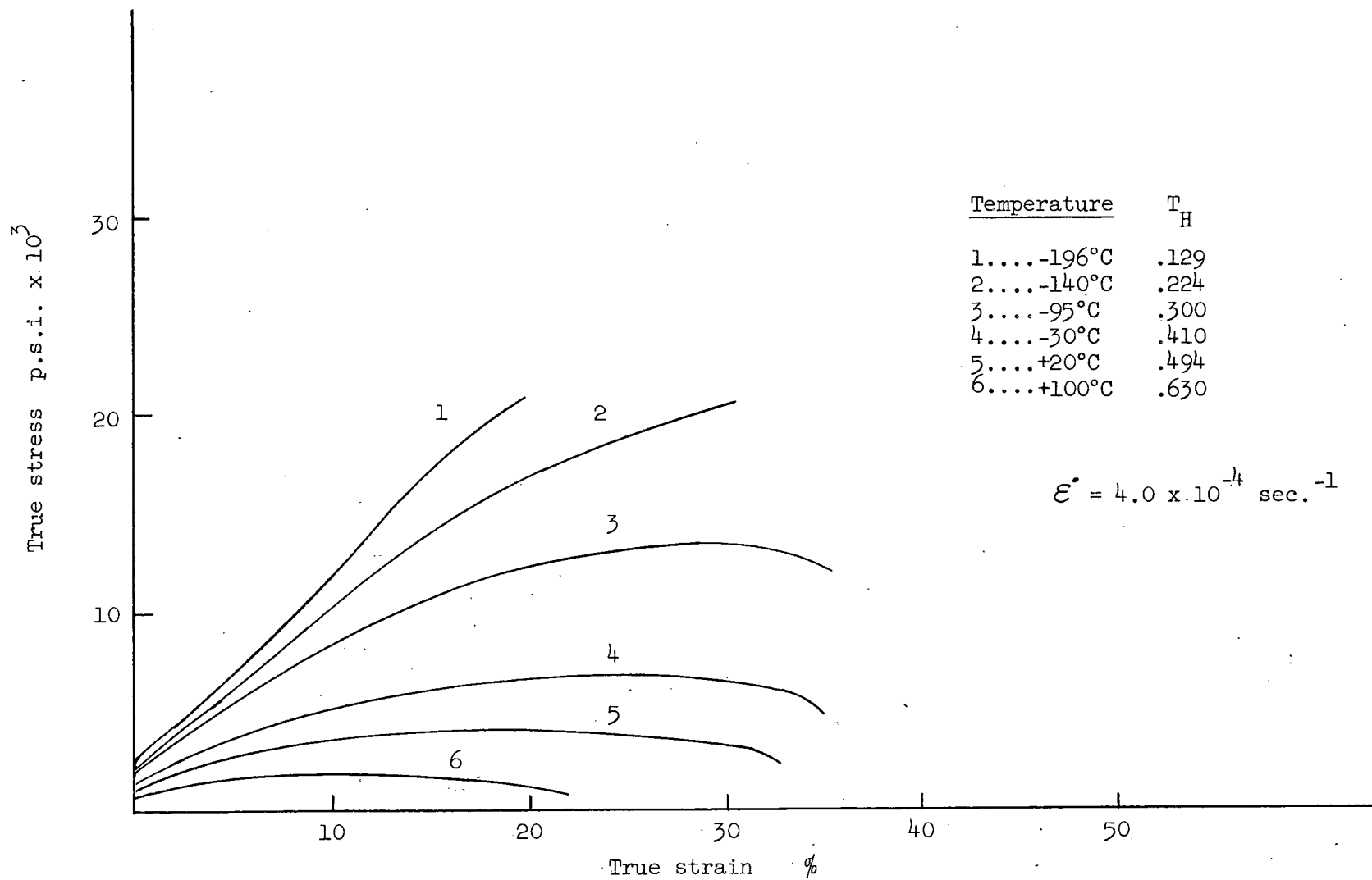


Fig. 5 Stress-strain curves for 400μ cadmium.

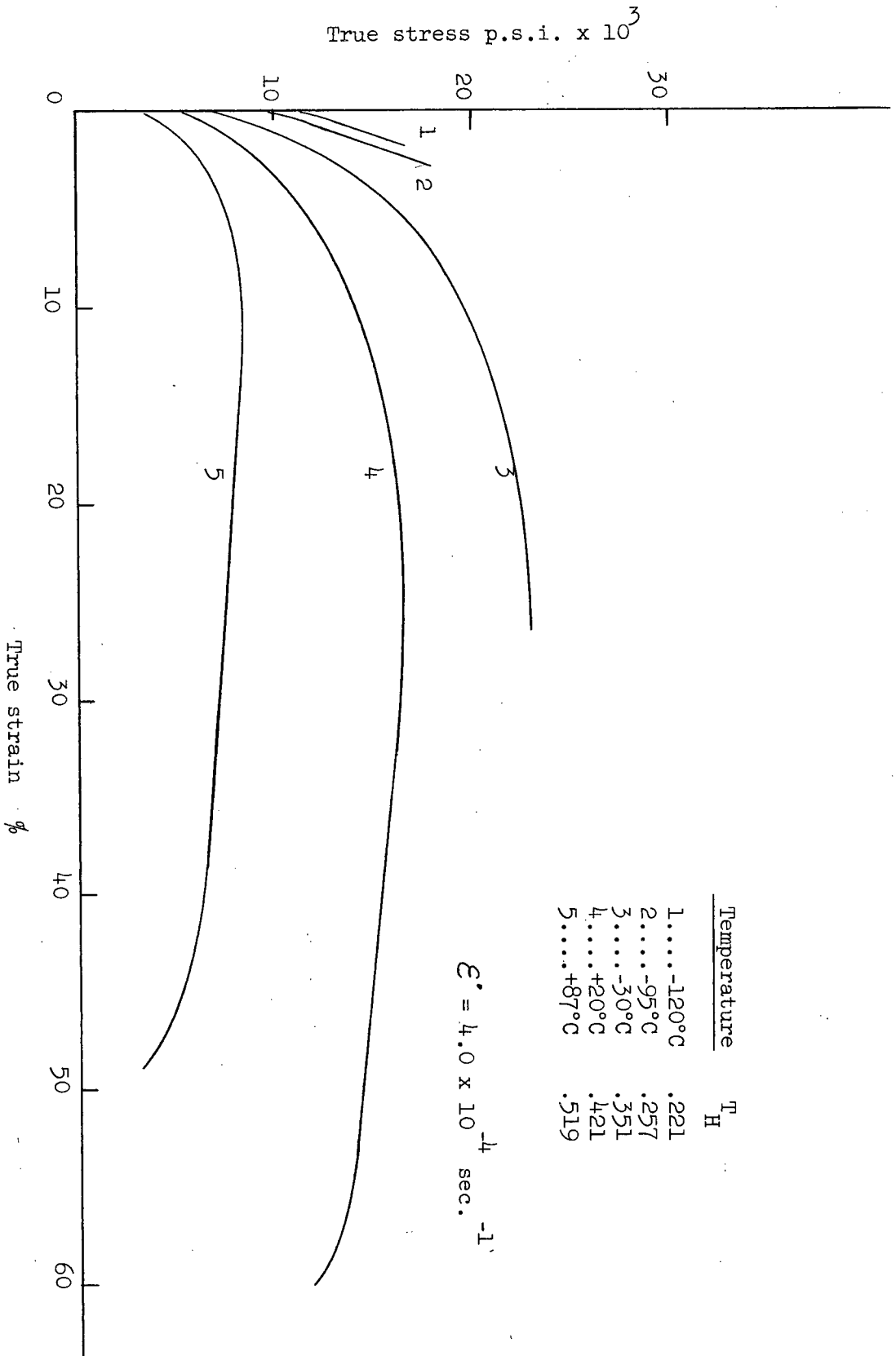


Fig. 6 Stress-strain curves for 20μ zinc.

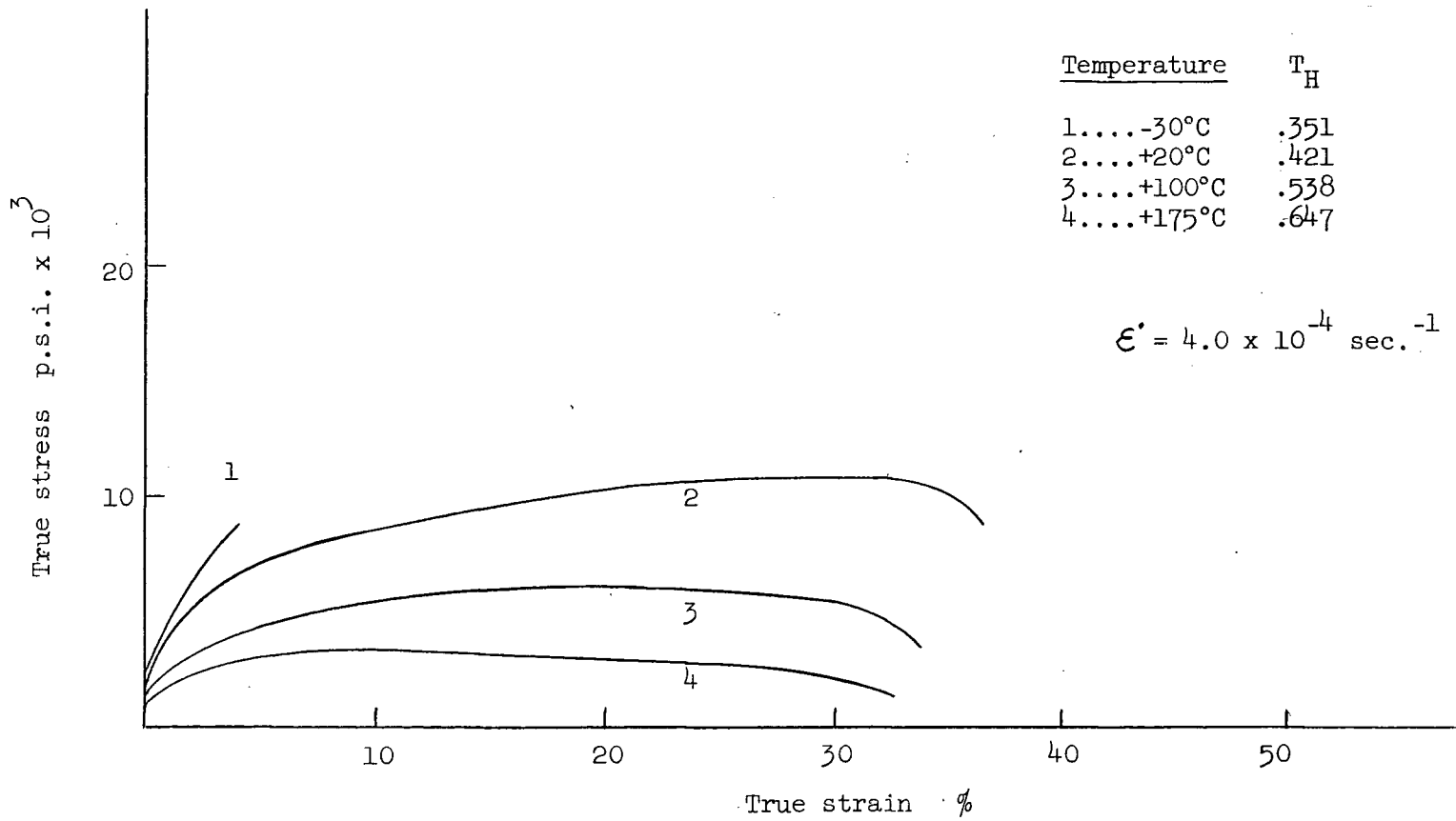


Fig.7 Stress - strain curves for 400μ zinc

### 1.3.2 Ductility

- 14 -

Ductility will be given only in terms of percent elongation or true strain as it was not practical to obtain reduction in area values because of the specimen dimensions. As an aid to interpretation, ductility is given not only as the true strain to fracture but also in terms of the true strain to maximum stress conditions. This is important when considering deformation at high values of  $T_H$  because of the large amounts of deformation associated with negative work hardening.

#### 1.3.2 a) Cadmium

The effect of temperature on the ductility of 25 $\mu$  and 400 $\mu$  cadmium is shown in Figures 8 and 9. It is observed that there is an increase in the strain to fracture as the temperature decreases to -120°C. This increase is more pronounced with an increase in grain size. At -120°C both grain sizes have approximately the same strain to fracture of about 40%. Below -120°C there is a steady decrease in ductility independent of grain size, in agreement with the results of Stoloff and Gensamer. This decrease corresponds to a change in the fracture mode from ductile shear to intergranular fracture.

From Figures 8 and 9 it is also observed that above -120°C,

- 1) the true strain to maximum stress is greater for 400 $\mu$  than for 25 $\mu$  cadmium
- 2) the percentage of the total ductility which is associated with negative hardening after maximum stress conditions have been realized is greater for the 25 $\mu$  cadmium.

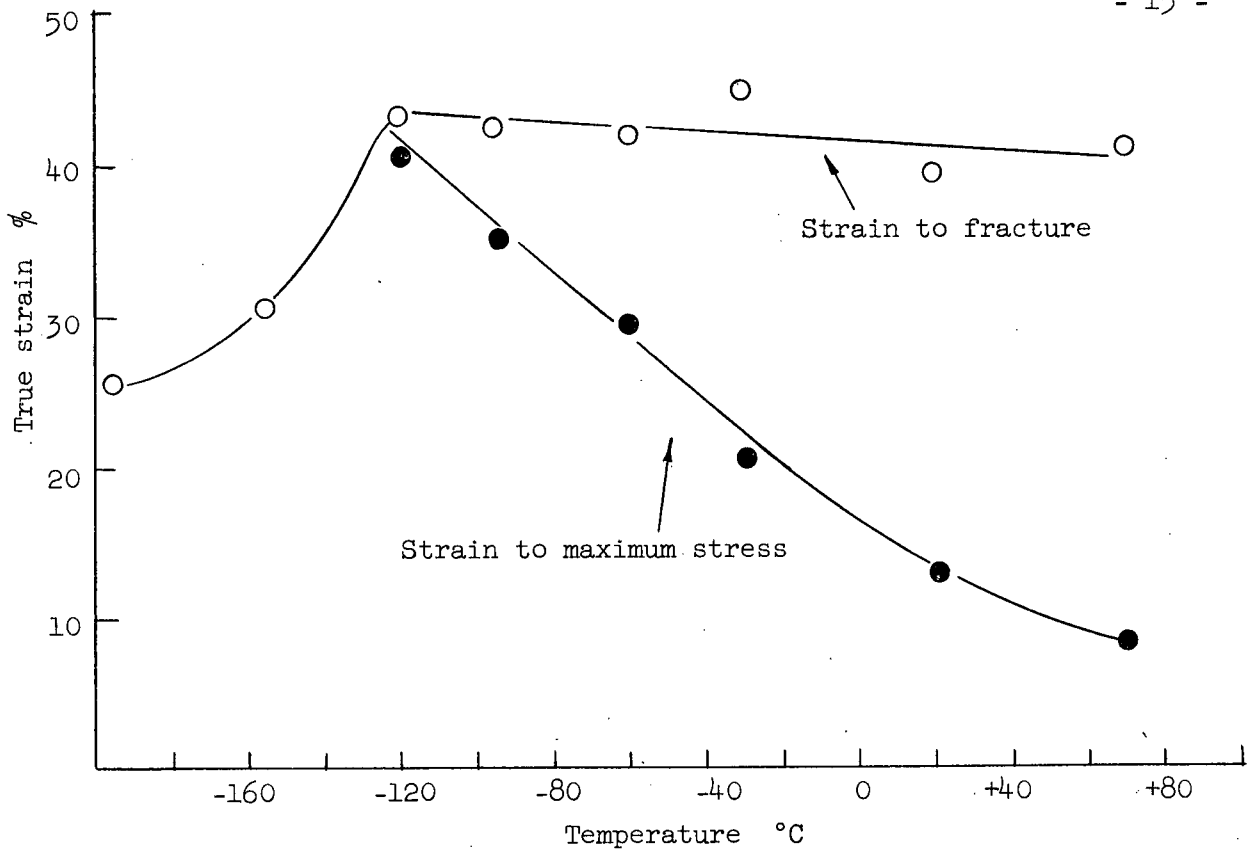


Fig.8 The effect of temperature on the ductility of 25 $\mu$  cadmium.

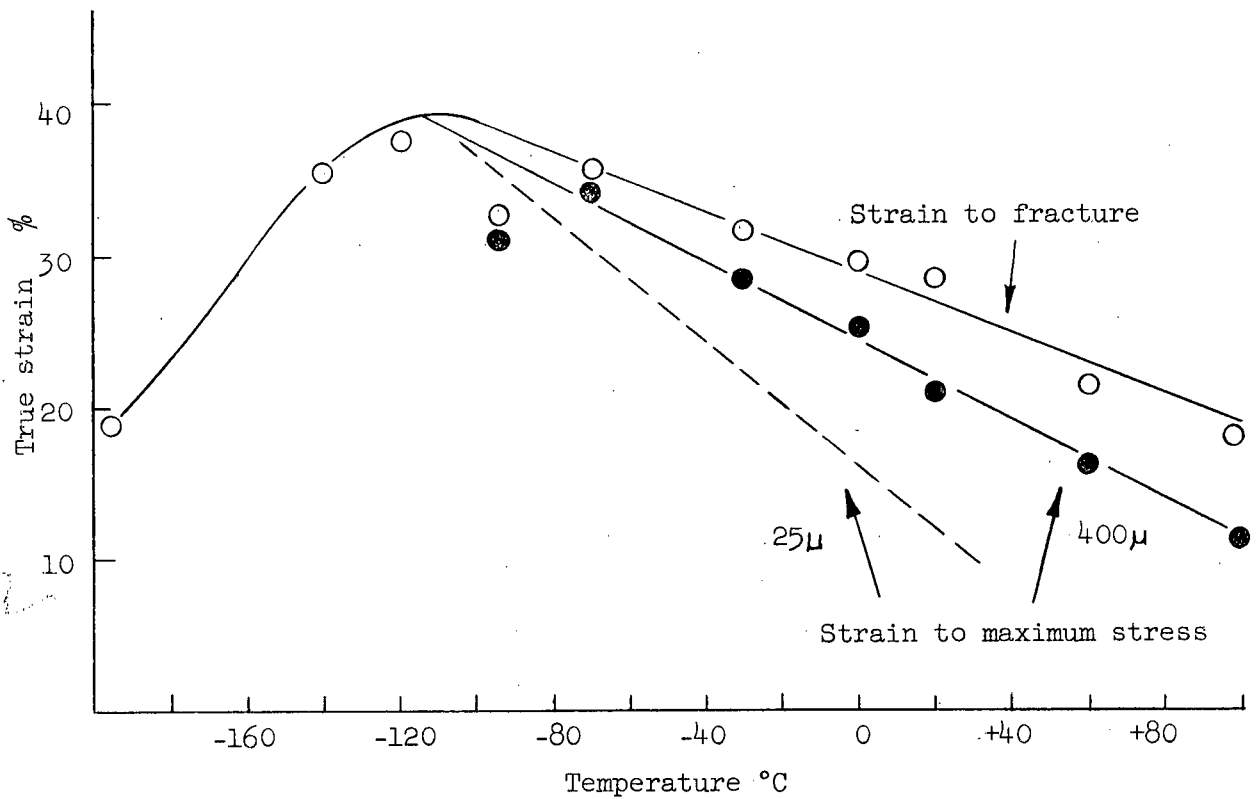


Fig.9 The effect of temperature on the ductility of 400 $\mu$  cadmium.

### 1.3.2 b). Zinc

The results for zinc are qualitatively the same as those for cadmium except for the occurrence of a distinct ductile to brittle transition due to cleavage fracture.

From Figure 10 it is observed that this transition is shifted about 50°C as the grain size is increased from 25 $\mu$  to 400 $\mu$ . Above the transition temperature it is observed that both the total strain to fracture and the true strain to maximum stress decrease with increasing temperature in a manner similar to cadmium. Likewise the percentage of the total ductility at fracture which is associated with negative work hardening is greater for 20 $\mu$  zinc than for 400 $\mu$  zinc. Also the true strain to maximum stress is greater at the same temperature for 400 $\mu$  zinc than for 20 $\mu$  zinc. This is in agreement with observations (1) and (2) of the previous section on cadmium.

The effect of strain rate on the ductile to brittle transition is shown in Figure 11. Changing the strain rate by a factor of 10 shifted the transition for 20 $\mu$  zinc by about 25°C.

### 1.3.3 Grain Boundary Effects

The observations of the previous section with regard to grain size effects indicate that some form of recovery and recrystallization are operative during deformation at elevated temperatures. These processes are expected because of the high purity and high effective temperatures. However Stoloff found no evidence of recrystallization during testing at 20°C.

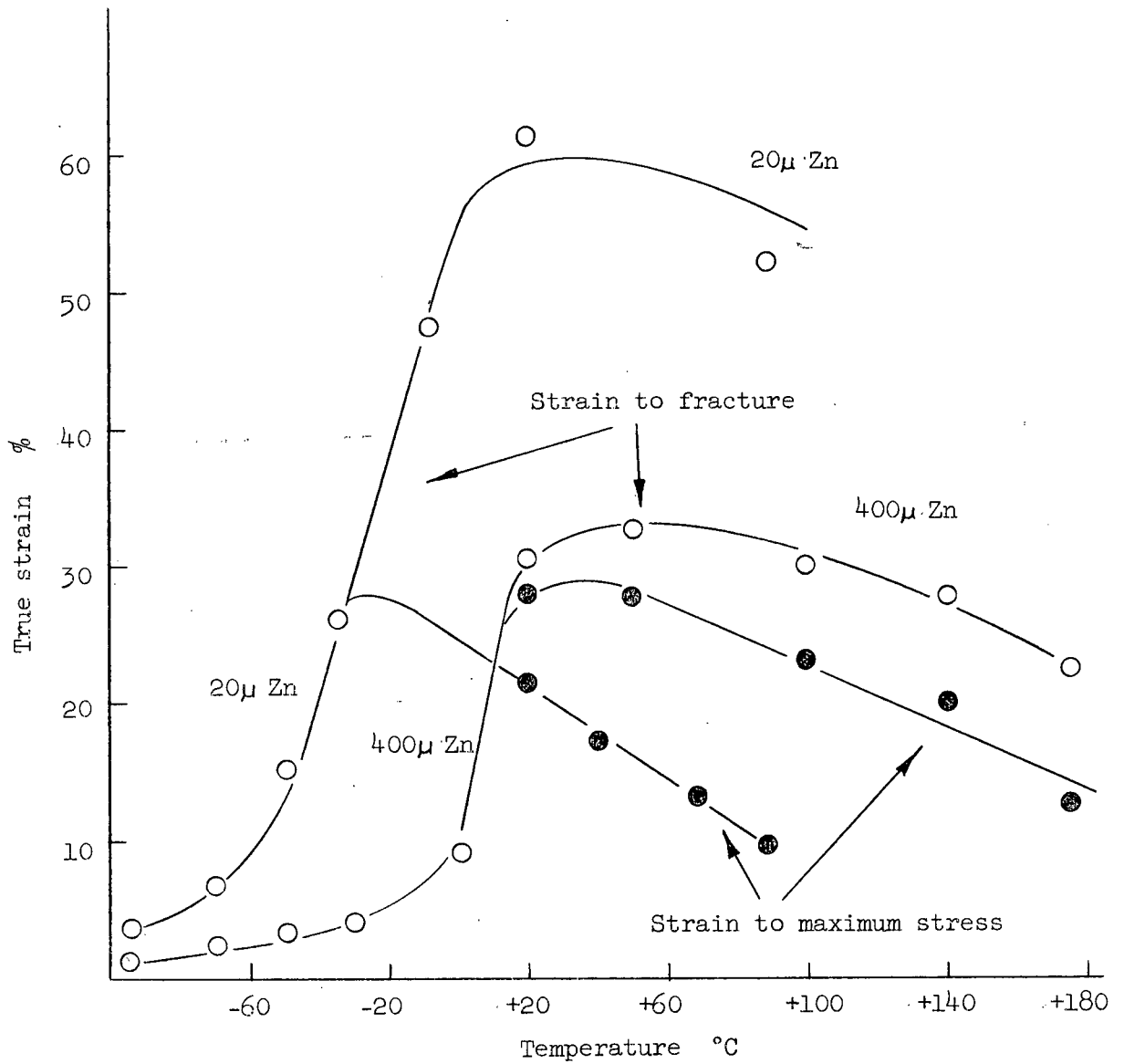


Fig.10 The effect of grain size on the ductility of zinc.

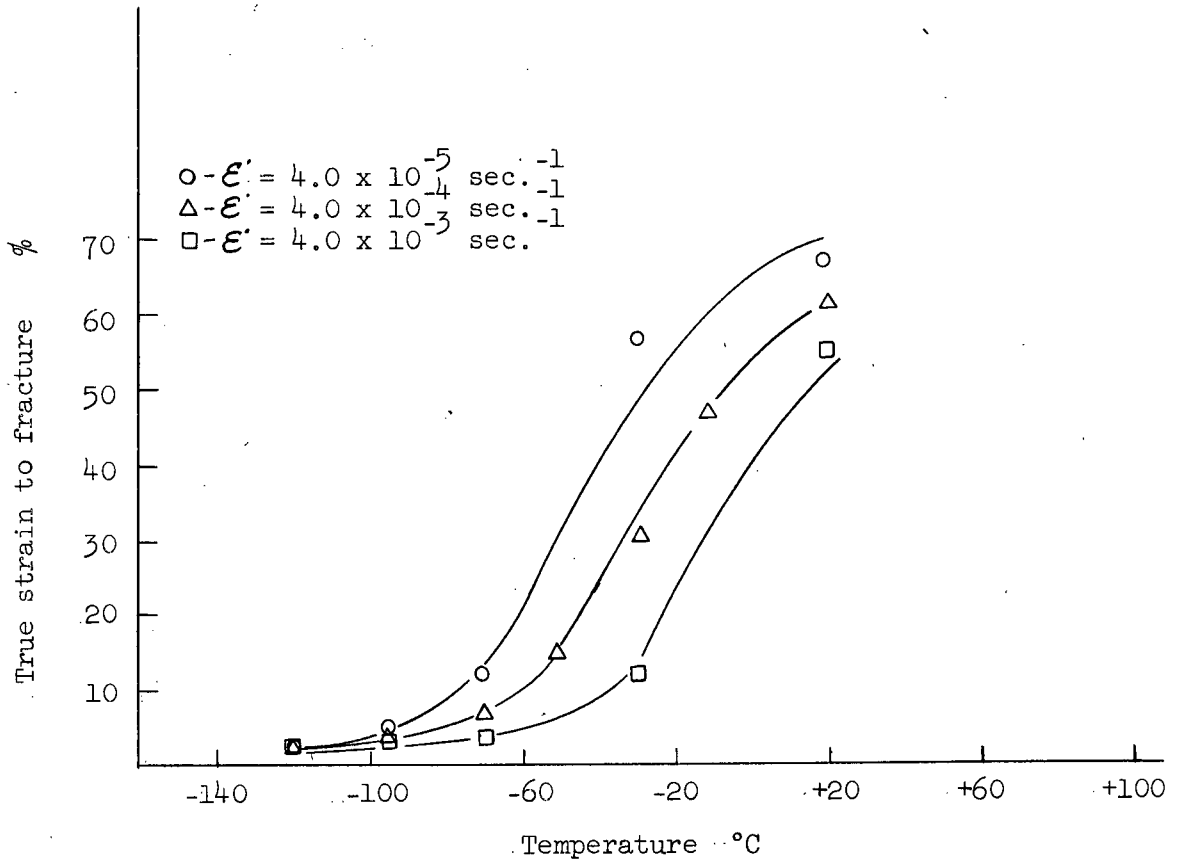


Fig. 11 The effect of temperature on the ductility of 20μ zinc.

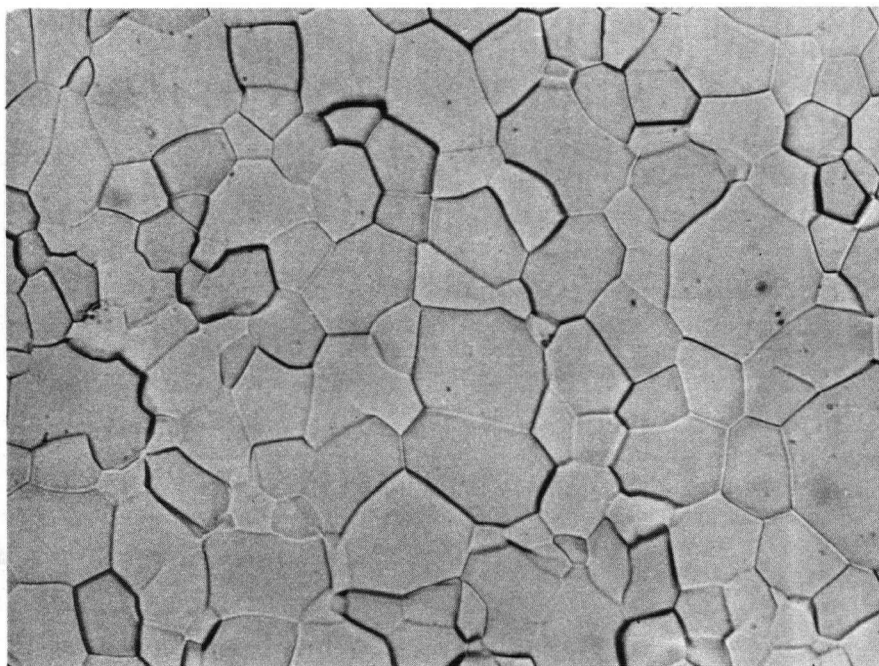
Figure 12 shows the relative grain boundary structures in 25 $\mu$  cadmium before and after 7% deformation at room temperature. The boundaries have become very jagged in appearance indicating considerable grain boundary migration during deformation.

Figure 13 shows other examples of boundary motion in 400 $\mu$  zinc and cadmium. With decreasing temperature the migrating boundaries show a more continuous type of migration along the boundary (Fig.13b) opposed to the corrugated type observed at room temperature and above (Fig.13d). At a given temperature these boundary effects were much more prominent in fine grained material.

Figure 13(b) shows a "stepped" type of boundary migration similar to that observed by Chang and Grant<sup>31</sup> during creep of polycrystalline aluminum at elevated temperatures. They interpreted such observations in terms of alternate processes of shear and migration.

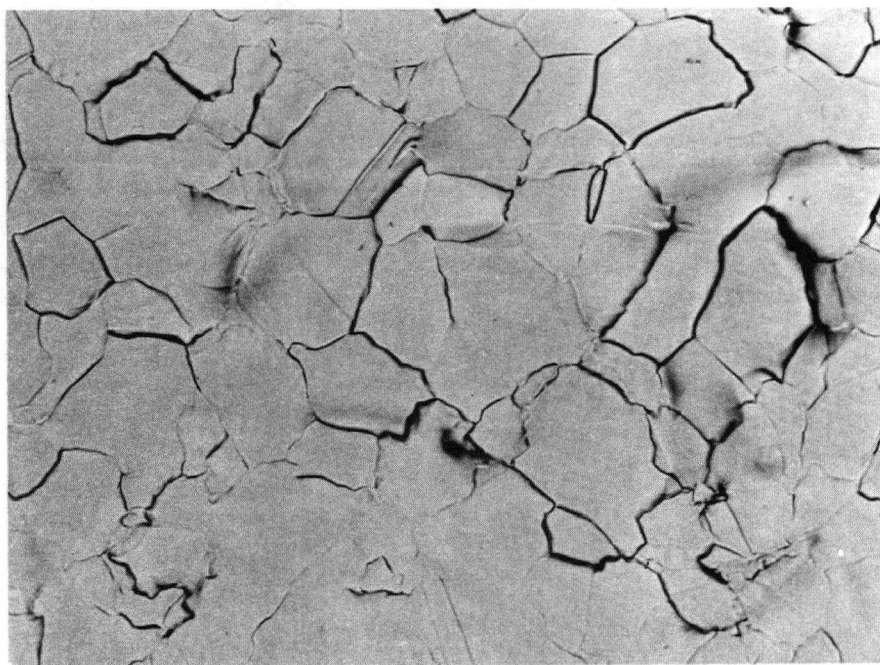
In order to obtain a quantitative assessment of the importance of shear as a deformation process, polished 400 $\mu$  specimens were finely marked by means of a soft brush and then deformed. As shown in Figure 14, shear was observed in both systems at room temperature. It was not necessarily associated with migration. Only a few boundaries showed visible offsets and such offsets could only be seen at rather high magnifications.

The effect of boundary migration and shear processes on the stress strain curve is not fully understood. Shear is basically a work hardening process and involves the deformation and subsequent hardening of areas adjacent to the boundaries. On the other hand migration occurs



(a) undeformed

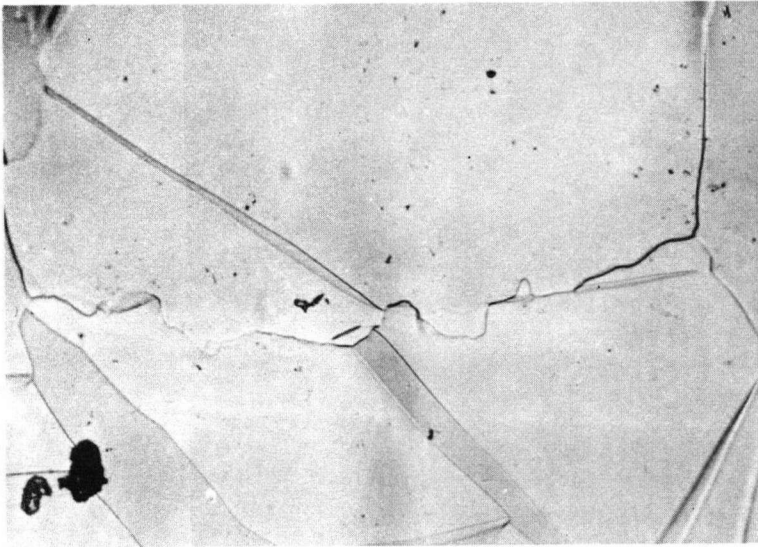
X 240



(b) deformed and immediately repolished

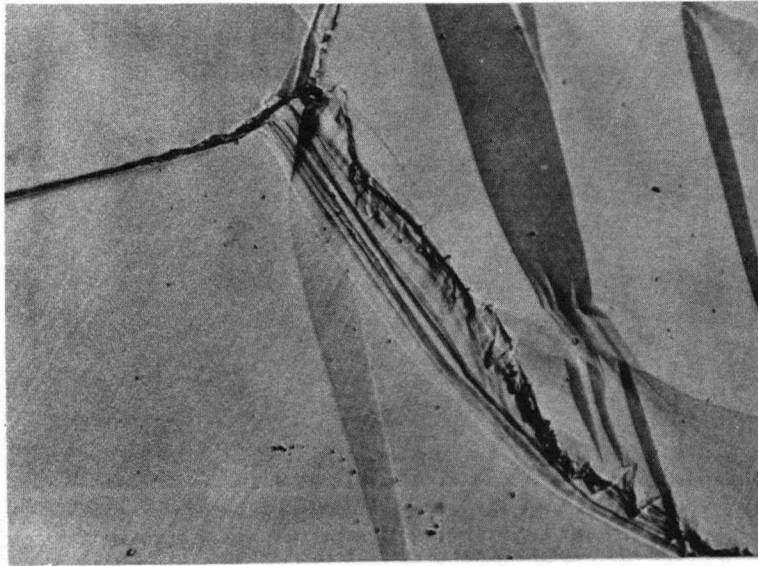
X 240

Fig.12 Grain boundaries in 25 $\mu$  cadmium before and after 7% deformation at +20°C.



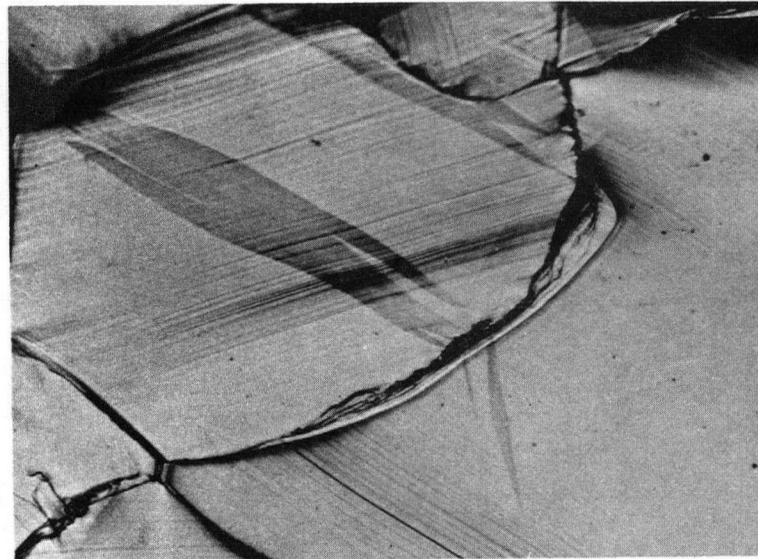
(a) corrugated grain boundary in cadmium deformed 7% at +20°C and repolished.

X 240



(b) cadmium deformed 7% at -30°C.

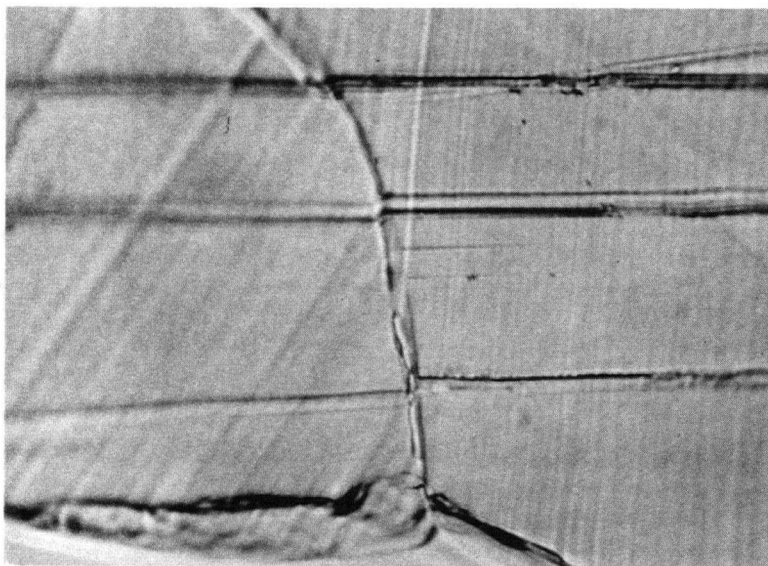
X 650



(c) zinc deformed 7% at +20°C.

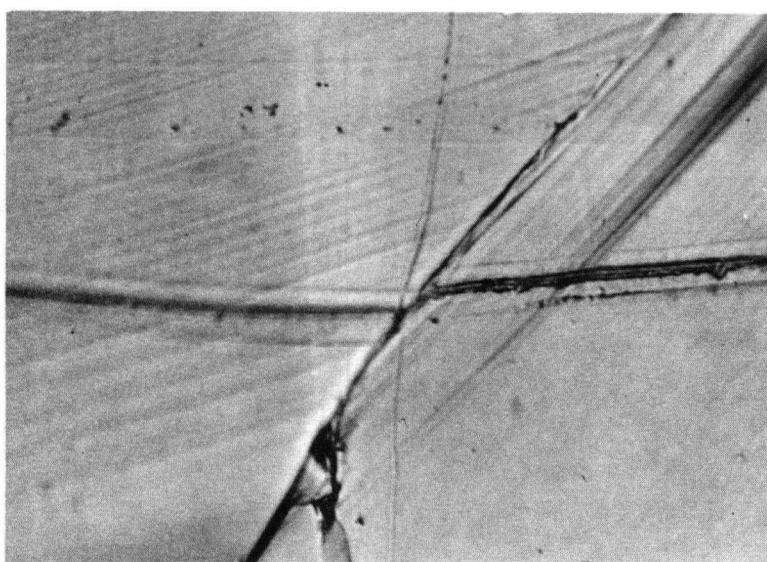
X 240

Fig.13 Grain boundary motion in 400 $\mu$  zinc and cadmium.



X 700

(a) cadmium at 10% strain.



X 700

(b) zinc at 7% strain.

Fig.14 Grain boundary shear in 400 $\mu$  zinc and cadmium at +20°C.

because of a net difference in free energy across the boundary caused by differences in the dislocation configurations associated with the work hardened states on each side of the boundary. If when a boundary moves it leaves behind a strain free region into which deformation can then proceed, the migration is essentially a recovery process acting as a prelude to recrystallization. Therefore any co-operative process of shear and migration represents a hardening and recovery cycle. Very small amounts of migration and shear were observed in cadmium at  $-95^{\circ}\text{C}$  ( $T_H = .30$ ), where migration was observed more as a slight grain boundary corrugation and did not involve gross boundary movement. More detailed studies will have to be made to accurately determine the temperature dependence of these processes. Dorn<sup>22</sup> observed substantial shear in polycrystalline magnesium at  $+20^{\circ}\text{C}$  ( $T_H = .32$ ). The possibility exists therefore that the ductility transition in cadmium at  $-120^{\circ}\text{C}$  is associated with the cessation of grain boundary recovery. If ductile shear as opposed to intergranular fracture occurs because of boundary recovery then it is necessary that the activation energy associated with migration be available down to  $T_H = .26$ .

The activation energy controlling boundary mobility is not known. However Winegard<sup>95</sup> has shown that the activation energy associated with grain growth in ultra pure metals can be related to the liquid self diffusion energy. This is usually in the range from .1 e.v. to .4 e.v. Although the driving force is somewhat different in each case it is not expected that the actual rate controlling mechanism during boundary migration will be different than that associated with grain growth. Therefore it is probable that the energy required for boundary migration will be sufficiently low that some boundary instability can occur in cadmium

at temperatures down to  $-120^{\circ}\text{C}$ .

Boundary migration in polycrystalline zinc poses a difficult problem for the development of successful zinc alloys with good creep resistance. It is desirable to obtain as fine a grain size as possible in order to improve strength and mechanical working characteristics. With such a structure however it is then necessary to stabilize the boundaries by a suitable alloying technique.

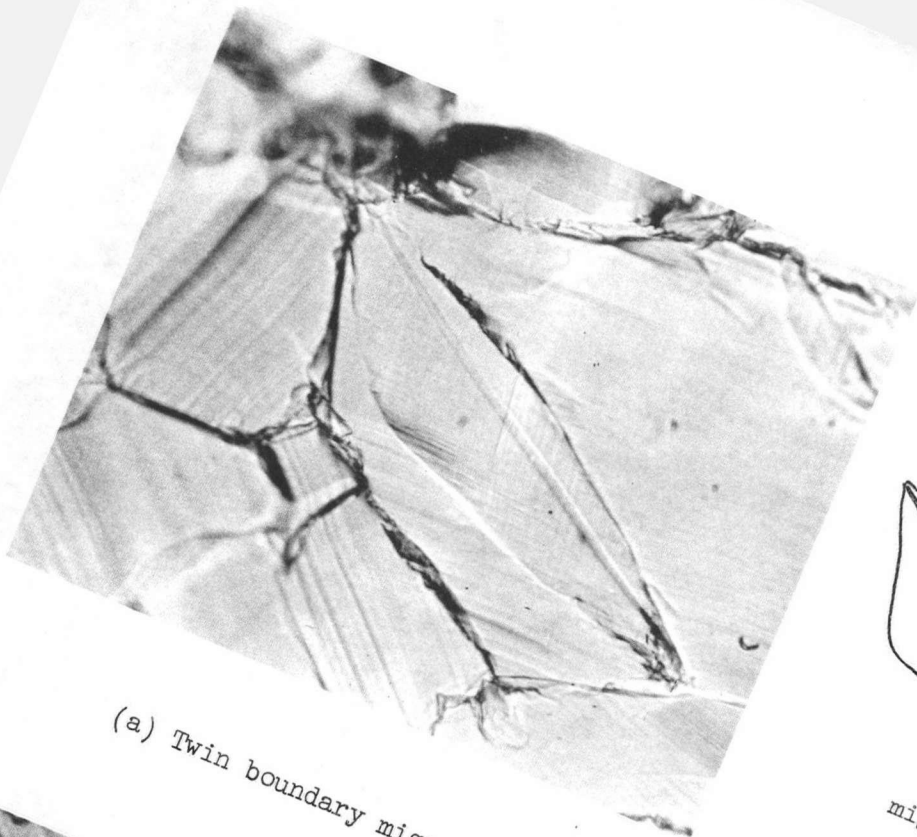
Since climb is known to occur at temperatures above  $-30^{\circ}\text{C}$ , it is probable that the ductile-brittle transition is related to the ease with which climb can occur as a dynamic recovery mechanism to allow for the circumvention of points of stress concentration. This interpretation however does not explain the known grain size dependence of the transition temperature.

This dependence on grain size may be explained in terms of easier crack propagation in large grained material. It may also be explained in terms of the relative amount of material being recovered by the action of boundary migration. Cleavage cracks are usually nucleated at grain boundaries, twin intersections etc. where stress concentration occurs. If these points of stress concentration can be removed by boundary migration then cleavage fracture should not occur. If it is assumed that the deformation processes do not change significantly with grain size, then the increased ductility of zinc with decreasing grain size at low temperatures may be related to the increased importance of grain boundary migration as a recovery mechanism. At any given value of strain and boundary migration rate, the amount of recovered material will increase as the grain size decreases.

#### 1.3.4 Recrystallization

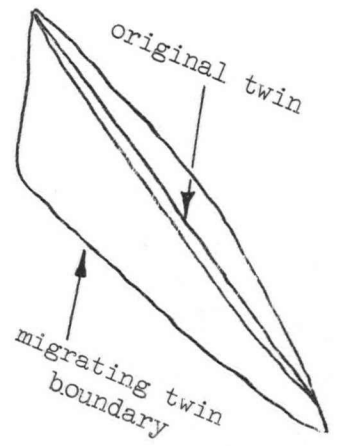
Grain boundary migration always preceded the introduction of new recrystallized grains which had their origin on the grain boundaries. A recrystallized grain which subsequently deformed is shown growing from the boundary in Figure 15(b). The growth of the new grain appears to have been stepped similar to the migration of existing boundaries. Fig. 15(a) illustrates the movement of twin boundaries into the parent grain by a diffusion process. This process is distinct from stress dependent twin growth which is a shear transformation. The original twin which formed is still visible due to surface distortion.

Recrystallized grains were never observed before maximum stress conditions, but were associated with the negative work hardening slope obtained at elevated temperatures above  $T_H = .40$ . At all temperatures studied, recrystallization never went to completion during testing except in the final necked area. At room temperature in 20 $\mu$  zinc, about 50% of the specimen volume remained unrecrystallized after 60% deformation. Recrystallized grains were rarely observed in 400 $\mu$  specimens at any temperature. This is reflected by the smaller amount of ductility from maximum stress to failure (Figure 9). The lower ductility to maximum stress for 20 $\mu$  Zn and 25 $\mu$  Cd at high temperatures as opposed to that for 400 $\mu$  material is merely a reflection of more pronounced boundary migration and the earlier introduction of recrystallization in the fine grained material.



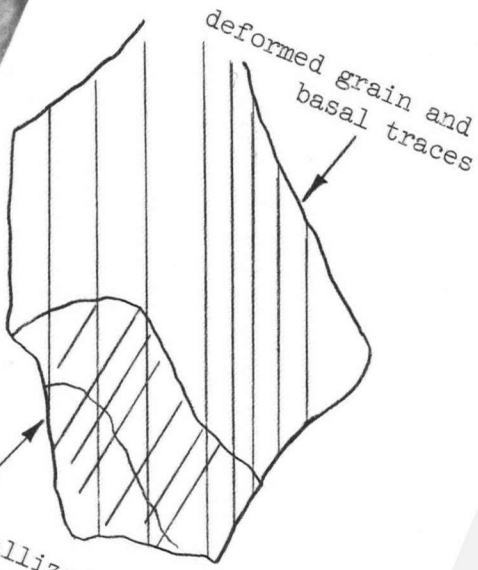
(a) Twin boundary migration.

X 650



(b) Recrystallized grain growing into a deformed grain.

X 650



recrystallized grain and subsequent basal traces

Fig.15 Recrystallization in 25 $\mu$  cadmium deformed 20% at +20°C.

### 1.3.5 Maximum Stress Variation with Temperature and Strain Rate

Stoloff using 500 $\mu$  cadmium found a plateau in ultimate tensile strength below about -160°C. The results of the present work are shown in Figure 16 and indicate that the occurrence of this plateau is grain size dependent. Continuously increasing strength values can be obtained to lower temperatures with a fine grain size.

Similar relationships are observed for zinc at high temperatures (Fig.17). However with the onset of cleavage fracture that accompanies decreasing temperature, there is a gradual decrease in maximum stress which levels off at a more or less constant value when ductility becomes less than 1%, indicating a temperature independent fracture process. The effect of strain rate on fracture stress is shown in Figures 18 and 19. It is seen from Figure 19 that in zinc when fracture occurs by cleavage as opposed to ductile shear, the macroscopic fracture stress is strain rate independent over the range of strain rates used.

With cadmium (Fig. 18) the strain rate dependence of maximum stress varies only slightly above 77°K. At 77°K where fracture is completely intercrystalline, there is virtually no strain rate dependence of maximum stress.

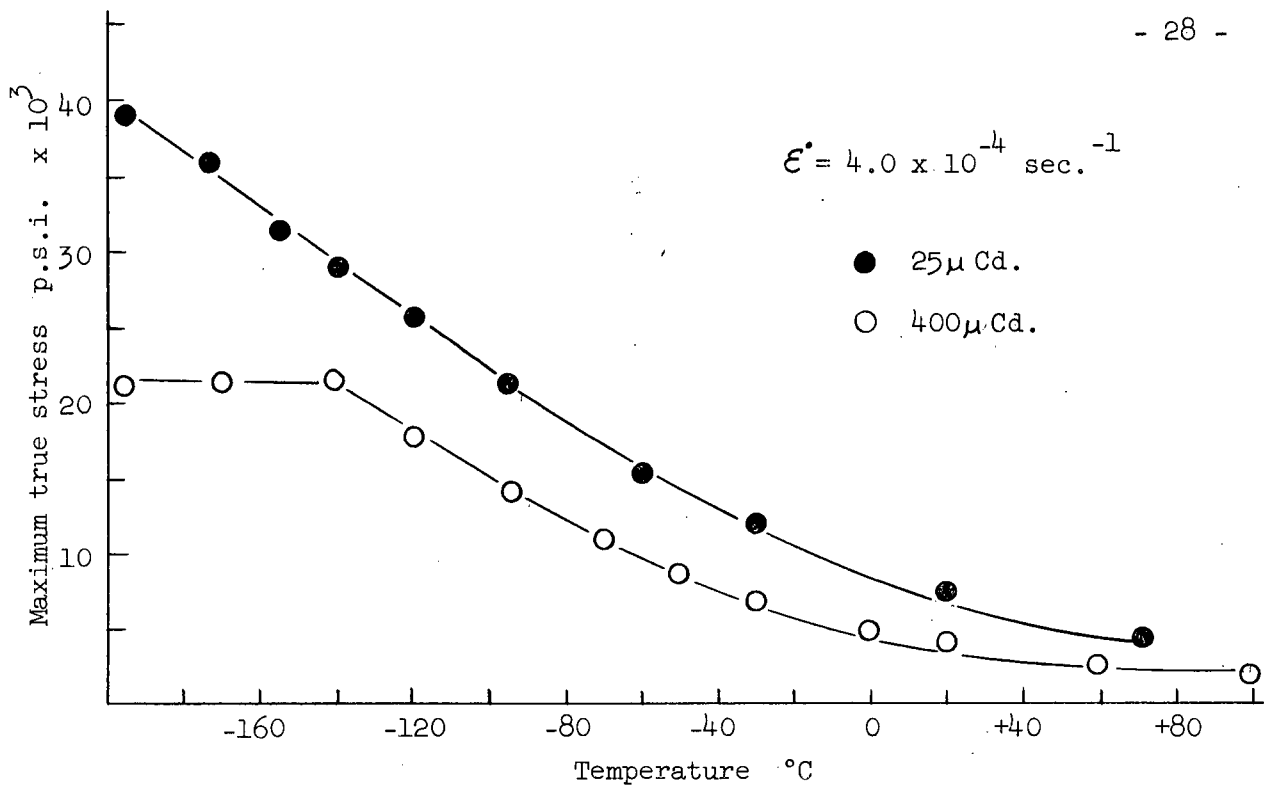


Fig.16 The temperature dependence of the maximum stress in cadmium.

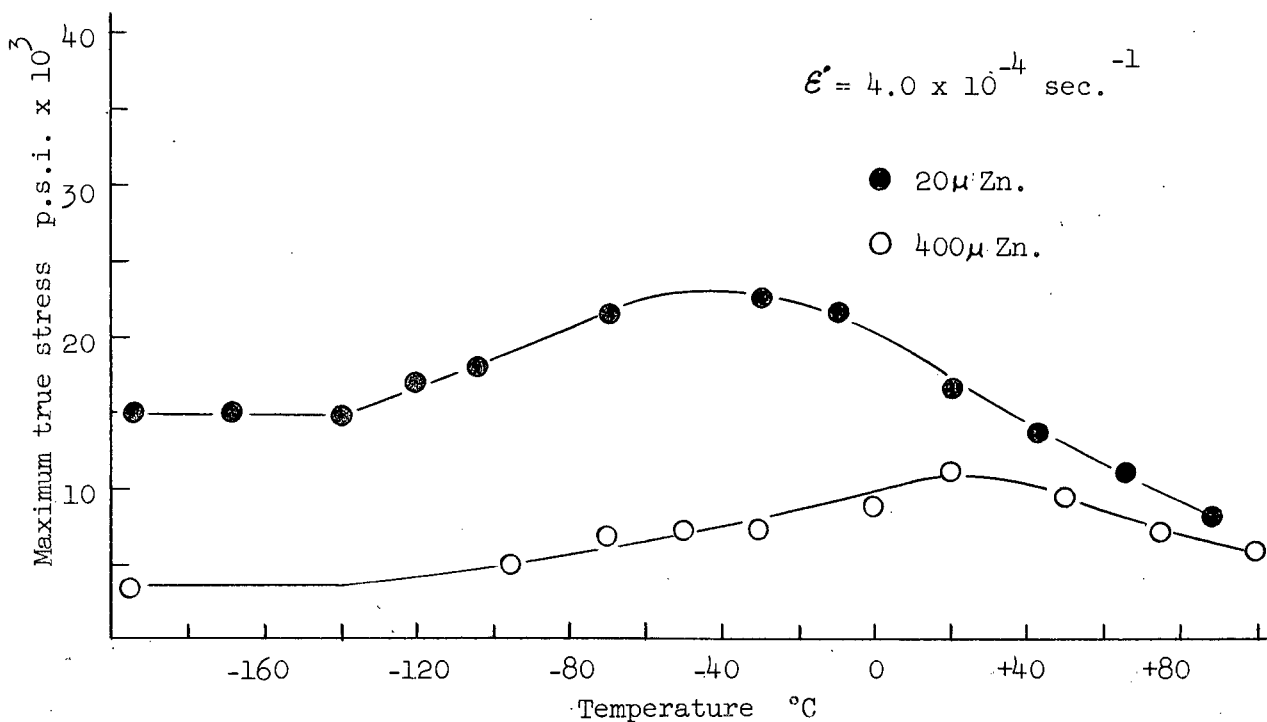


Fig.17 The temperature dependence of the maximum stress in zinc.

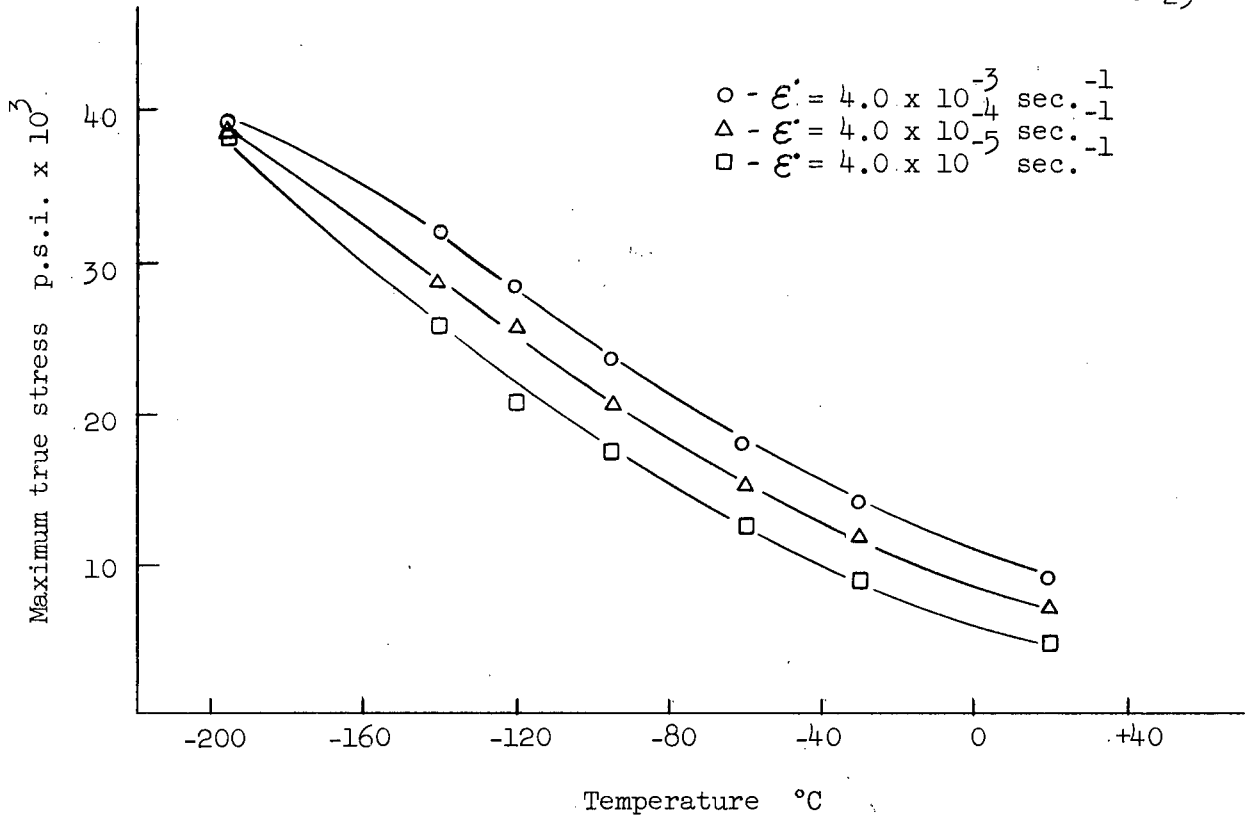


Fig. 18 The effect of strain rate on the maximum stress in 25μ cadmium.

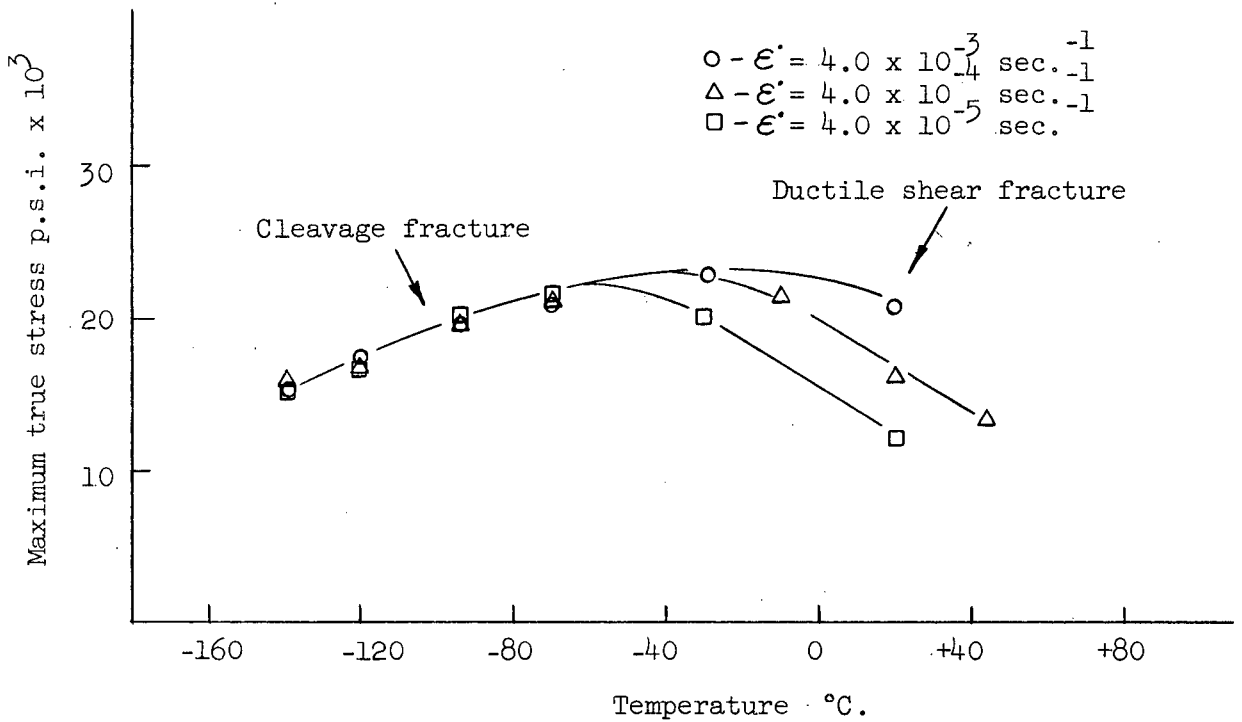


Fig. 19 The effect of strain rate on the maximum stress in 20μ zinc.

## 1.4 DEFORMATION MODES IN ZINC AND CADMIUM

In 1928 Von Mises<sup>32</sup> showed that it was necessary for five independent slip systems to be operative before a polycrystalline material can undergo a general homogeneous strain by slip. In many systems however other mechanisms such as twinning, bending and kinking may occur thereby reducing the number of distinct slip systems required.

### 1.4.1 Slip

The predominant slip system in zinc and cadmium is the basal system (0001)  $\langle 11\bar{2}0 \rangle$ . It has been a popular belief that if and when non basal slip does occur it will do so much more readily in systems which have  $c/a$  ratios equal to or less than ideal. This argument follows from relative close packing considerations. Seeger<sup>33</sup> has suggested however that in addition to the  $c/a$  ratio, the stacking fault energy will have a strong influence on deformation modes in as much as it controls the cross slip process. Stoloff and Davies<sup>34</sup> using hexagonal close packed Zn-Ag alloys of slightly varying axial ratios showed that the  $c/a$  ratio is not the only criterion for non basal slip.

The possible pyramidal slip systems are indicated in Figure 20. Tables 2 and 3 show the results of previous investigations into the non basal slip characteristics of zinc and cadmium. All studies were carried out using single crystals. Gilman<sup>43</sup> observed prismatic slip  $\{10\bar{1}0\} \langle 11\bar{2}0 \rangle$  in cadmium but only at higher temperatures than those used in the present investigation. The only non basal system that has been reliably reported as being operative in zinc is the second order pyramidal  $\{11\bar{2}2\} \langle 11\bar{2}3 \rangle$ .

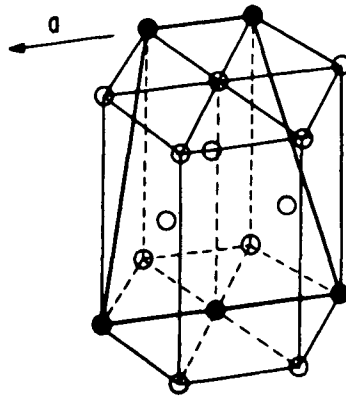
However both pyramidal systems  $\{10\bar{1}1\}\langle 11\bar{2}0\rangle$  and  $\{11\bar{2}2\}\langle 11\bar{2}3\rangle$  have been observed in cadmium by Price using dislocation free platelets.<sup>40-41</sup> This is interesting in that the first order pyramidal is a possible cross slip plane. Alden<sup>45-46</sup> using zinc and cadmium single crystals found that zinc has a much higher net hardening rate than cadmium during alternating tension-compression tests. This he interpreted to be due to the greater ease of cross slip in cadmium. However the 1st order pyramidal system has never been observed during the deformation of bulk crystals. On the other hand Price failed to observe any cross slip from basal to pyramidal planes. His pyramidal dislocations were all nucleated on the pyramidal planes.

Metallographic studies for this work indicated that non basal slip is a common occurrence. All observations were made using 400 $\mu$  material because of the difficulty in resolving traces on fine grained surfaces. Qualitatively it appeared that the occurrence of non basal slip increased in frequency with decreasing grain size. However any quantitative results will have to wait an extensive electron microscopy replica study.

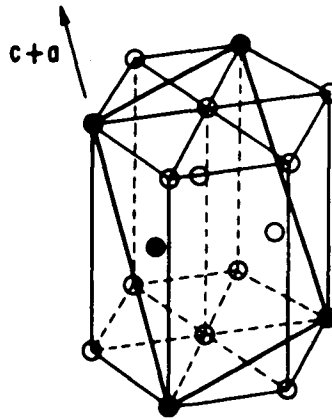
#### 1.4.1 a) Zinc

Non basal traces were much more prevalent at +20°C in zinc than in cadmium at an equivalent temperature. Figure 21 shows slip line traces in zinc over a series of strains at +20°C. Approximately 50% of the grains in zinc showed non basal traces at fracture. These traces were usually wavy and discontinuous in nature at +20°C and did not completely traverse a grain. They would start near grain boundaries and gradually progress across the grain (Grain A, Fig. 21). Many grains showed two different traces and a few three (Grain B).

(a) First-order pyramidal glide occurs when dislocations with a  $\frac{1}{2}[\bar{1}210]$  Burgers vector move on  $(10\bar{1}1)$  planes. (b) Second-order pyramidal glide occurs when dislocations with a Burgers vector  $\frac{1}{2}[\bar{1}\bar{1}23] = c+a$  move on  $(11\bar{2}2)$  planes.



(a)



(b)

Fig. 20 Pyramidal glide systems in zinc and cadmium (after Price<sup>39</sup>).

TABLE 2

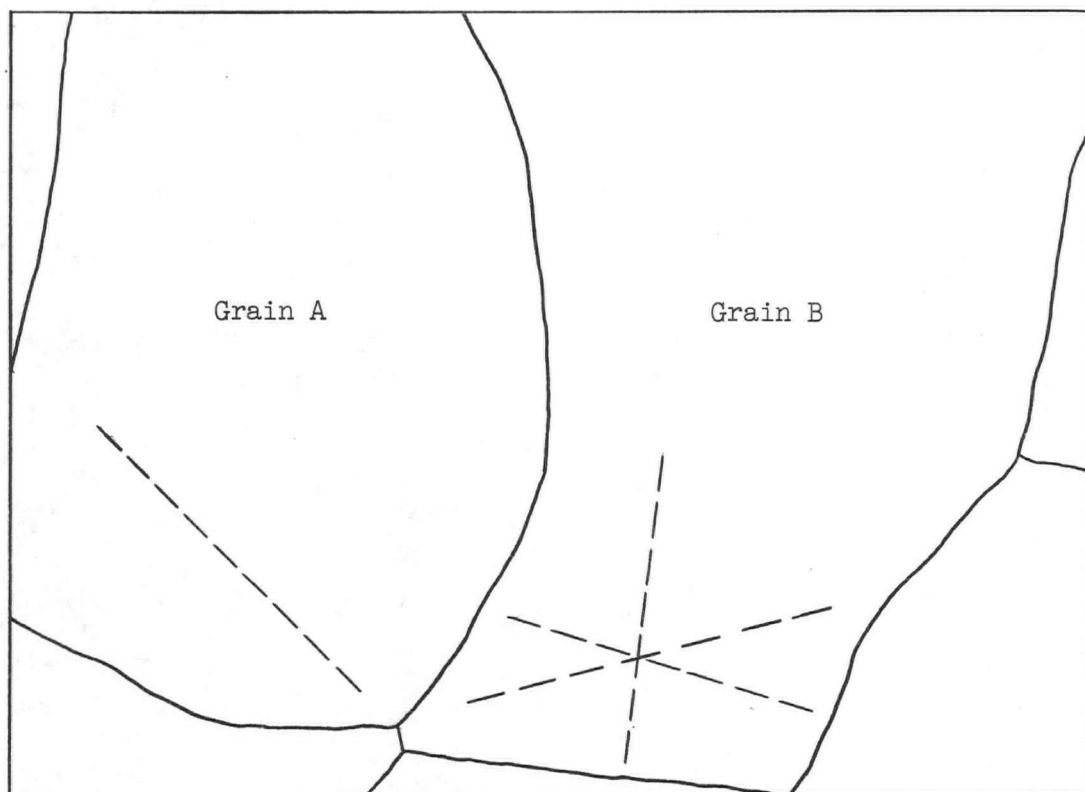
Non Basal Slip Systems Observed in Zinc

| Author                               | Temperature    | Loading                              | Non Basal System   | Remarks   |
|--------------------------------------|----------------|--------------------------------------|--|---|
| Rosenbaum <sup>35</sup>              | +20°C          | Bending                              | $\{11\bar{2}2\} \langle 11\bar{2}3 \rangle$  | etch pitting on basal planes  |
| Bell and Cahn <sup>36</sup>          | +20°C          | Tension    to basal planes           | $\{11\bar{2}2\} \langle 11\bar{2}3 \rangle$  | slight departure from $\{11\bar{2}2\}$ - slip plane may be irrational                 |
| Price <sup>37,38,39</sup>            | +20°C → -150°C | Tension                              | $\{11\bar{2}2\} \langle 11\bar{2}3 \rangle$  | dislocation free platelets  |
| Predvoditelev <sup>42</sup>          | +20°C          | Compression    to c axis             | $\{11\bar{2}2\} \langle 11\bar{2}3 \rangle$  | etch pit studies  |
| Gilman <sup>43</sup>                 | +20°C → +150°C | Compression    to basal planes       | $\{11\bar{2}2\} \langle 11\bar{2}3 \rangle$<br>$\{10\bar{1}0\} \langle 11\bar{2}0 \rangle$ | Prismatic only at elevated temperatures   |
| Stofel, Wood and Clark <sup>44</sup> | 25°C and -78°C | Tension and Compression    to c axis | $\{11\bar{2}2\} \langle 11\bar{2}3 \rangle$  | rate of work hardening = $7.5 \times 10^5$ psi. decreases with decreasing temperature |

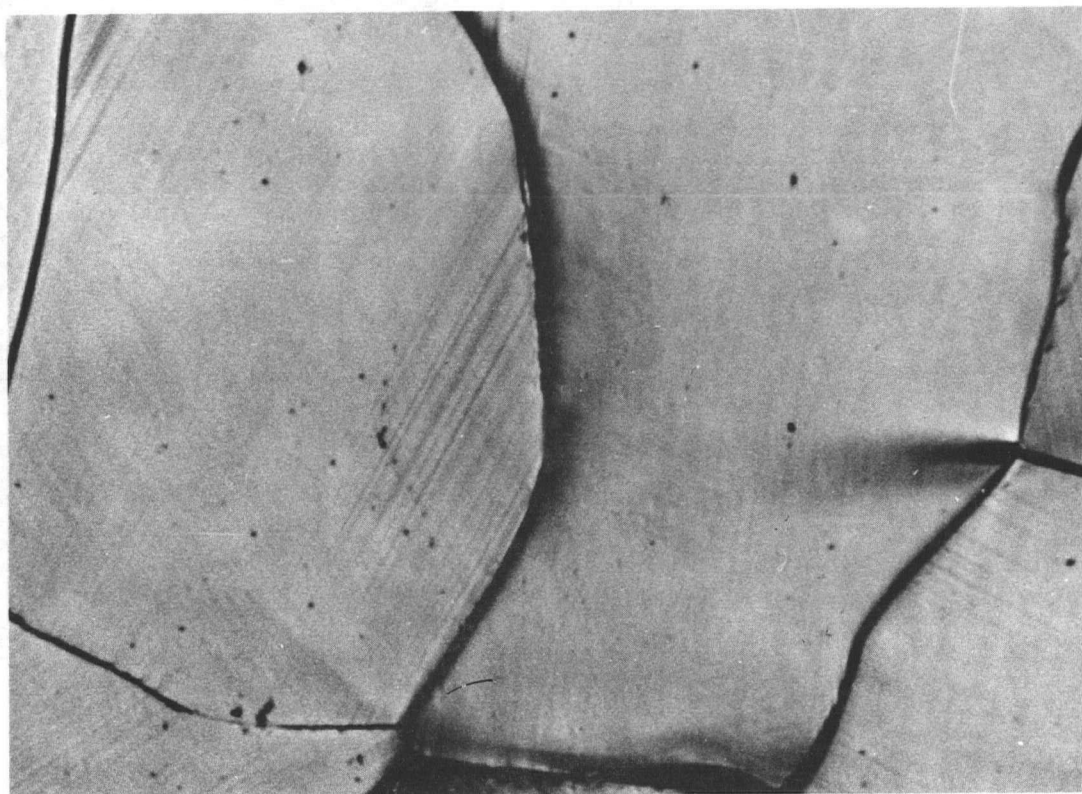
TABLE 3

## Non Basal Slip Systems Observed in Cadmium

| Author                             | Temperature    | Loading                 | Non Basal System   | Remarks  |
|------------------------------------|----------------|-------------------------|--|--|
| Stoloff and Gensamer <sup>47</sup> | +20°C → -196°C | bending and compression | $\{11\bar{2}2\} \langle 11\bar{2}3 \rangle$  | Single crystals used   |
| Price <sup>40-41</sup>             | +20°C → -150°C | tension                 | $\{11\bar{2}2\} \langle 11\bar{2}3 \rangle$<br>$\{10\bar{1}1\} \langle 11\bar{2}0 \rangle$ | Dislocation free platelets<br>$\{1011\}$ predominates at elevated temperatures |
| Gilman <sup>48</sup>               | +150°C → 275°C | tension                 | $\{10\bar{1}0\} \langle 11\bar{2}0 \rangle$  | Only at elevated temperatures  |
| Wernick and Thomas <sup>49</sup>   | +25°C → -150°C | compression             | $\{11\bar{2}2\} \langle 11\bar{2}3 \rangle$  | etch pit studies   |

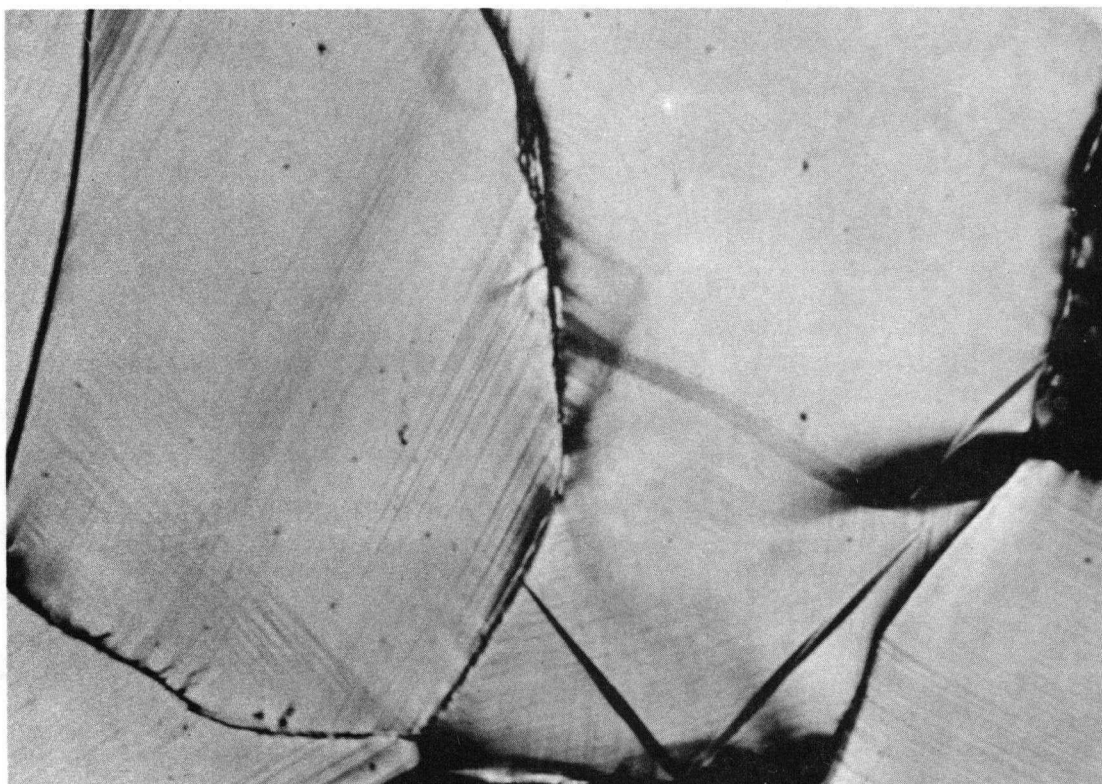


(a) schematic diagram

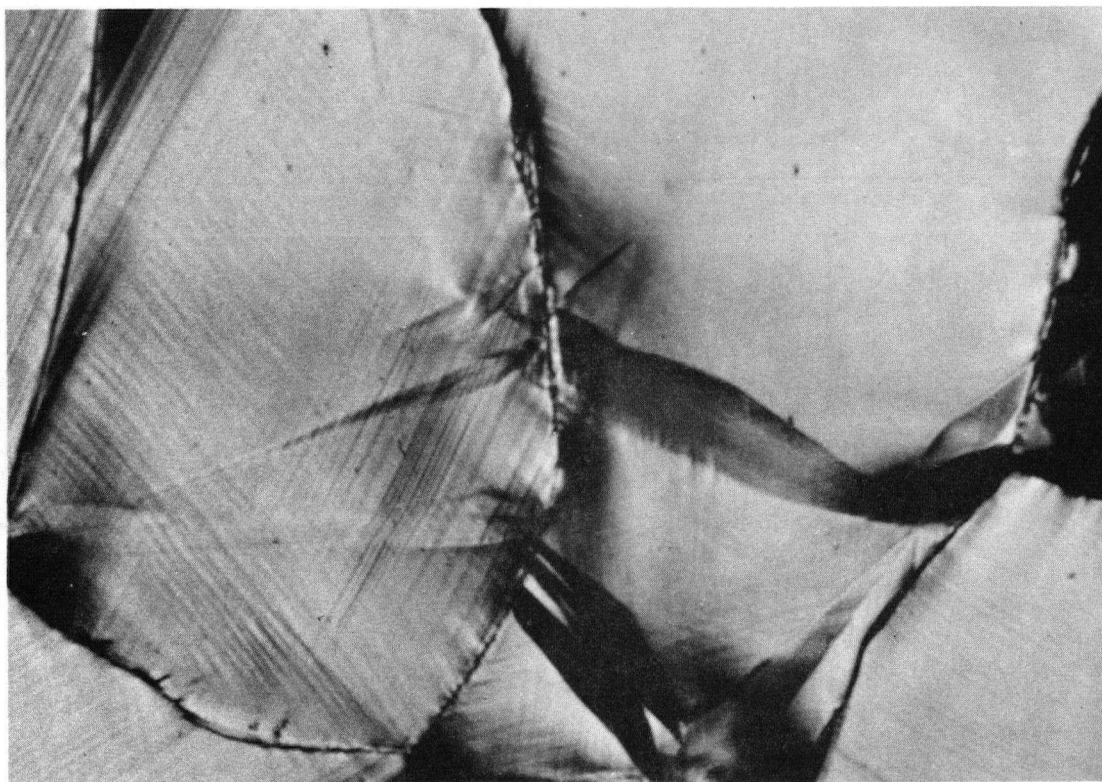


(b) 1.7 % strain

Fig. 21       $\{11\bar{2}2\}$   $\langle 11\bar{2}3 \rangle$  slip in 400 $\mu$  zinc at various strains.  
Temperature = +20°C.      Magnification X 400



(b) 4.7 % strain



(c) 7.1 % strain

Fig. 21  $\{11\bar{2}2\} \langle 11\bar{2}3 \rangle$  slip in  $400\mu$  zinc at various strains.  
Temperature =  $+20^{\circ}\text{C}$  Magnification X 400

By a trace analysis technique similar to that described by Reed-Hill and Baldwin,<sup>65</sup> all non basal traces were identified as originating from  $\{11\bar{2}2\} \langle 11\bar{2}3 \rangle$  slip. The technique can only be used if at least 3 twin traces and the basal slip traces can be observed. Then by an appropriate measurement of angles it is possible to arrive at a possible solution for the non basal traces. Because of the slight ambiguity associated with this procedure, it was checked against X-Ray determination of the orientation for two selected grains showing non basal traces. In both cases, the two techniques indicated 2nd order pyramidal slip.

Price observed that screw dislocations with a Burgers vector  $\frac{1}{3} [\bar{1}\bar{1}23]$  cross glided frequently between planes containing the  $[\bar{1}\bar{1}23]$  direction. This could explain the wavy nature of the traces at room temperature.

With decreasing temperature the non basal traces became straighter and tended to concentrate into bands, an observation made previously by Stoloff<sup>47</sup> in cadmium and Gilman<sup>43</sup> in zinc. These bands may easily be mistaken for fine twins. However as seen in Figure 22 they readily intersect one another and were removed by polishing.

#### 1.4.1. b) Cadmium

At 30°C and above non basal slip was less extensive in cadmium than in zinc. With decreasing temperature it became more prevalent as shown in Fig. 23. These low temperature markings were very similar to those observed in zinc at equivalent temperatures. As in zinc, trace

analysis showed them to originate from  $\{11\bar{2}2\}\langle 11\bar{2}3\rangle$  slip. In no case was first order pyramidal observed.

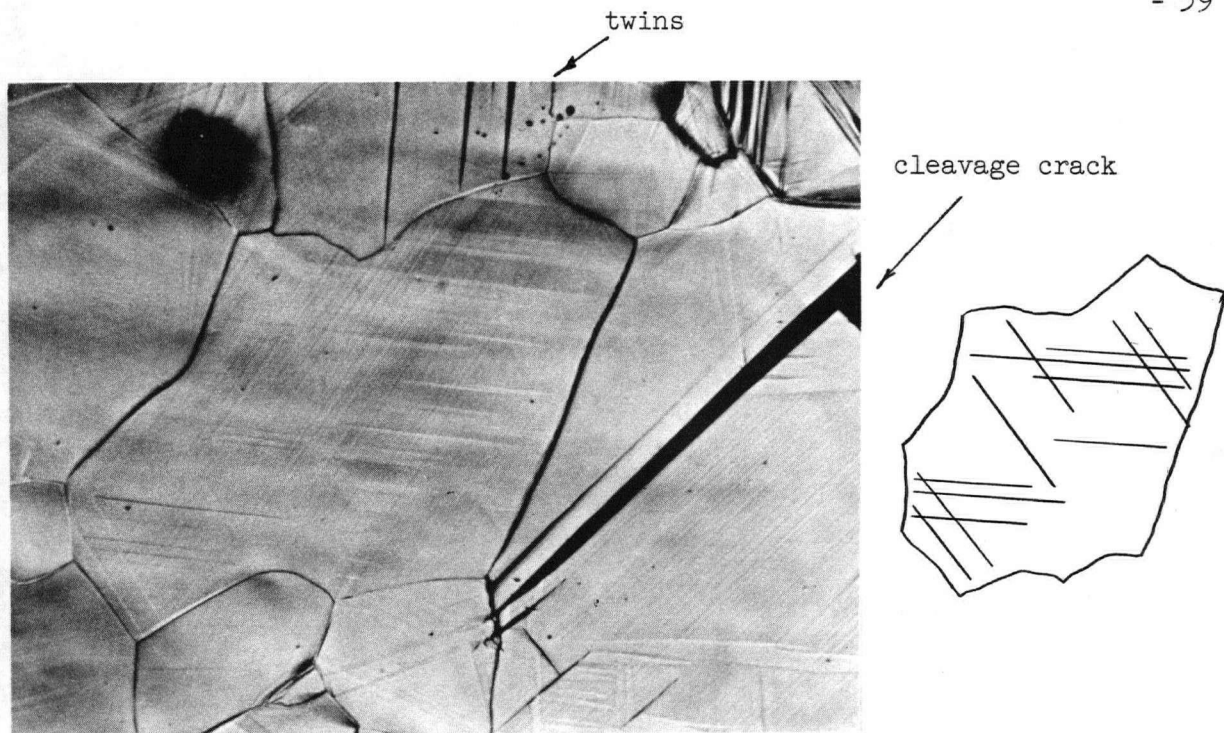
The observation of extensive  $\{11\bar{2}2\}\langle 11\bar{2}3\rangle$  slip in zinc and cadmium is not unexpected. As reviewed by Dorn<sup>86</sup>, this system is the only one which can promote extensive deformation parallel to the c axis. The contribution that twinning can make is not significant in terms of the total strain. No combination of  $\{0001\}\langle 11\bar{2}0\rangle$ ,  $\{10\bar{1}0\}\langle 11\bar{2}0\rangle$ , and  $\{10\bar{1}1\}\langle 11\bar{2}0\rangle$  can provide the five independent systems required for homogeneous deformation. However the operation of  $\{11\bar{2}2\}\langle 11\bar{2}3\rangle$  is sufficient by itself in providing the number of required systems. Table 4 shows the number of independent systems for each of the prominent slip systems.

TABLE 4

Slip Systems in Hexagonal Metals

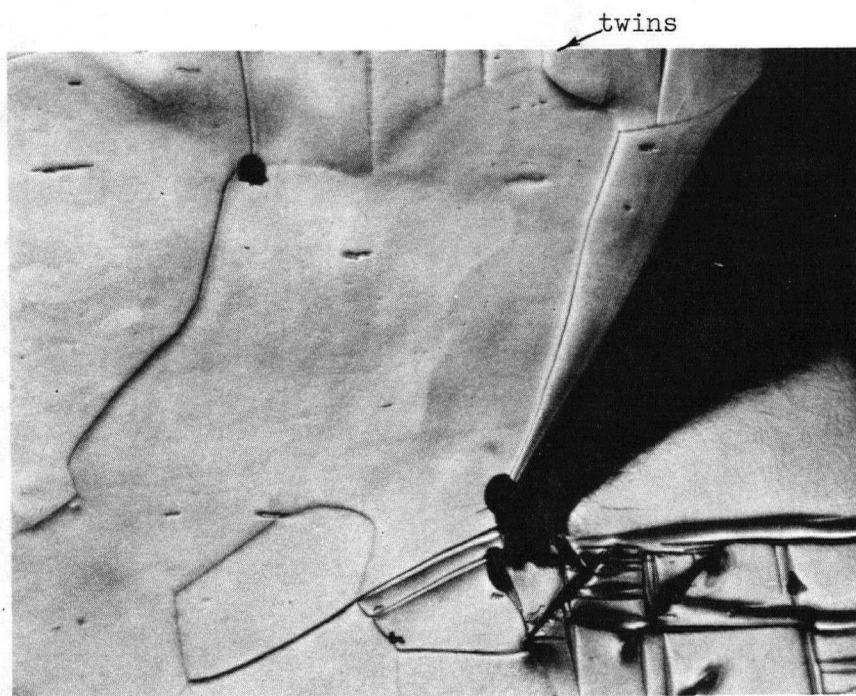
| No. | Slip System                               | Burgers Vector | Number of Independent Systems |
|-----|---|----------------|-------------------------------|
| 1   | $\{0001\}\langle 11\bar{2}0\rangle$       | a              | 2                             |
| 2   | $\{10\bar{1}0\}\langle 11\bar{2}0\rangle$ | a              | 2                             |
| 3   | $\{10\bar{1}1\}\langle 11\bar{2}0\rangle$ | a              | 4                             |
| 4   | $\{11\bar{2}2\}\langle 11\bar{2}3\rangle$ | c + a          | 5                             |
| 5   | 1 + 2 + 3                                 | a              | 4                             |

(after Dorn<sup>86</sup>).



X 240

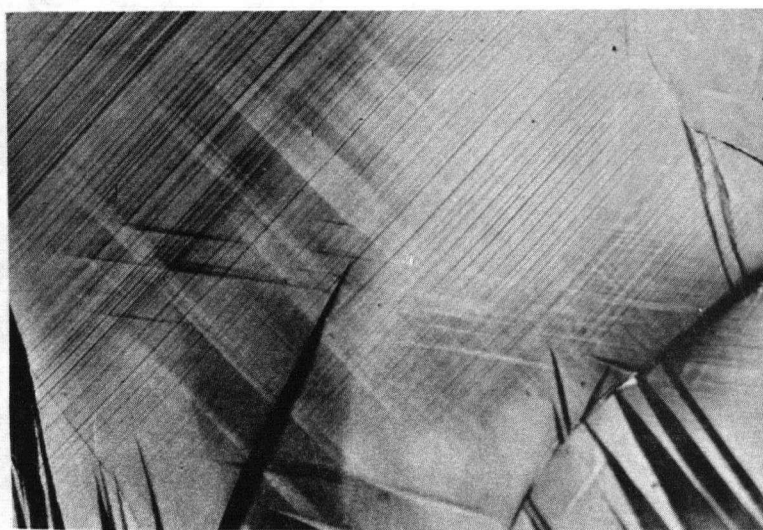
(a) Non basal traces near fracture surface.



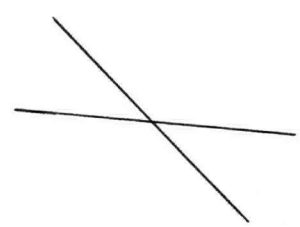
X 240

(b) As above after polishing.

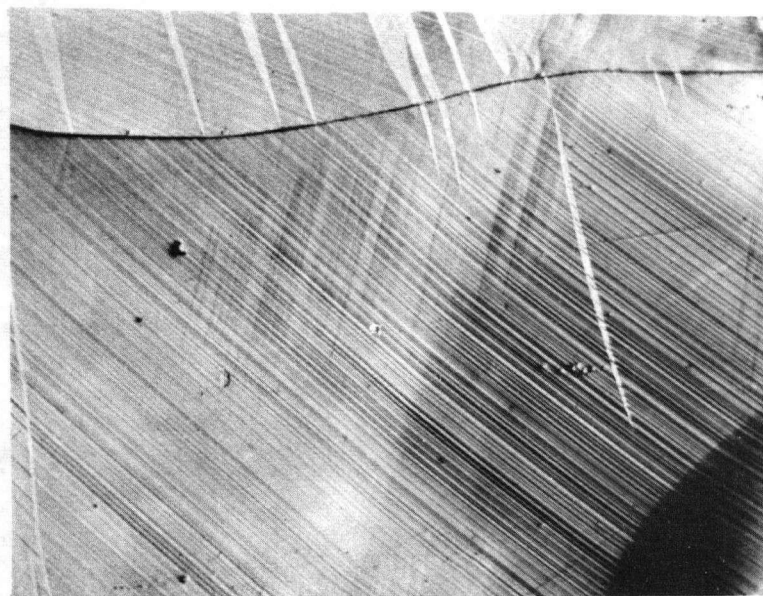
Fig. 22  $\{11\bar{2}2\} \langle 11\bar{2}3 \rangle$  slip in  $400\mu$  zinc at  $-196^\circ\text{C}$ .



(a)



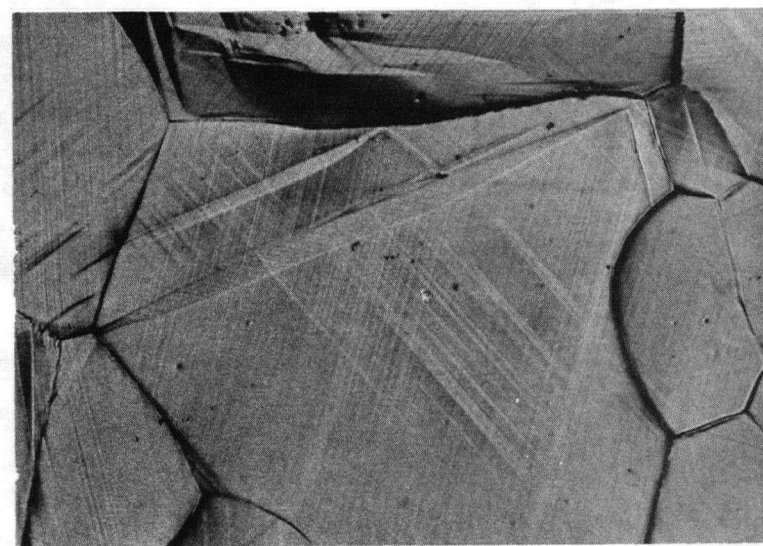
X 240



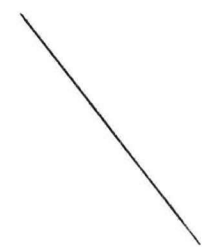
(b)



X 240



(c)



X 240

Fig. 23  $\{11\bar{2}2\}$   $\langle 11\bar{2}3 \rangle$  traces on  $400\mu$  cadmium deformed 7% at  $-196^\circ\text{C}$ .

#### 1.4.2 Twinning

In both zinc and cadmium twinning occurs on the  $\{10\bar{1}2\}$  planes in the  $\langle 10\bar{1}1 \rangle$  directions. However slight differences occur in the two systems in the frequency of twinning.

In the absence of general grain boundary migration the amount of twinning did not vary appreciably with temperature. As the temperature decreased the twins became finer indicating restricted twin growth with decreasing temperature. A comparison of the deformation markings after 7% strain at +20°C and -196°C in 400  $\mu$  cadmium is shown in Figures 24 and 25.

The amount of twinning under equivalent conditions of temperature and strain was slightly less in zinc than in cadmium. However Price observed that in dislocation free platelets, twins formed more readily and grew to larger sizes in zinc than they did in cadmium. This he explained in terms of the greater shear associated with twinning in cadmium (.171) as opposed to zinc (.139) and the possibility therefore of a more difficult process of twin nucleation in cadmium. However one could easily argue that twins should nucleate and grow more readily in cadmium because they represent a more effective deformation mechanism.

The lower frequency of twinning in zinc may also be due to the fact that second order pyramidal slip occurs more readily in polycrystalline zinc than in cadmium and the amount of twinning needed to meet Von Mises' requirements is therefore reduced.



X100

Fig. 24 Microstructure of 400μ cadmium deformed 7% at +20°C.



X 100

Fig. 25 Microstructure of 400μ cadmium deformed 7% at -196°C

The amount of twinning in both systems was always governed by the relative temperature and strain. In the region of room temperature with increasing boundary migration accompanying increasing strain, twin formation became much less frequent. Once distinct recrystallization started twin formation was not observed. Therefore cadmium which had fractured at 20% strain at  $-196^{\circ}\text{C}$  always showed more twinning than cadmium deformed to 20% strain at  $+20^{\circ}\text{C}$  since at the latter temperature migration is occurring. Migration affects twinning due to its recovery effect on areas of stress concentration required for twin nucleation. Therefore true comparisons of relative twinning could only be made either at low values of strain before extensive migration had started, or at low temperatures.

On this basis of comparison and keeping in mind the greater tendency for migration and recrystallization with decreasing grain size it was observed that the amount of twinning did not vary significantly with grain size.

At temperatures above  $+20^{\circ}\text{C}$ , where extensive migration occurs, very little twinning occurred as shown in Fig. 26.

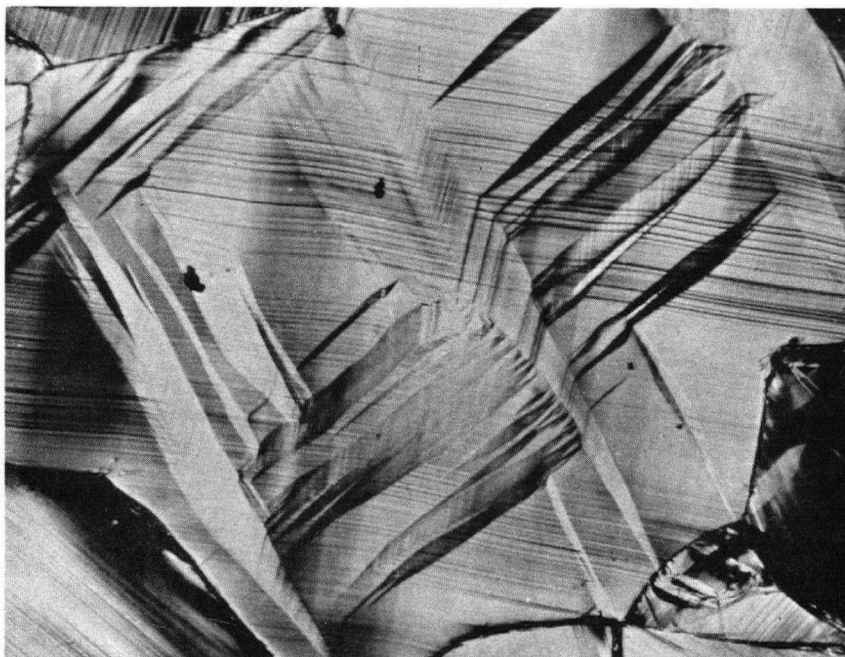
Stoloff observed less basal slip in twinned regions with a decrease in temperature. This was not observed as indicated in Figure 27 which shows extensive twin basal slip at  $-196^{\circ}\text{C}$ . The finer nature of basal traces at low temperatures makes them more difficult to resolve.

When twinning on one particular twin plane was stopped by a twin on another plane as shown in Figure 27, extensive slip would occur in basal planes of the latter and eventually cause twin nucleation on the opposite side of the twin. This process of twin nucleation was a common occurrence especially in cadmium.



X 260

Fig. 26 Lack of twinning in the presence of boundary migration.  
( 25 $\mu$  cadmium deformed 10% at +60°C.)



X 120

Fig.27 Twin basal slip and twin nucleation.  
( 400 $\mu$  cadmium deformed 7% at +20°C )

### 1.4.3 The Formation of Low Angle Boundaries during Deformation

Low angle boundaries have been observed to form during the deformation of both single crystals and polycrystals in many materials. Such boundaries have been referred to by a variety of nomenclatures which has confused their nature of formation and their importance as a deformation process.

The formation of "kinks" in single crystals of cadmium was first observed and discussed by Orowan<sup>54</sup>. Hess and Barrett<sup>52</sup>, Gilman<sup>55-56</sup> and Washburn and Parker<sup>51,53</sup> studied the nature of kinking in zinc single crystals. Gilman distinguished between compression kinks and tension kinks, postulating that the latter form only due to crystal inhomogeneities. Compression kinks were further subdivided into "ortho" (formed under low stress conditions) and "para" (formed at high stresses in crystals which have been extensively deformed). Compression ortho kinks were observed by Gilman in which the kink planes were always perpendicular to surface basal traces. They were observed to form in zinc at temperatures down to  $-196^{\circ}\text{C}$  indicating that the process of their formation is more likely one of stress induced dislocation rearrangement on the basal planes than one of dislocation climb which is thermally activated.

Boundary formation in polycrystals is more complicated because of the nature of the stresses. It has therefore been referred to by a variety of terms such as mosaic walls, cell formation and non crystallographic boundary formation. Gifkins<sup>50</sup> reported the formation of "cells" during the deformation of polycrystalline zinc above  $200^{\circ}\text{C}$ . Dorn<sup>21-22</sup> studying magnesium observed temperature independent "non crystallographic"

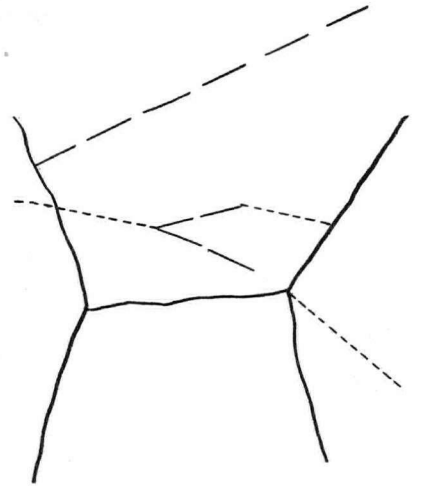
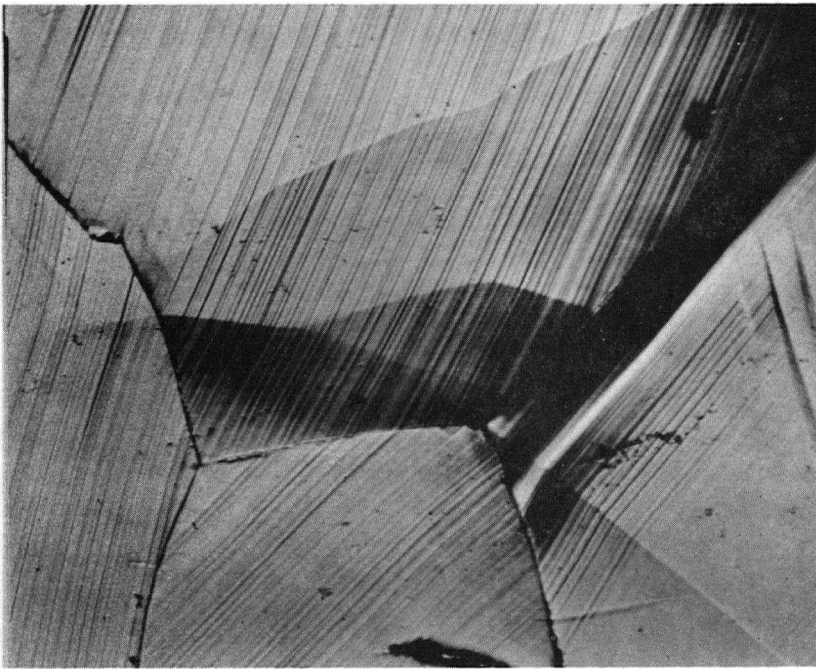
boundary formation which in many cases crossed grain boundaries. He postulated that these boundaries formed because of the bending of the lattice associated with the non homogeneous deformation of underlying grains.

The observations of the present work indicate that the formation of boundaries is similar in degree and type in both zinc and cadmium. "Non crystallographic" boundaries similar to those observed by Dorn are shown in Figure 28 and 29. From Figure 28 it is also observed that these boundaries can cross grain boundaries.

On close examination of Figure 28 it is observed that some boundaries seem to be "crystallographic" in that they are perpendicular to the basal slip traces. Similar boundaries are shown in Figure 30. These boundaries are similar to the ortho kink planes of Gilman. They were distinguished by three distinct features:

- 1) The misorientation of the basal traces was always greater across the crystallographic "kinks" than across non crystallographic boundaries.
- 2) Crystallographic boundaries formed in those grains which had the most prominent basal traces and few if any twins.
- 3) The boundaries were sometimes observed to be composed of two or more smaller boundaries (Figure 30) similar to those of Washburn and Parker.

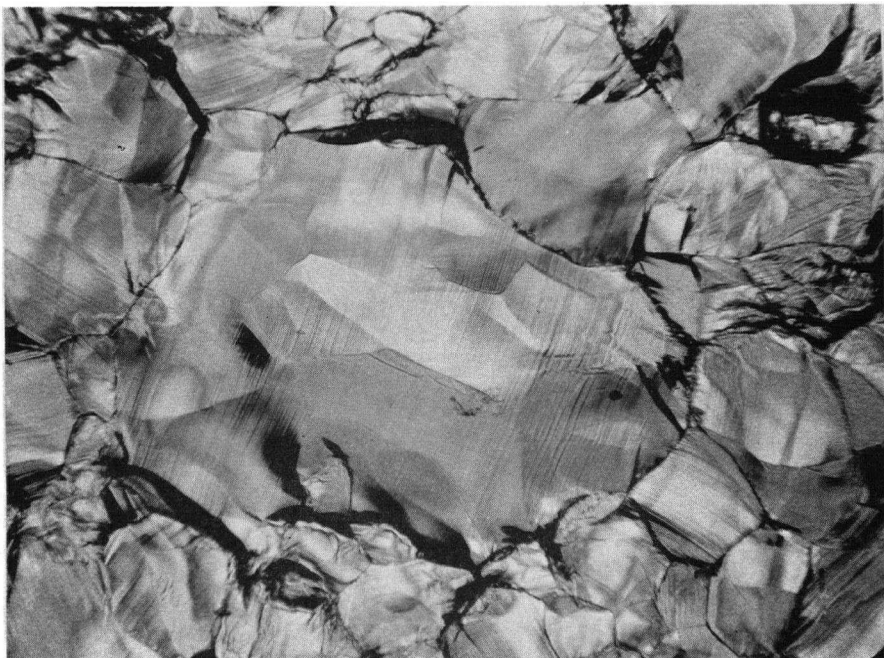
It would appear that the "crystallographic kinks" form only under fairly simple stress conditions such as bending or compression of the basal planes. The boundaries become non crystallographic however where



----- crystallographic  
----- non " "

X400

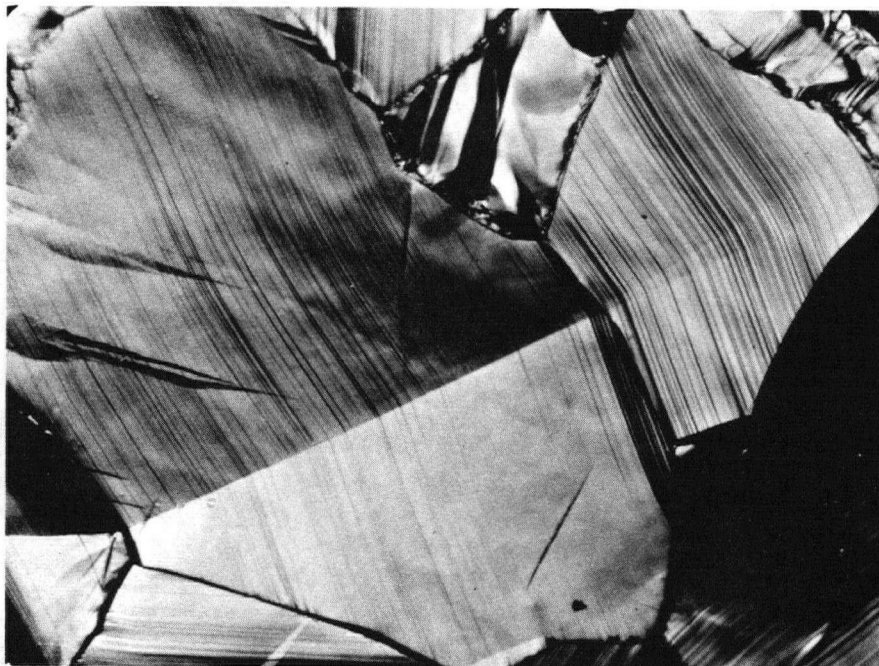
Fig.28 Low angle boundaries in cadmium deformed 7% at -30°C .



X 120

Fig.29 The formation of non crystallographic boundaries in cadmium due to underlying small grains.

( deformed 15% at +20°C.)



X240

(a) cadmium deformed 15% at +20°C.



X240

(b) zinc deformed 7% at +20°C.

Fig. 30 Crystallographic boundary formation in  $400\mu$  Zn and Cd.

boundary restraints on a given grain become more complicated. The extensive non crystallographic boundary formation of Figure 29 is due to the restraints imposed by the underlying fine grain structure.

## 1.5 YIELD STRESS AND WORK HARDENING

### 1.5.1 The Temperature Dependence of Yield

The flow stress-temperature relationships found by Stoloff are shown in Figure 31. He found that the yield stress was independent of temperature below about  $-80^{\circ}\text{C}$  and that the work hardening rate was constant over an increasing strain region as the temperature decreased. The results at  $4.2^{\circ}\text{K}$  are somewhat in doubt due to the different specimen geometry.

The definition of yield in polycrystalline zinc and cadmium is difficult because of the gradual nature of the yield process. Therefore the yield stress for the purpose of this work was defined by an offset technique using  $.1\%$  strain as the yield strain. In order to compare the temperature dependence of yield in zinc and cadmium, the yield stresses were normalized in each case by dividing by the shear modulus  $G$ . Shear modulus values were obtained from the tables of Koster<sup>57</sup>. The yield stress-effective temperature relationships are shown in Figure 32.

It is seen that below the critical temperature where yield is completely thermally activated the yield stress appears to increase linearly with decreasing temperature. The temperature dependence of yield for both grain sizes is slightly greater for zinc than for cadmium. The normalized yield stress is also somewhat higher for zinc. In  $400\mu$  material the

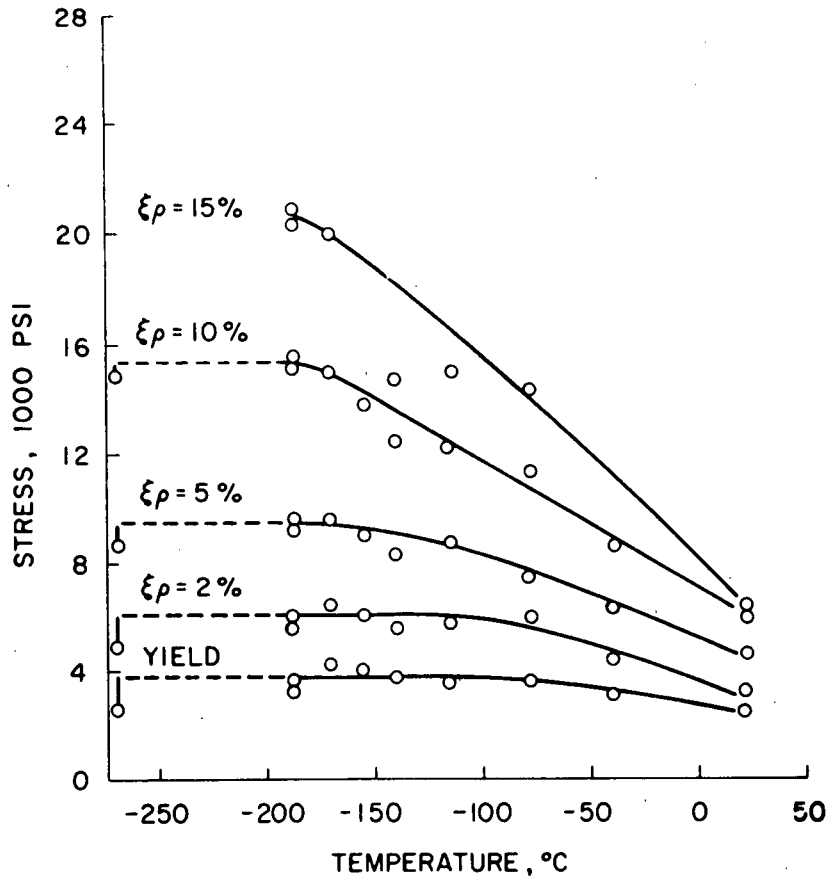


Fig. 31 Flow stress-temperature relationships for 0.020 inch grain diameter cadmium as found by Stoloff.

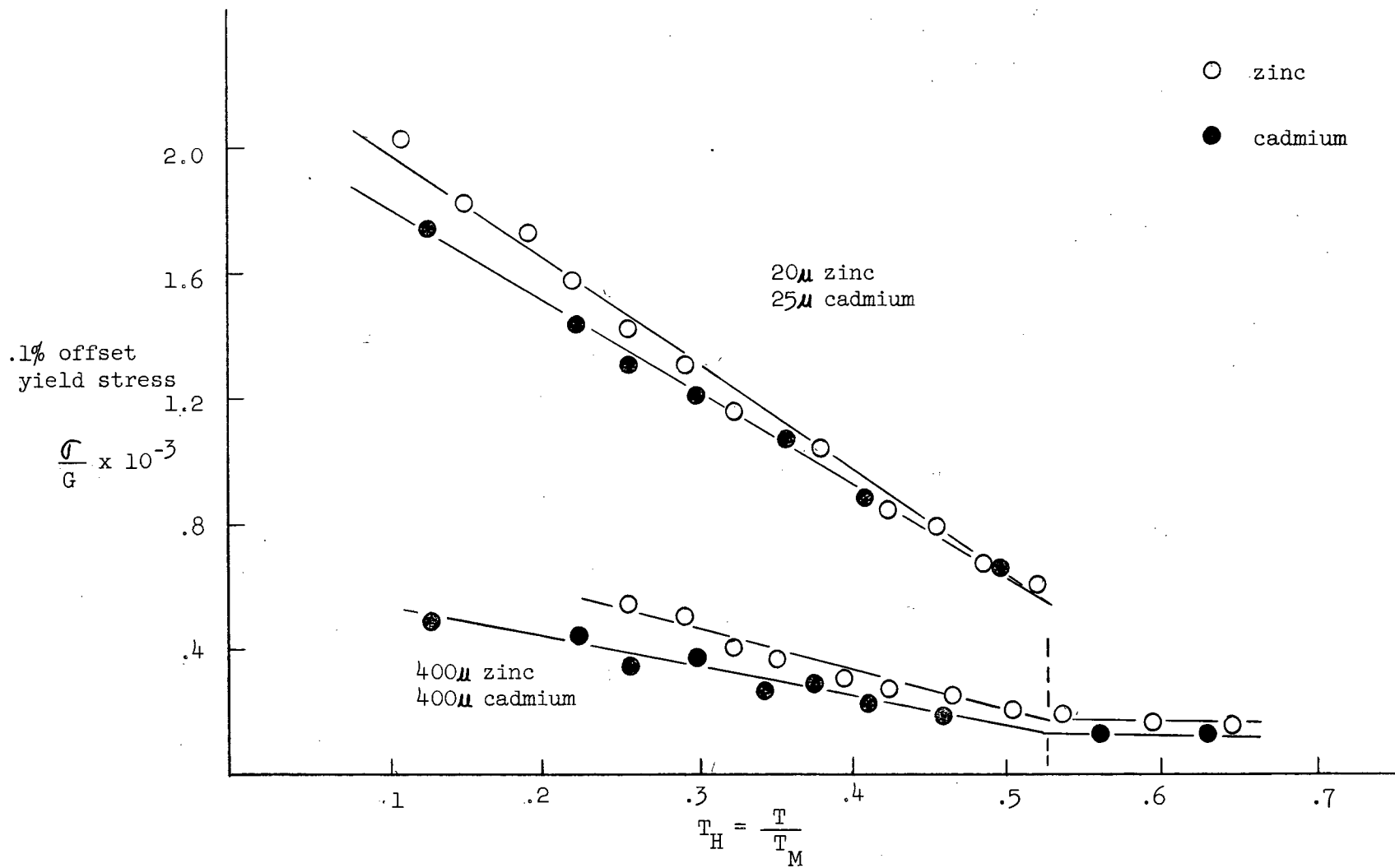


Fig.32 Temperature dependence of the yield stress in polycrystalline zinc and cadmium

critical temperature ( $T_c$ ) is approximately the same for both zinc and cadmium ( $T_H = .520$ ). Tests could not be done on fine grained material above about  $T_H = .5$  due to grain growth at these temperatures.

### 1.5.2 Temperature Sensitivity of the Flow Stress

Bullen<sup>58-60</sup> using polycrystalline copper found a linear relationship between the flow stress (at constant strain), and temperature over a range of temperature from 4.2°K to 450°K. He postulated that the hardening mechanism in copper remained the same over the temperature range studied but that the lower flow stress values obtained with increasing temperatures were due to either a different rate of obstacle formation with strain, or to a temperature dependent dynamic recovery process which tended to remove obstacles once formed. On the other hand Russell<sup>4</sup>, again using polycrystalline copper found that the work hardening rate was linear, and temperature insensitive below a certain critical temperature. The amount of strain involved with this constant linear hardening was also a function of temperature, and increased with decreasing temperature. His results are shown in Figure 33. Stoloff (Figure 31) also indicated a linear and temperature insensitive work hardening rate for cadmium at low temperatures where the flow stress itself was not a function of temperature.

#### 1.5.2 a) Cadmium

Flow stress-temperature relations for 25 $\mu$  and 400 $\mu$  cadmium obtained during this study are shown in Figures 34 and 35.

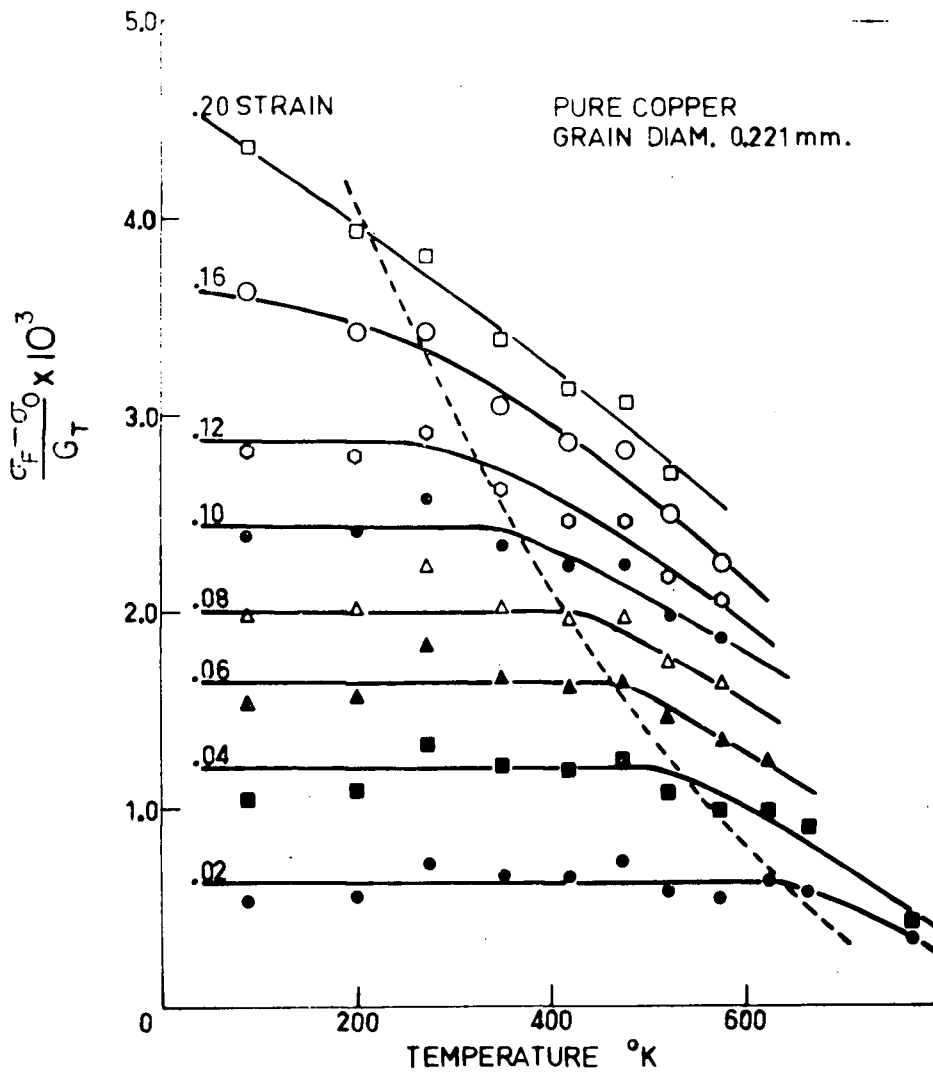


Fig.33 The temperature dependence of the strain hardening parameter of polycrystalline copper as found by Russell .

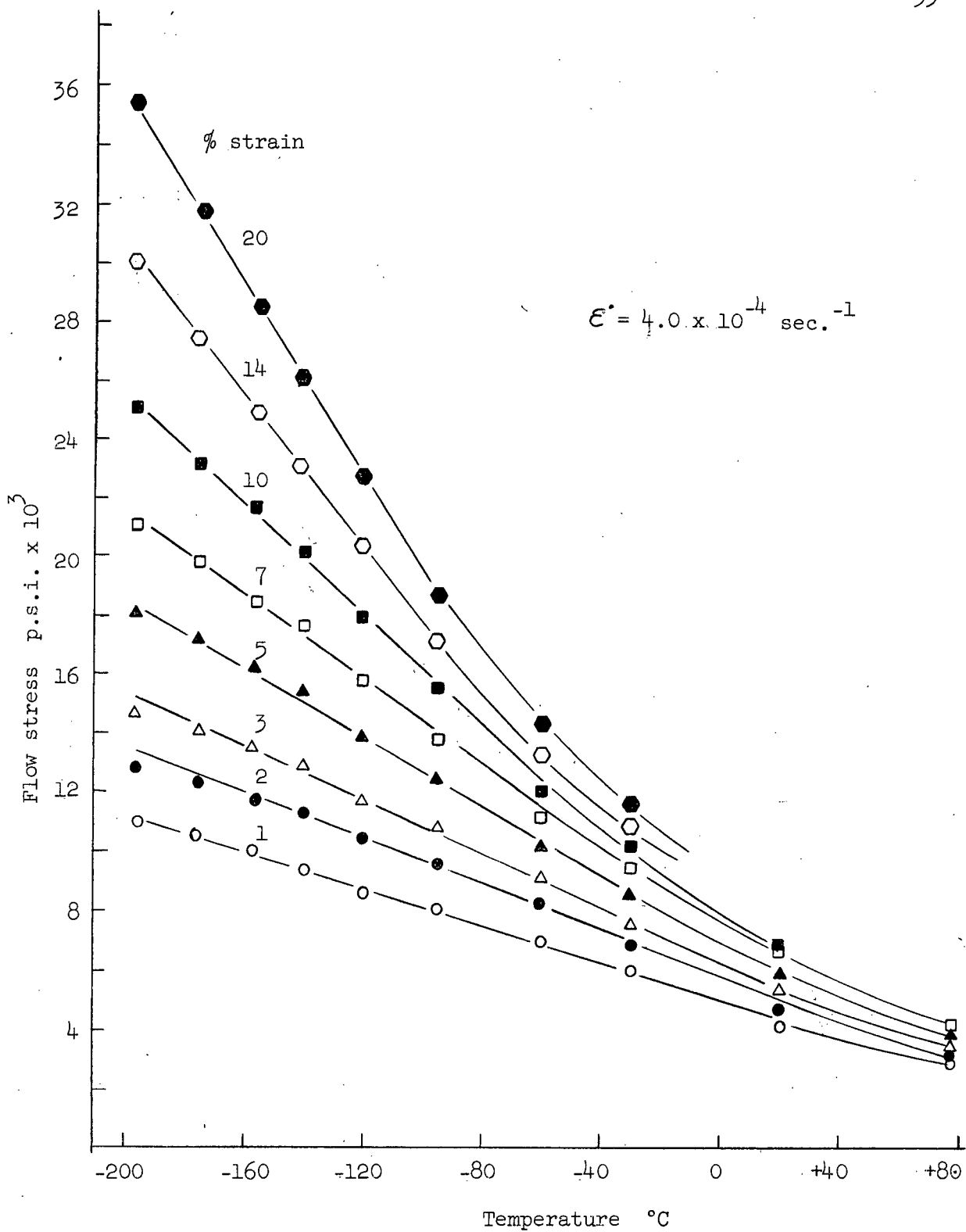


Fig. 34 Flow stress-temperature relationships for 25  $\mu$  cadmium.

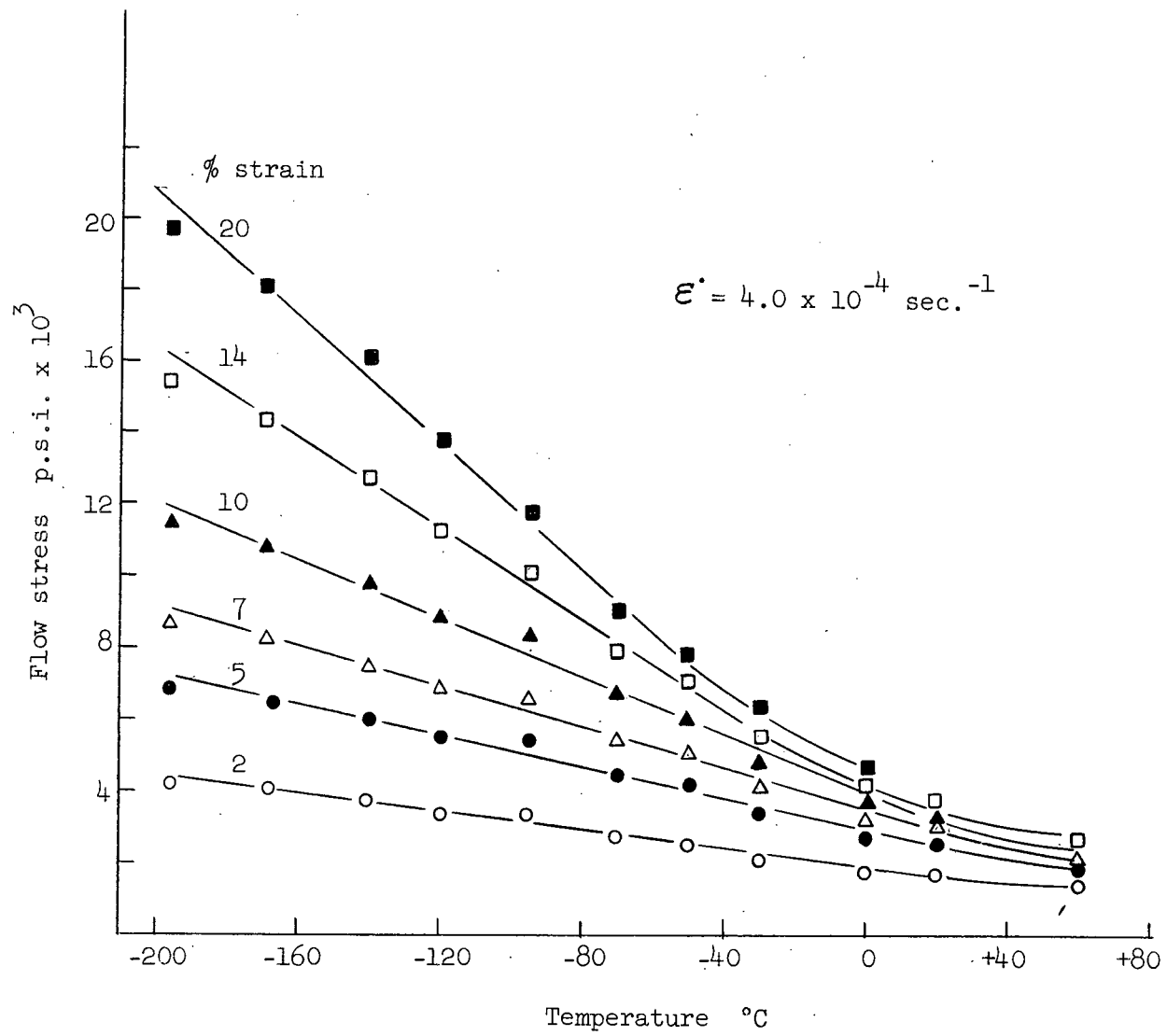


Fig. 35 Flow stress-temperature relationships for 400 $\mu$  cadmium.

It is seen that as opposed to Stoloff's results, the flow stress continues to increase with decreasing temperature down to  $-196^{\circ}\text{C}$ . Until tests can be performed below  $-196^{\circ}\text{C}$  it is not known whether this trend continues.

In order to obtain a more direct comparison of the stress strain relationships, the yield stress was subtracted from the flow stress for each point giving plots of the work hardening parameter ( $\sigma_{\text{flow}} - \sigma_{.1\% \text{ strain}}$ ) vs. temperature. These are shown in Figures 36 and 37. It is seen that in both cases, a region of temperature independent work hardening develops below  $-120^{\circ}\text{C}$  similar to that observed by Russell. With increasing temperature the amount of strain involved decreases. The temperature independent work hardening region covers the same temperature range for both grain sizes. However larger amounts of strain in  $400\mu$  material show temperature independent work hardening than that found for  $25\mu$  (i.e. 14% strain at  $-196^{\circ}\text{C}$  for  $400\mu$  and 7% for  $25\mu$ ).

#### 1.5.2 b) Zinc

Because of the limited ductility of  $400\mu$  zinc, no similar evaluation could be made. However the results obtained for  $20\mu$  zinc are shown in Figures 38 and 39. Temperature independent work hardening is observed below approximately  $-95^{\circ}\text{C}$ . Table 4 shows a comparison between zinc and cadmium of the maximum temperature for this region at the arbitrary value of 1% strain. It is seen that temperature independent work hardening occurs below a common equivalent temperature of  $T_H = .26$  in both systems.

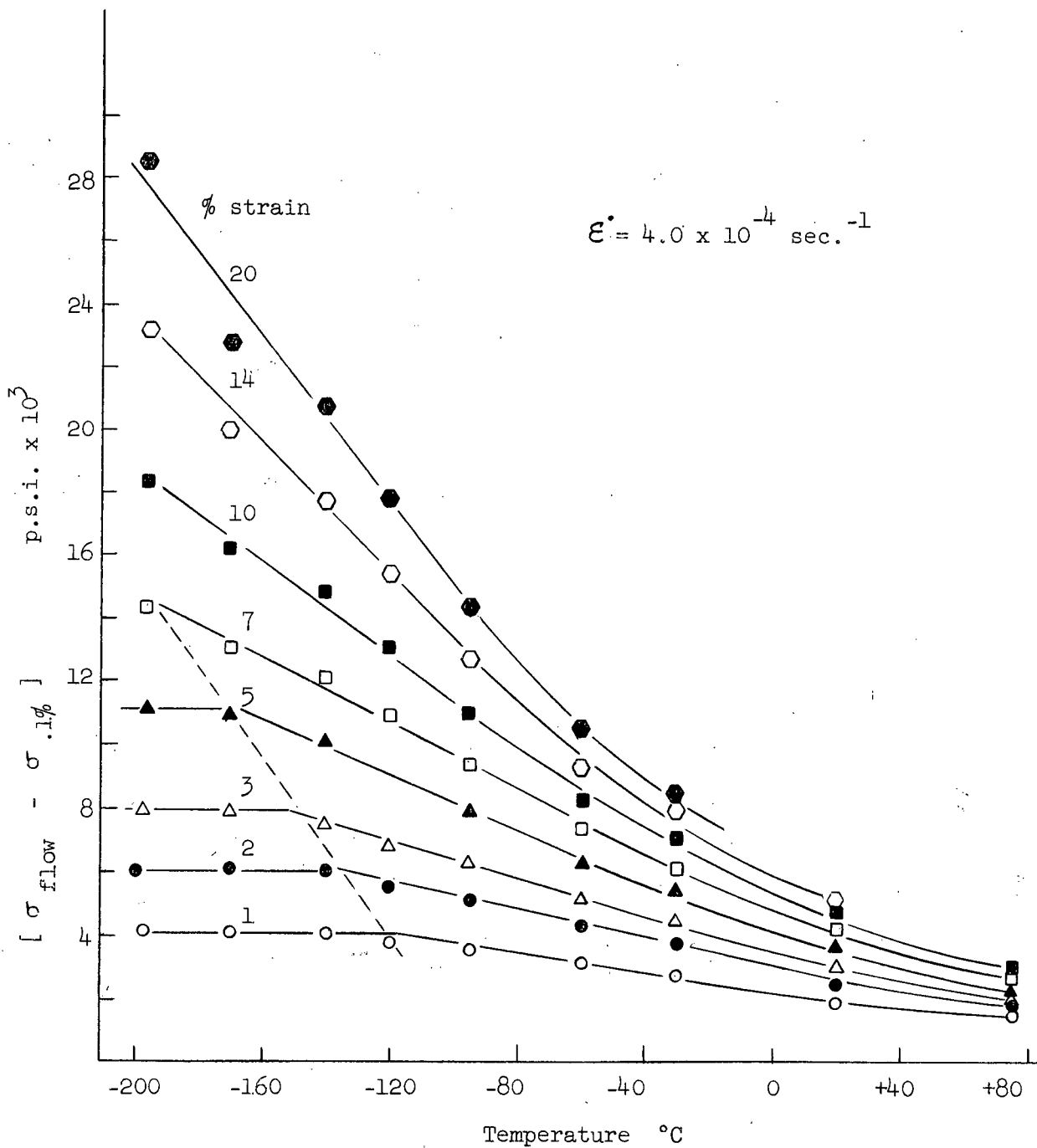


Fig. 36 The variation with temperature of the work hardening parameter in 25μ cadmium.

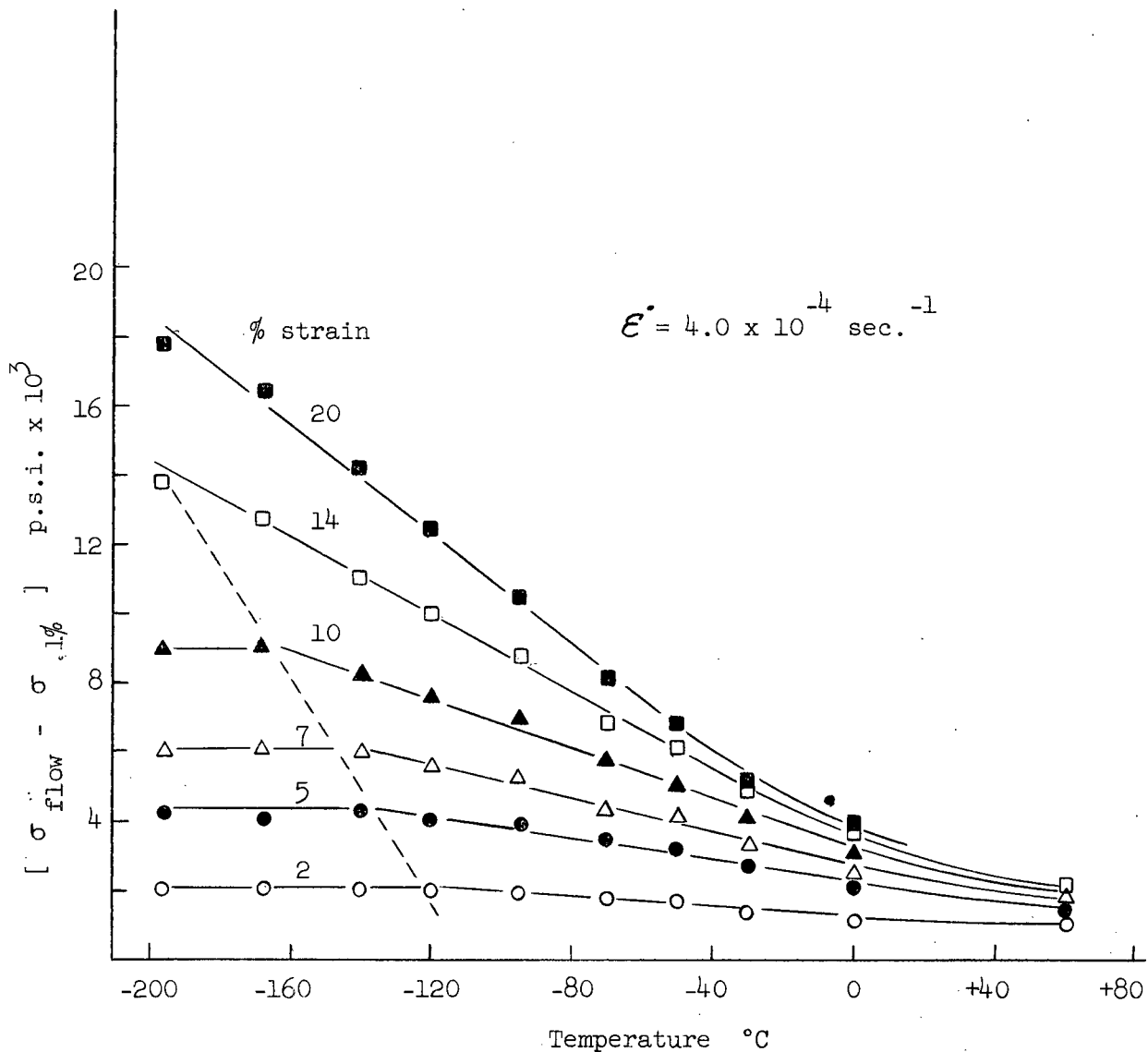


Fig. 37 The variation with temperature of the work hardening parameter in 400μ cadmium.

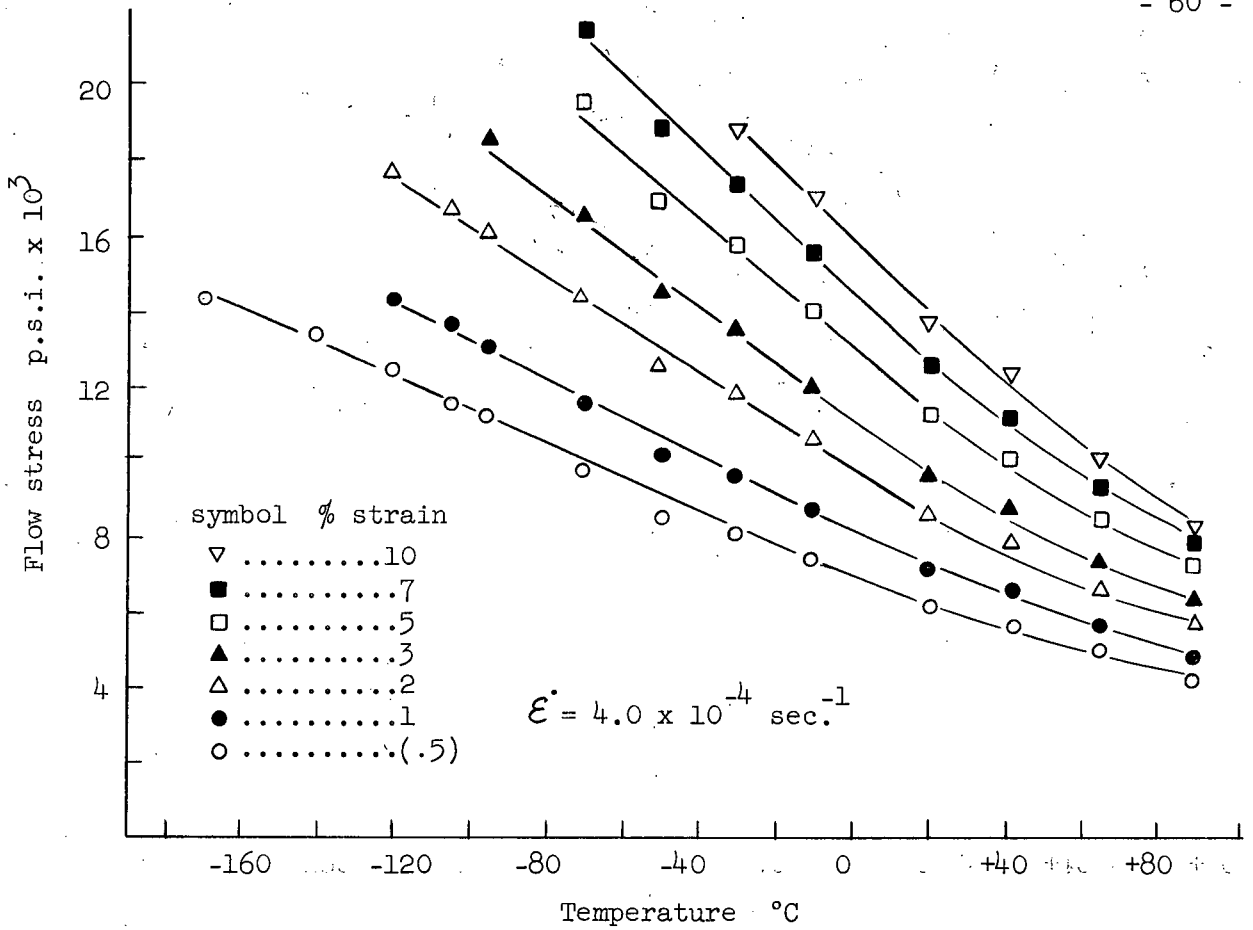


Fig.38 Flow stress-temperature relationships for 20μ zinc.

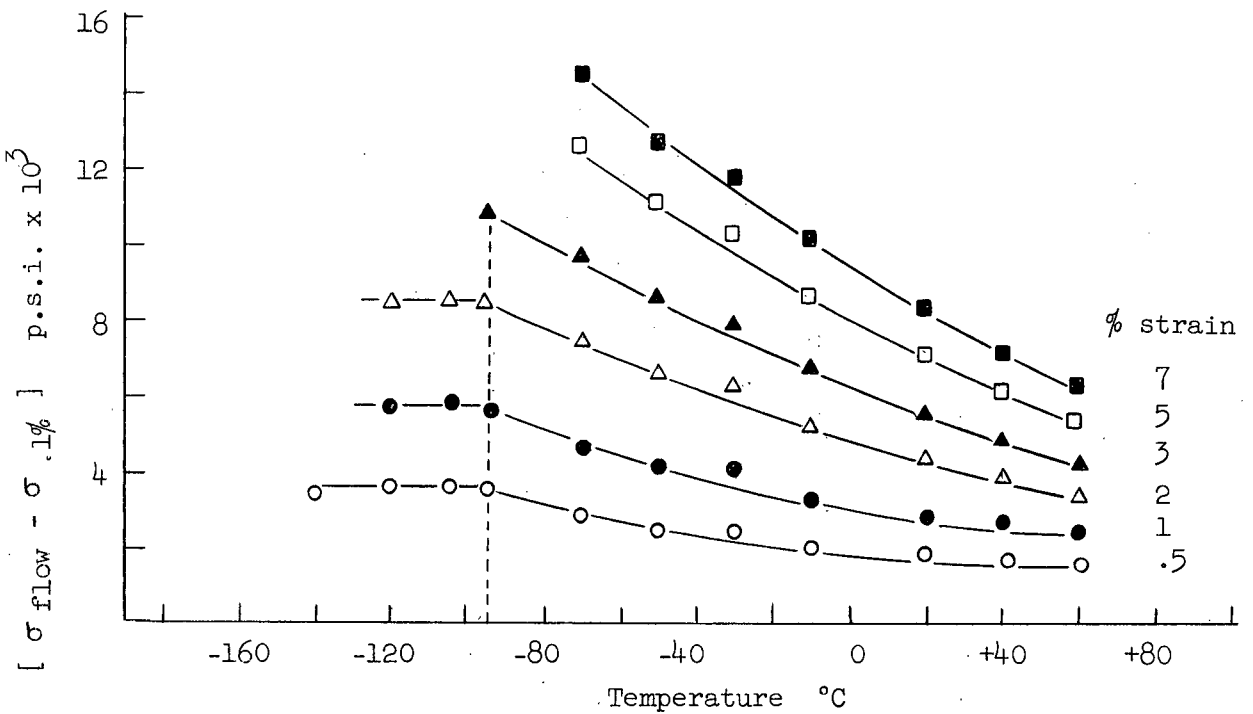


Fig.39 The variation with temperature of the work hardening parameter in 20μ zinc.

The comparison of the work hardening behaviour of zinc and cadmium in the temperature insensitive hardening region is shown in Figure 40. Taking into account the shear modulus of each system, it is seen that the work hardening of fine grained zinc and cadmium is identical. Except for a parabolic region below 1% strain, the hardening is also linear.

TABLE 5

Upper temperature limits for linear hardening in polycrystalline zinc and cadmium

|  | Zinc  | Cadmium |
|--|-------|---------|
| Maximum Temperature for linear hardening | -95°C | -120°C  |
| Maximum Equivalent Temperature<br>$T_H$  | .26   | .26     |

### 1.5.3 Strain Rate Sensitivity of the Flow Stress

The effect of strain rate on the flow stress was investigated for 20 $\mu$  Zn and 25 $\mu$  Cd over the temperature range from -196 to +20°C. Tests were not done with 400 $\mu$  material because of the poorer reproducibility of flow stress values. Five strain rates between  $4.0 \times 10^{-3} \text{ sec}^{-1}$  and  $4.0 \times 10^{-5} \text{ sec}^{-1}$  were used. Linear relationships were obtained for all test conditions between flow stress at constant strain, and the natural logarithm of the strain rate as illustrated for 20 $\mu$  zinc in Figure 41.

$\frac{\Delta\sigma}{\Delta \ln \dot{\epsilon}}$  was chosen as a strain rate parameter and values obtained as a function of strain are shown in Figures 42 and 43 for cadmium and zinc respectively.

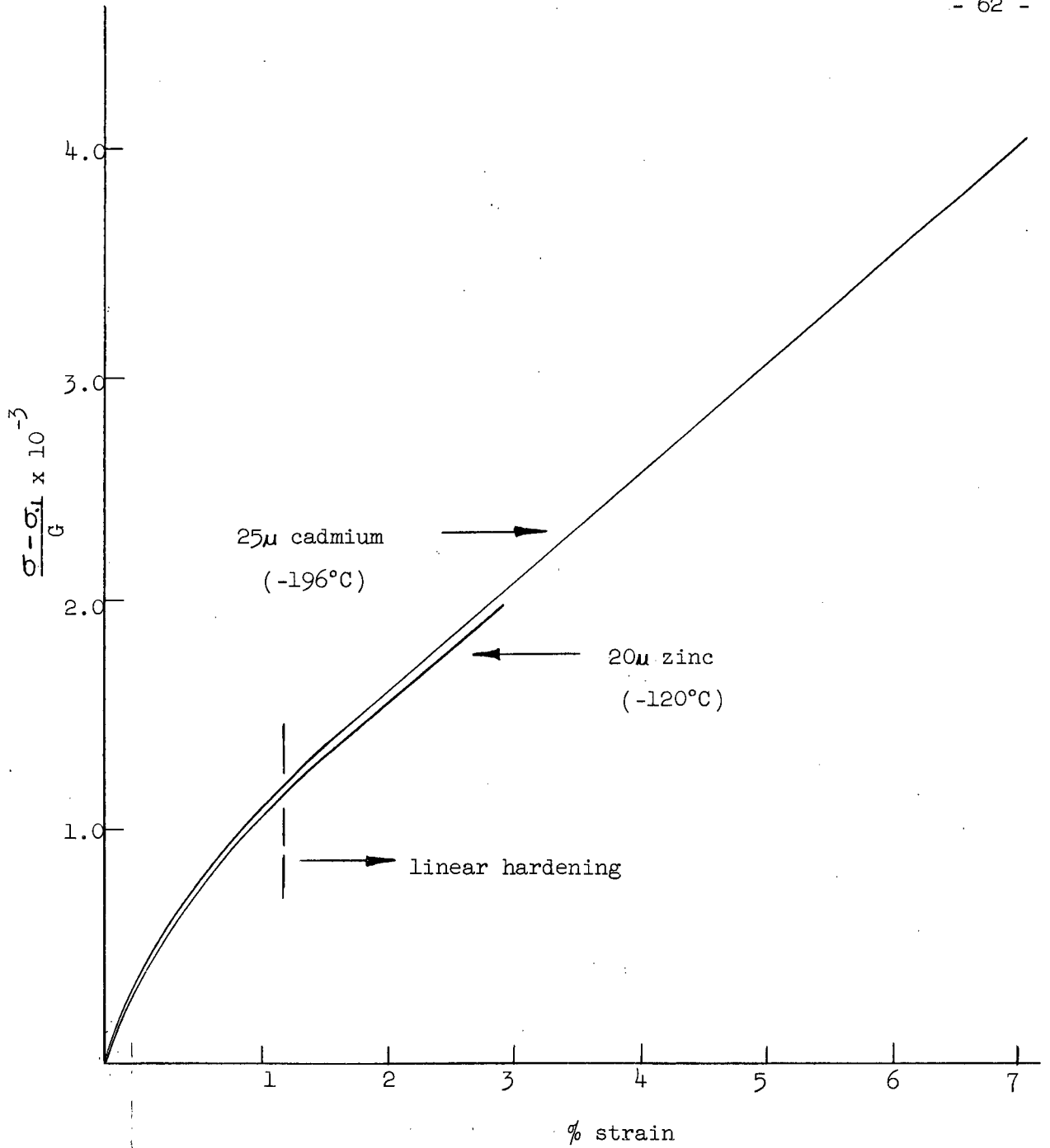


Fig. 40 Linear hardening of polycrystalline zinc and cadmium below  $T_H = .26^\circ$

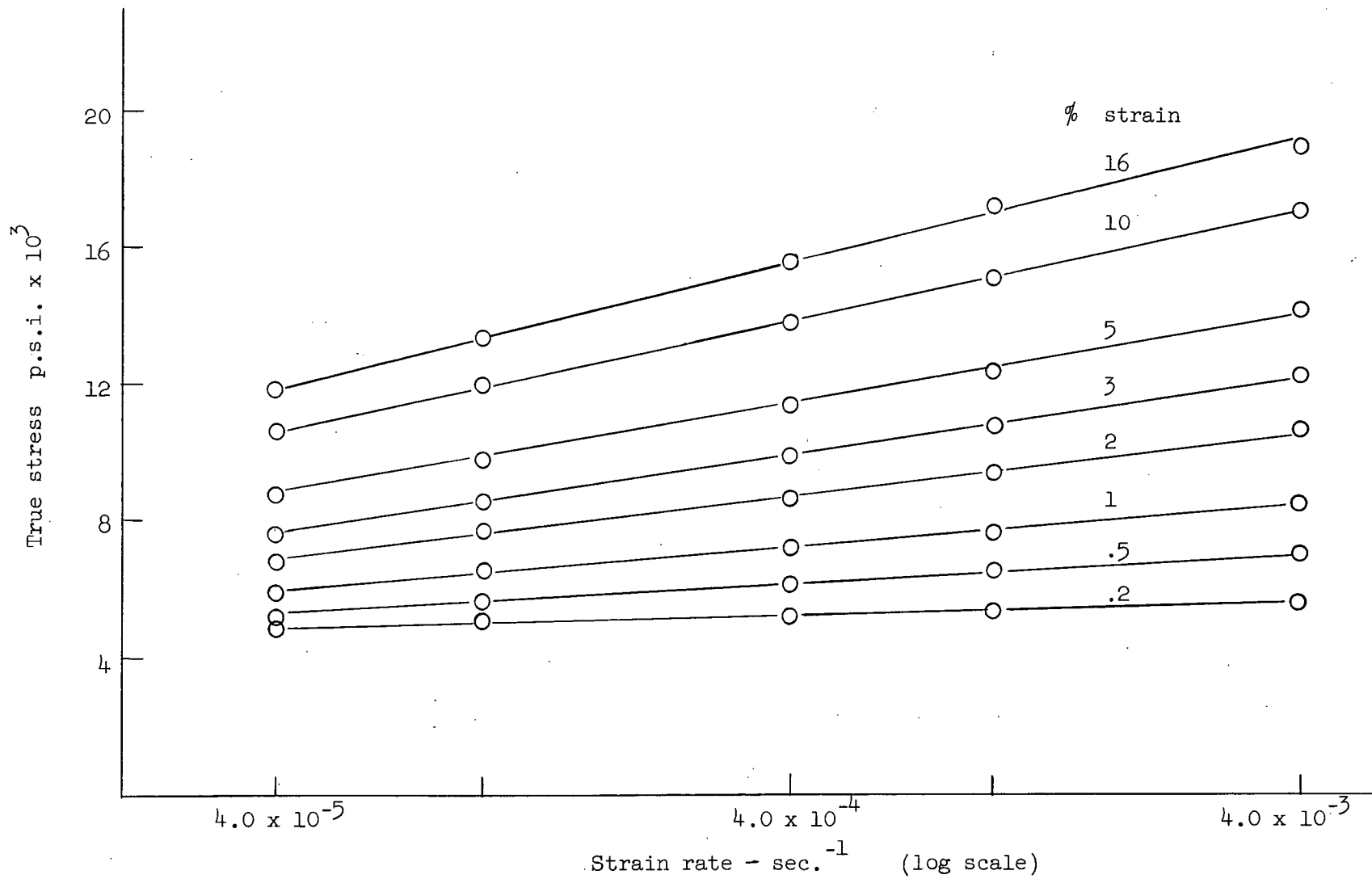


Fig.41 The effect of strain rate on the flow stress of 20μ zinc at +20°C.

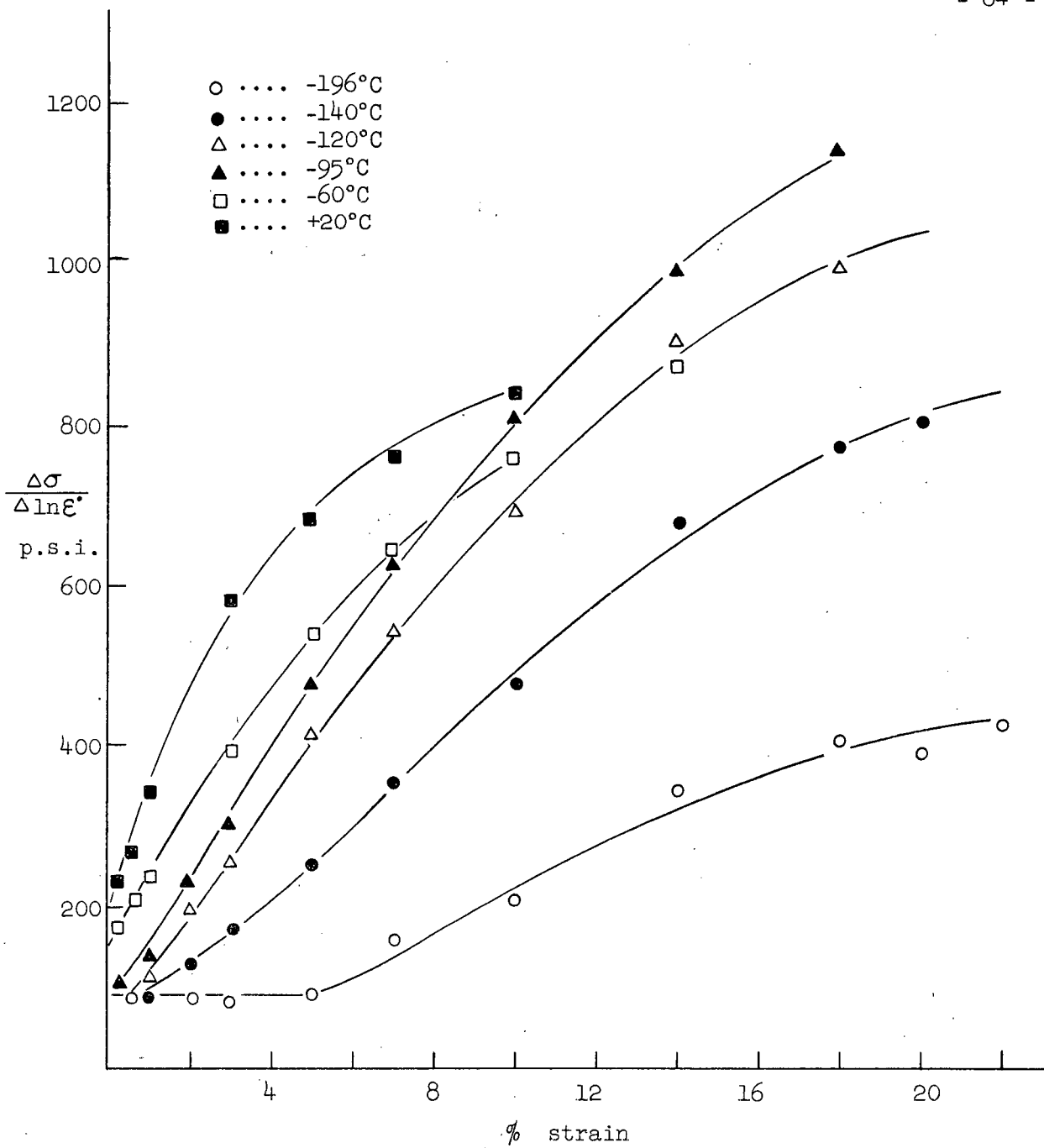


Fig.42 The variation of the strain rate parameter  $\frac{\Delta\sigma}{\Delta \ln \dot{\epsilon}}$  with temperature and strain in 25μ cadmium.

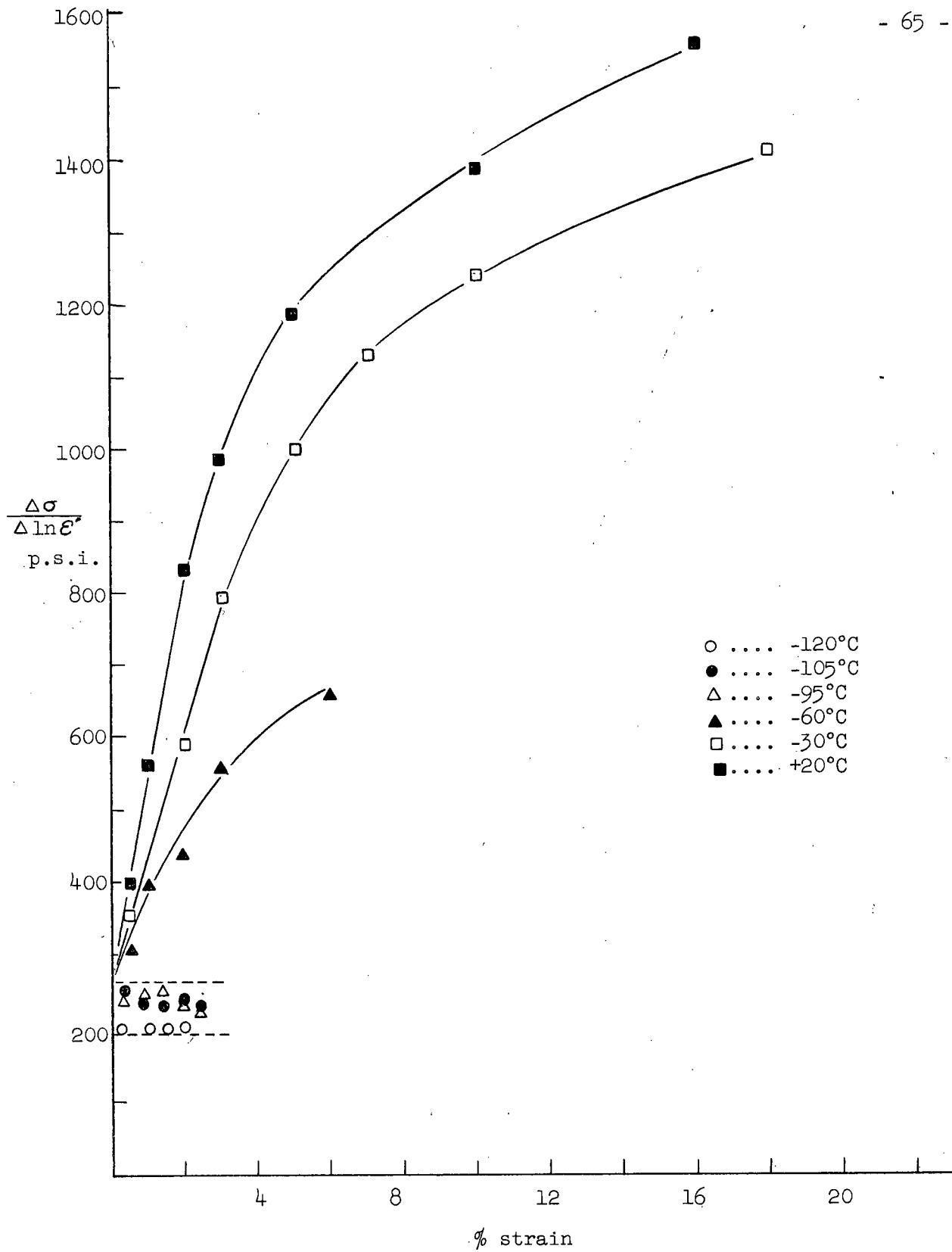


Fig. 43 The variation of the strain rate parameter  $\frac{\Delta\sigma}{\Delta\ln\dot{\epsilon}}$  with temperature and strain in 20μ zinc.

From Figure 42 for 25 $\mu$  cadmium it is seen that at -196°C there is an almost constant value of strain rate sensitivity up to about 6% strain above which the sensitivity increases. This implies a strain rate insensitive rate of work hardening in this region. This region of strain at -196°C is approximately the same that showed temperature insensitivity of the hardening rate.

Between -95°C and -196°C there is a continual increase of sensitivity with increasing temperature and strain. At about -60°C and above however it is seen that, at high values of strain the increase in sensitivity with strain is much less. It is in this region that grain boundary migration is known to occur to a significant degree.

The results for zinc are qualitatively the same (Fig. 43). Below -95°C the strain rate sensitivity does not vary with strain. This again is the same temperature region which gives a temperature independent work hardening rate.

#### 1.5.4 The Deformation of Cadmium Single Crystals

Russell has proposed that the deviations which occur from linear hardening at high values of strain or with increased temperature in copper are due to a dynamic recovery mechanism involving cross slip. He has associated the initial linear hardening region of polycrystals with second stage single crystal hardening. Therefore in order to have a better understanding of the deformation behaviour of cadmium it was decided to undertake some study of single crystal behaviour.

Resolved shear stress-shear strain curves for cadmium single crystals of identical orientations are shown in Figs. 44 and 45. The orientation used was as shown in Fig. 44 with the angle between tensile axis and slip plane and tensile axis and slip direction being  $36^\circ$  and  $38^\circ$  respectively. At  $+20^\circ\text{C}$  a three stage hardening curve was obtained (Fig. 45) in which the initial stage is subdivided into two regions similar to that observed by Seeger<sup>25</sup> in zinc at room temperature. He also postulated that the transition from Stage I to Stage II hardening is due to the establishment of a critical density of immobile dislocation loops due to vacancy condensation.

At  $-50^\circ\text{C}$  and below the nature of the curves is somewhat different (Fig. 44). Stage I was linear at all temperatures down to  $-196^\circ\text{C}$  and did not show the "S" type of hardening observed in magnesium<sup>13</sup>. Of about 20 crystals tested all showed extensive twinning during Stage II. All possible care was taken in order to avoid crystal damage prior to testing and no observable twins were present. Therefore at low temperatures it must be concluded that twinning is a general feature of Stage II hardening. Lally<sup>89</sup> has reached a similar conclusion with respect to magnesium.

An interesting observation is that the resolved shear stress on the basal plane associated with initial twin formation was virtually independent of temperature as shown in Table 6. The shear strain increased with increasing temperature due to the lower rate of work hardening.

Although the maximum rate of hardening during Stage II is a function of the nature and extent of twinning, the transition from Stage I to Stage II cannot be associated with twinning. This follows from the experimental observation that a considerable proportion of the crystal remains untwinned in the transition region. The flow stress is derived

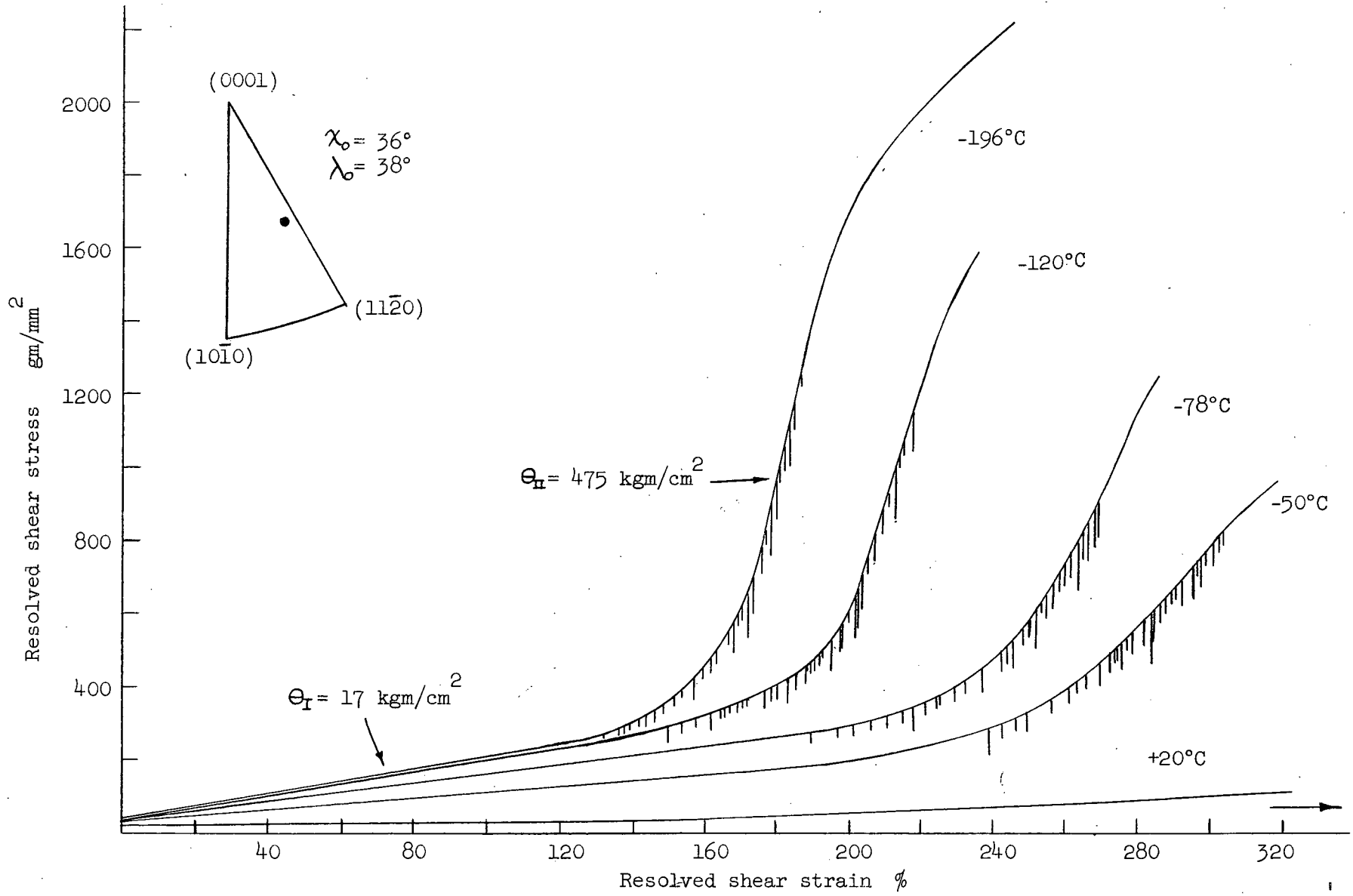


Fig. 44 Stress strain curves for cadmium single crystals at various temperatures

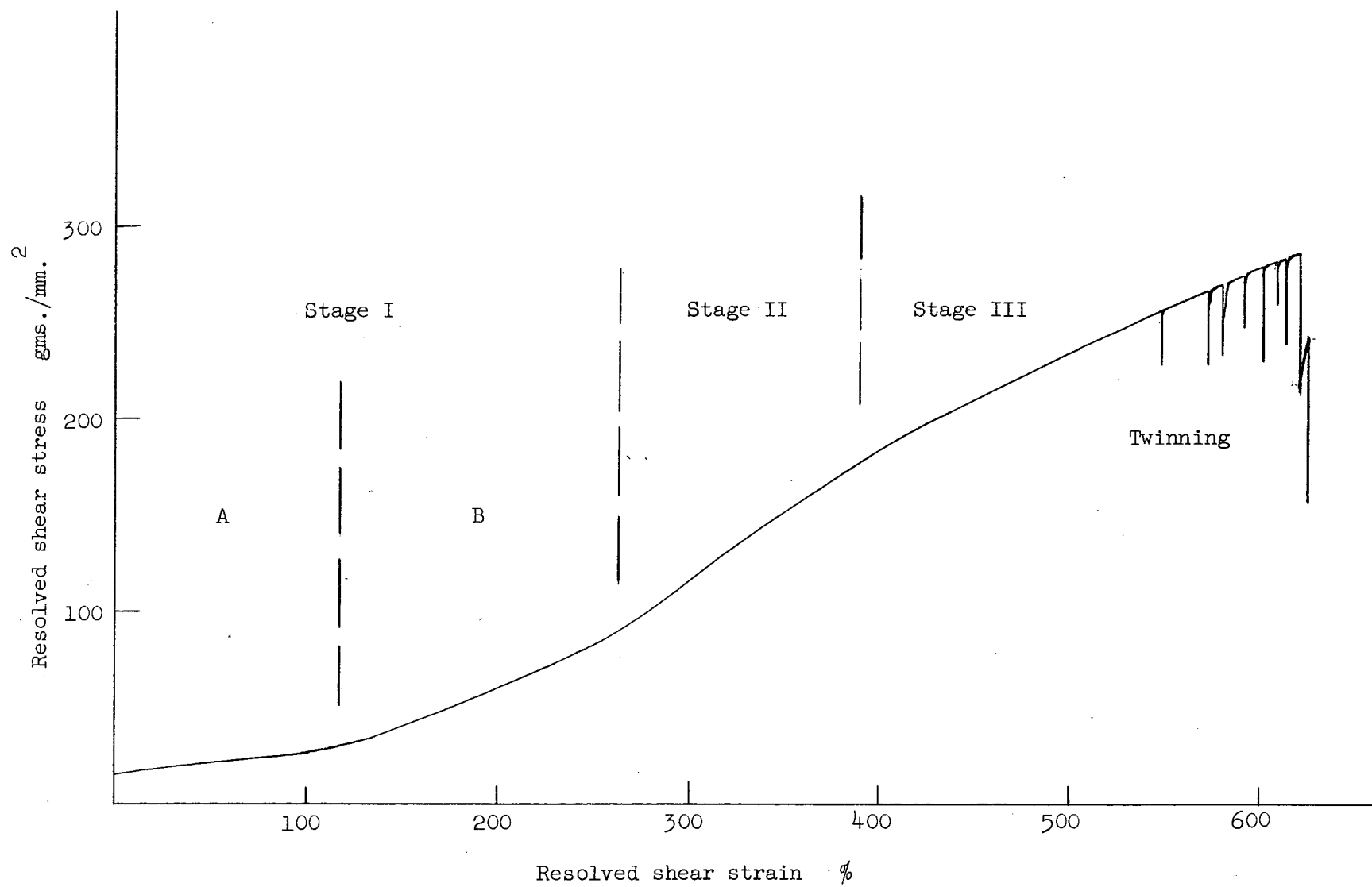


Fig. 45 Single crystal stress strain curve for cadmium at +20°C.

therefore only from the nature of the dislocation configuration in untwinned regions.

Due to the above reasoning it is more accurate to say that it is the stress associated with the end of Stage I which is independent of temperature. Twinning therefore is an "after the fact" consideration.

Somewhat similar observations were made by Lücke, et al.<sup>104</sup> during the deformation of zinc single crystals. They found that the stress associated with the end of Stage I hardening is independent of strain rate at +20°C. The related shear strain increased with decreased strain rates.

TABLE 6

Basal shear stress required for initial twin formation.

| Temperature | Shear stress on basal plane<br>gm/mm <sup>2</sup> | Shear strain<br>% |
|-------------|---|-------------------|
| +20°C       | 260   | 550               |
| -50°C       | 280   | 240               |
| -78°C       | 280   | 190               |
| -120°C      | 285   | 145               |
| -196°C      | 300   | 130               |

No attempt was made to calculate the macroscopic stress on the twinning system. It is known<sup>39</sup> that such calculations produce values that are at least an order of magnitude lower than the stress thought to be required for twin nucleation. It is impossible to estimate with any degree of accuracy the stress at points of stress concentration which is required

for twin nucleation in bulk crystals. However if one assumes a constant relationship between macroscopic shear stress and the value of stress at points of stress concentration it is then possible to predict a temperature independent twinning stress.

#### 1.5.5 Temperature Dependence of Work Hardening

The temperature dependence of the rate of work hardening in Stage I ( $\frac{\Theta_I}{G}$ ) and Stage II ( $\frac{\Theta_{II}}{G}$ ) is shown in Figures 46 and 47. It is seen that below  $-120^\circ\text{C}$  the work hardening rates are constant. Above this temperature for both hardening regions the rate of hardening decreases. Fahrenhorst and Schmid<sup>62</sup>, and Seeger and Trauble<sup>25</sup> have found similar relationships for Stage I hardening of zinc. The data of Seeger after normalizing for shear modulus changes is compared with that obtained during this study of cadmium in Figure 48. It is seen that the drop in the hardening rates occurs at the same equivalent temperature of  $T_H = .26$  in both systems. This is the same temperature below which temperature and strain rate insensitive hardening began in polycrystalline zinc and cadmium. If this decrease in hardening rate is associated with some dynamic recovery mechanism it would appear that such a mechanism is similar in both polycrystals and single crystals.

From Figure 48 it is also noted that this work hardening transition region has an upper temperature limit of about  $T_H = .40$  in both systems.

#### 1.5.6 The Grain Size Dependence of Hardening at $-196^\circ\text{C}$

Clarebrough<sup>2</sup> and Hargreaves have attempted an analysis of the similarities of Stage II hardening of f.c.c. single crystals and the initial deformation characteristics of polycrystals. This was based to a large

extent on the results of Feltham and Meakin<sup>3</sup> who observed a linear hardening region during the early regions of strain associated with the deformation of polycrystalline copper. They also observed that the magnitude of the polycrystalline linear hardening rate was comparable to that of Stage II hardening. There was therefore no appreciable effect of grain size on the work hardening rate. Similar conclusions were reached by Russell<sup>4</sup> who also correlated the stress at the end of polycrystalline hardening to that at the end of Stage II single crystal hardening. Parabolic hardening as opposed to linear hardening, occurs in f.c.c. polycrystals therefore, due to the action of cross slip in a similar manner to single crystals.

In order to test this concept, cadmium of 5 grain sizes was tested at  $-196^{\circ}\text{C}$ . Since the specimen dimensions were held constant it was thought that any consistent trend towards single crystal data might be observed.

Due to the extensive twinning during 2nd stage single crystal deformation at  $-196^{\circ}\text{C}$  the meaning of the resolved shear stress on the basal planes is clouded. Therefore for comparison with polycrystalline material it was decided to merely report the single crystal Stage II hardening in terms of the tensile hardening rate. This also avoids the difficulty associated with assigning some average shear stress value for polycrystals.

The polycrystalline stress strain curves obtained are shown in Figure 49. It is seen that with increasing grain size a two stage hardening curve gradually appears. Since it was desired to compare the 2nd stage hardening, the maximum hardening rate was used in all cases as shown. With decreasing grain size the region of linear hardening decreased to smaller

values of strain.

The comparison of hardening rates is made by a  $d^{-\frac{1}{2}}$  plot as shown in Fig. 50. It is seen that the rate of hardening varies linearly with  $d^{-\frac{1}{2}}$  and extrapolates to the single crystal value at  $d^{-\frac{1}{2}} = 0$ . There is an increase by a factor of about 3 in the hardening rate from the single crystal value to 25 $\mu$  material. Since all crystals are twinned to about the same degree, this increase reflects the nature of the hardening change with increasing grain boundary area per unit volume and decreasing proportion of grains with a free surface. Since no pyramidal slip was observed in single crystals and an increasing amount occurs in polycrystals as the grain size decreases, the increased hardening rate can be explained in terms of a gradual change in the nature and extent of the deformation mechanisms. However in copper single crystal and polycrystal hardening rates can be compared directly because the deformation mechanisms do not change with grain size.

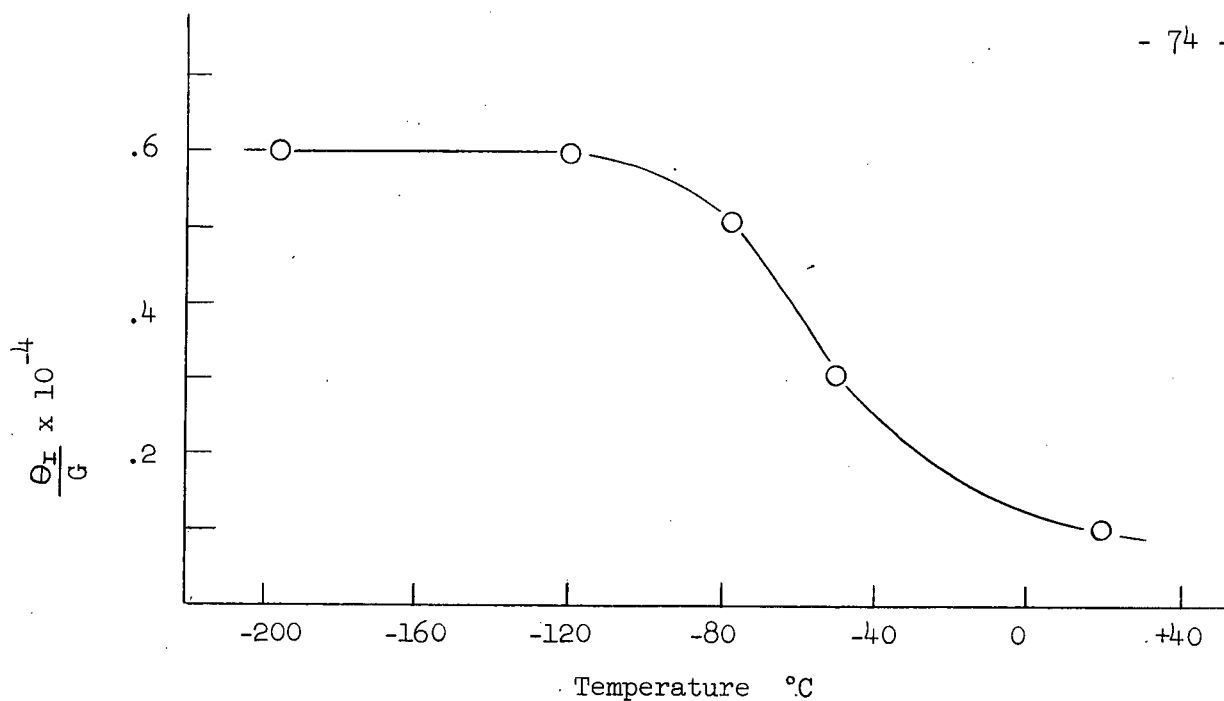


Fig. 46 The temperature dependence of stage I hardening in cadmium.

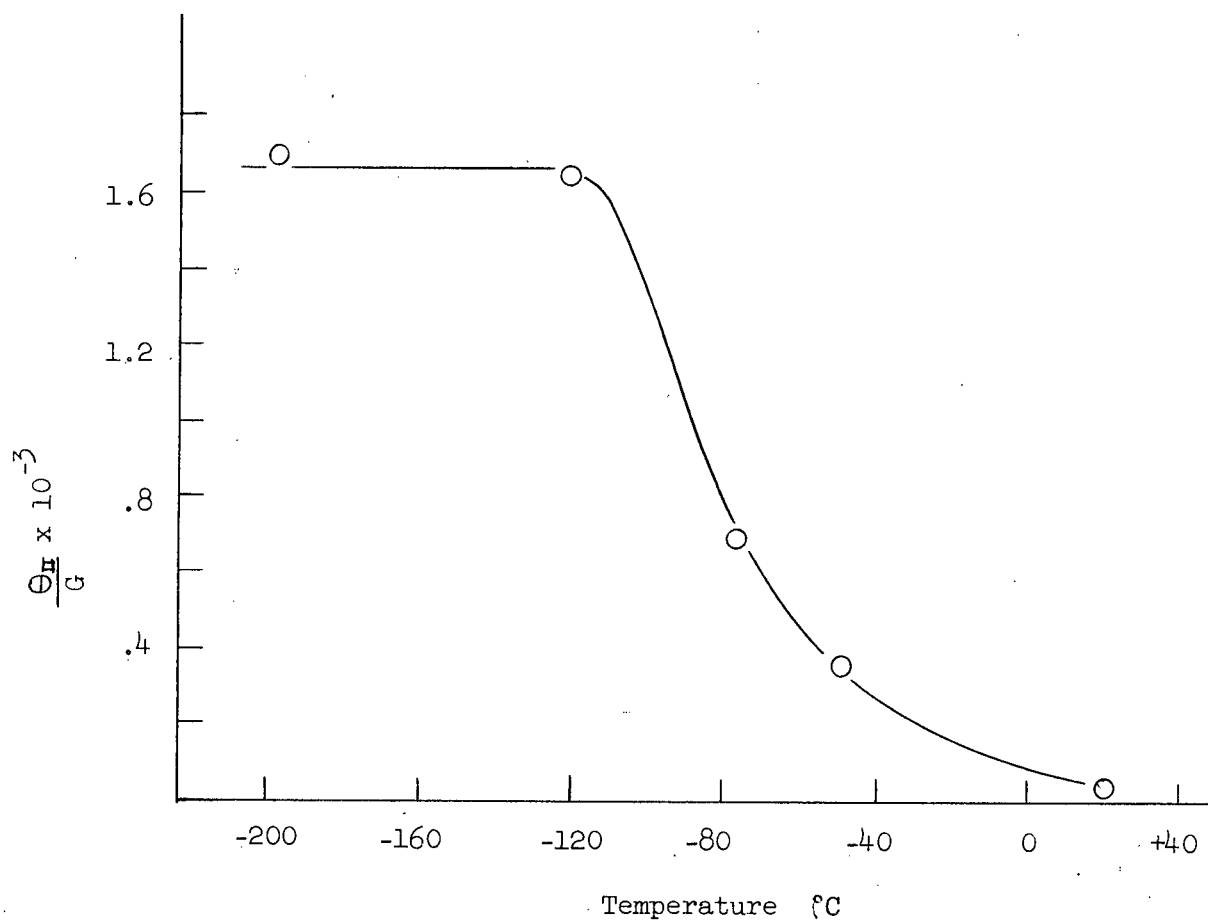


Fig. 47 The temperature dependence of stage II hardening in cadmium.

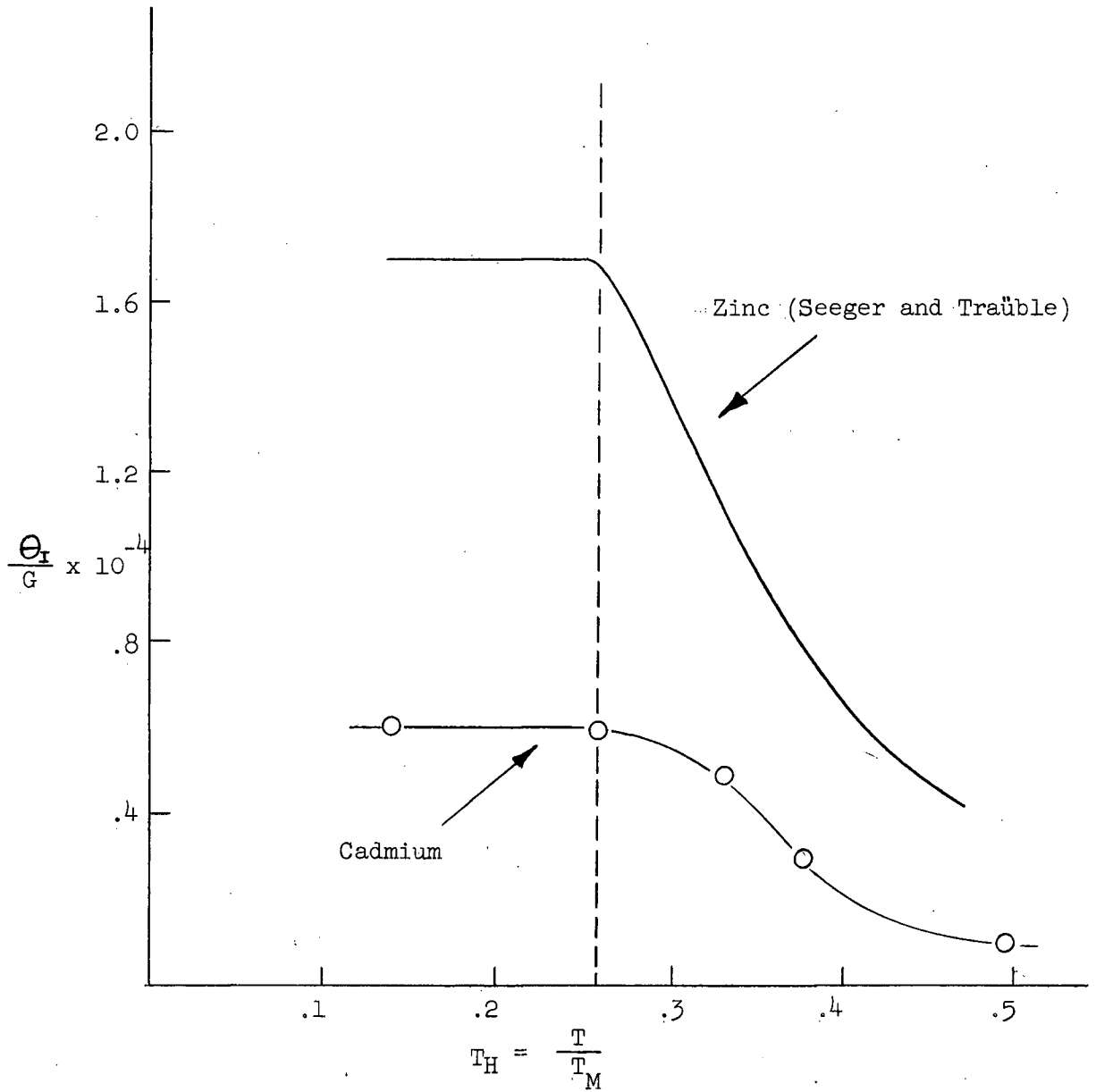


Fig. 48 Temperature dependence of the rate of work hardening during Stage I deformation

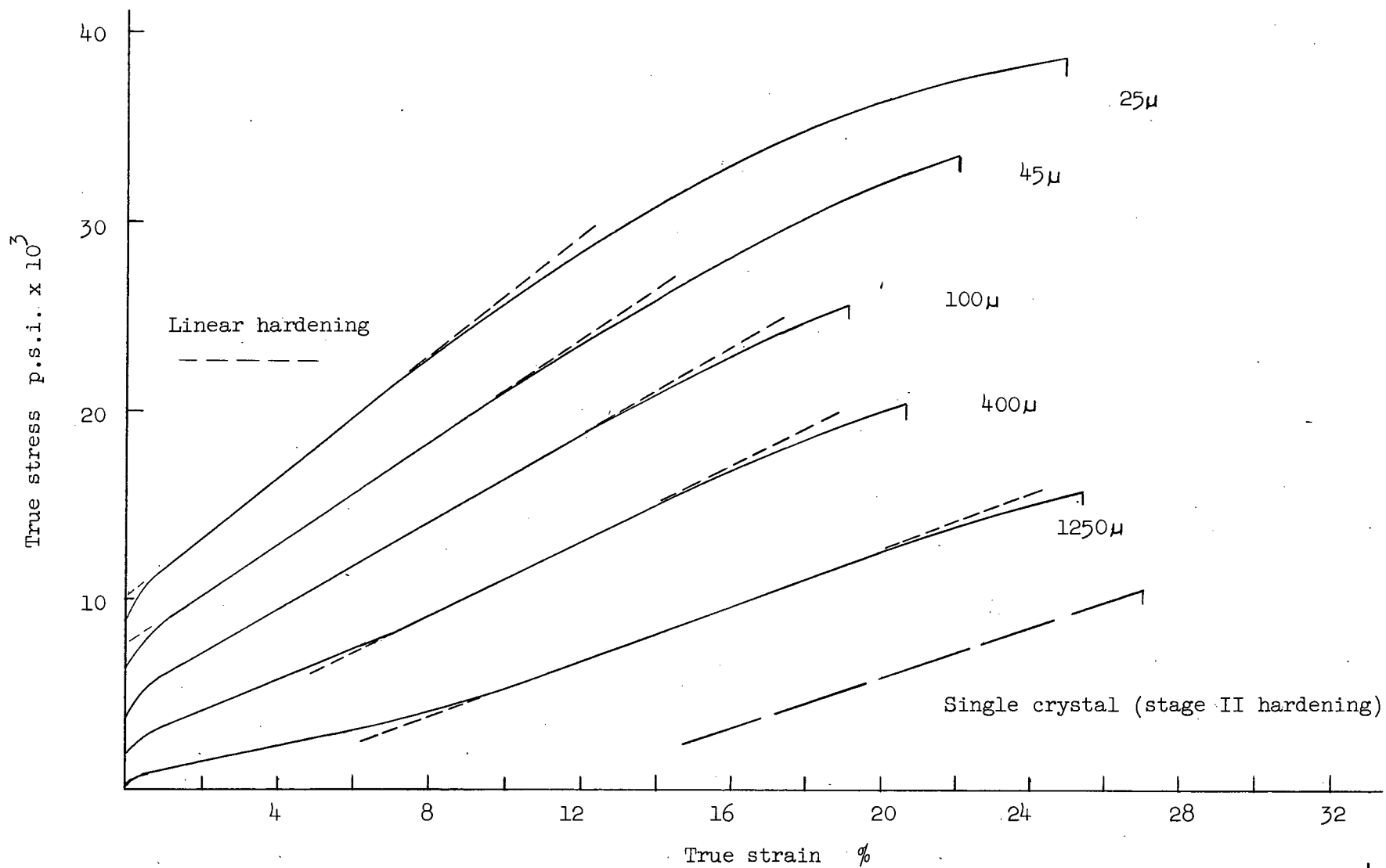


Fig. 49 Stress-strain curves for cadmium of various grain sizes at -196°C.

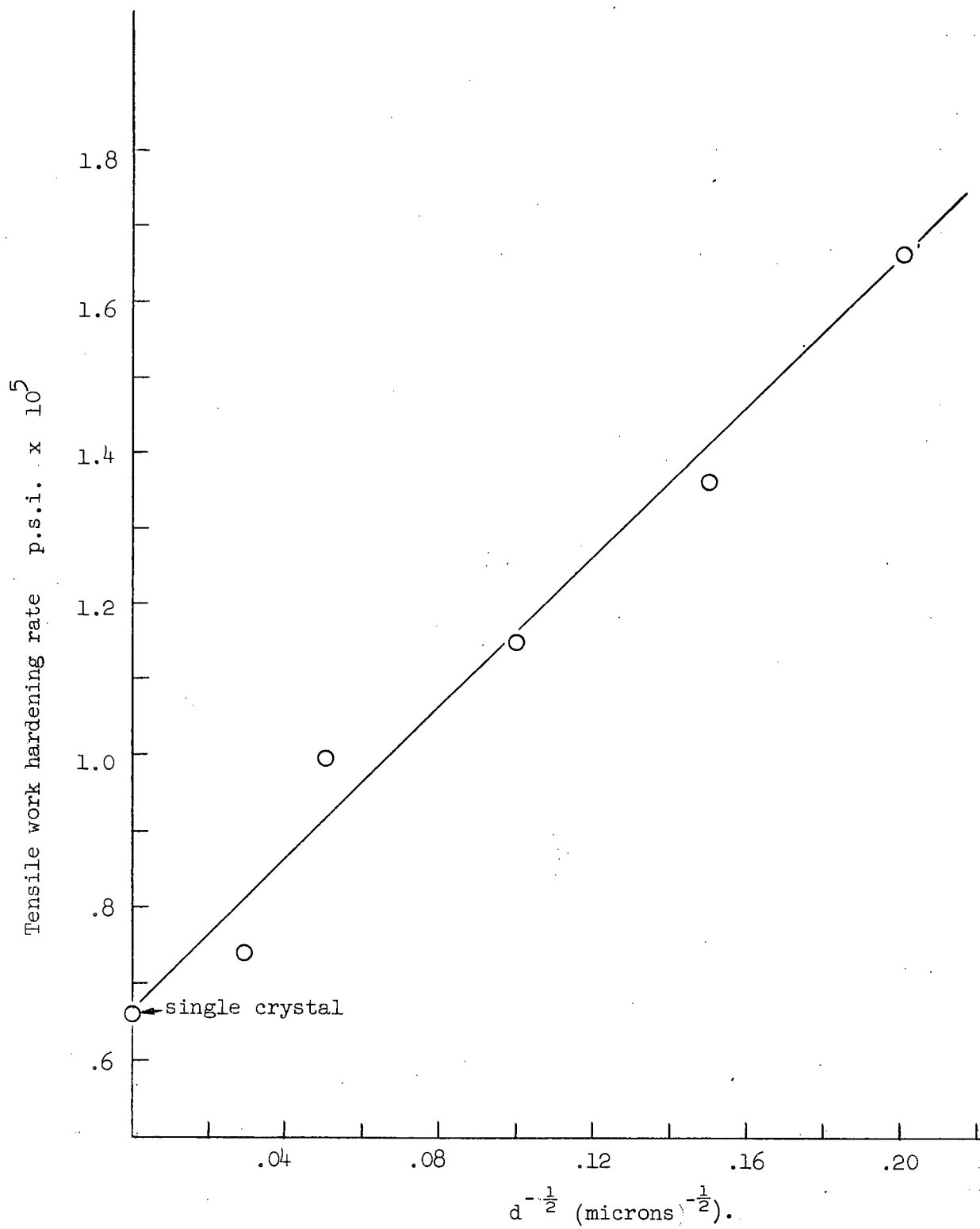


Fig. 50 The effect of grain size on the rate of linear hardening of cadmium at -196°C.

PART II

2. MECHANISMS OF HARDENING IN ZINC AND CADMIUM

2.1 INTRODUCTION

Many techniques have been used in recent years in an effort to evaluate the hardening mechanisms that control deformation. Some of the more prominent include the use of transmission electron microscopy, the study of Cottrell-Stokes Law obedience, and the application of rate theory to determine the rate controlling mechanisms. All have their limitations depending upon experimental procedures and theoretical assumptions.

Although transmission microscopy techniques have proven to be valuable in observing dislocation motion and behaviour, considerable difficulty is encountered in preparing specimens which truly represent bulk samples<sup>66,67</sup>.

Several authors have made detailed studies of the Cottrell-Stokes Law<sup>6,11-13,68-72</sup>. However there is considerable controversy as to the exact meaning of Cottrell-Stokes obedience.

The application of rate theory to deformation processes has been plagued by a multitude of formulations<sup>11,73-78</sup> all of which require certain simplifying assumptions to arrive at mathematical expressions which may be easily used to interpret experimental data.

Seeger<sup>79</sup> originally postulated that the applied stress could be considered as the sum of two components such that

$$\tau_a = \tau_G + \tau^* \dots\dots\dots(1)$$

where  $\tau^*$  is associated with short range obstacles which can be

overcome with the aid of thermal energy ( forest dislocations). Therefore it may be referred to as the thermal component of the applied stress.

and  $\tau_G$  is the athermal component of stress which arises due to long range elastic interactions such as those between parallel glide dislocations at distances large compared with "b". Such obstacles cannot be overcome with the aid of thermal energy.

The temperature dependence of yield as postulated by Seeger when the mechanism of yield does not change with temperature, is shown in Fig. 51. The internal stress  $\tau_G$  varies with temperature only through a change in the shear modulus. The increase in  $\tau_a$  below the critical temperature reflects the decrease in the amount of thermal energy available and subsequently the increased effective stress necessary for activation.

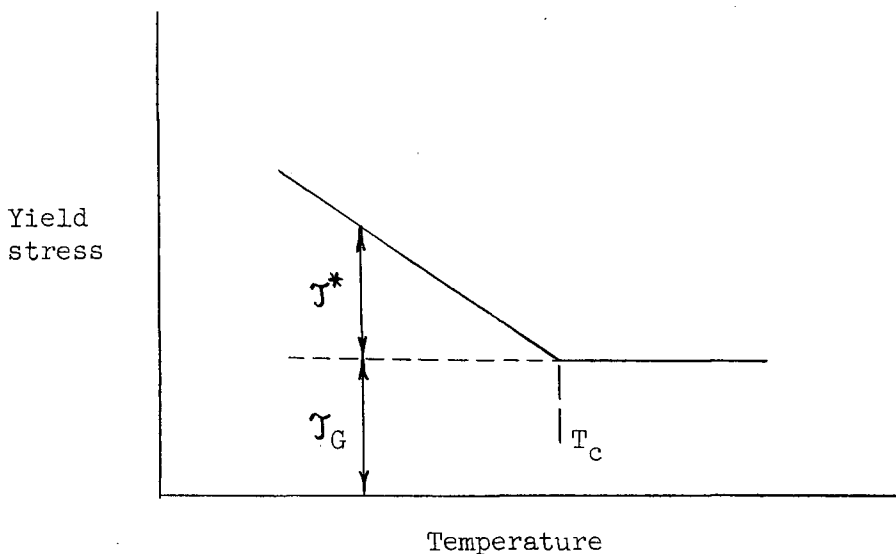


Fig. 51 The temperature dependence of yield in terms of the stress components (after Seeger).

Much of the work in deformation in recent years has been concerned with obtaining a better knowledge of the nature and origin of the stress components in various systems.

Basinski<sup>17</sup> postulated that because of Cottrell-Stokes obeyance in certain f.c.c. metals, the two components  $\tau_G$  and  $\tau^*$  arise from a single source ( the interaction of glide and forest dislocations ). Seeger<sup>66</sup> has since modified his original definition of  $\tau_G$  to include a short range elastic interaction term . However he maintains that a major portion of the flow stress of single crystals is still derived from long range interactions between parallel dislocations (Fig.52 ).

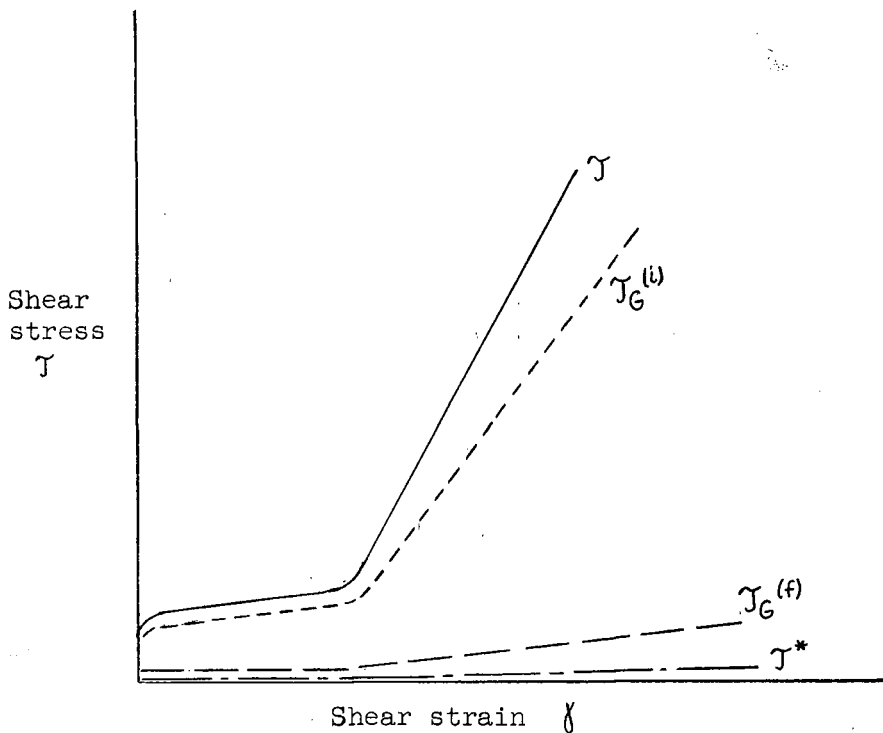


Fig.52 The components of the total flow stress in f.c.c. crystals.  
 $\tau_G^{(i)}$  = contribution of the long range internal stress  
 $\tau_G^{(f)}$  = elastic interaction between glide and forest dislocations  
 $\tau^*$  = thermal component of the stress (effective stress)

In the only consistent study to date, Mitra and Dorn have with the aid of rate theory separated the two components of the athermal stress in aluminum and copper single crystals. It would appear that short range elastic stresses as proposed by Basinski account for a greater proportion of the

total flow stress than has been indicated by Seeger.

In 1954 Cottrell and Stokes using aluminum single crystals found that the reversible change in flow stress ( $\Delta\tau^*$ ) during a temperature change test was directly proportional to the total flow stress and that the value of  $\frac{\Delta\tau^*}{\tau}$  was not only independent of strain but also of the prior thermal and mechanical history. Cottrell-Stokes obeyance occurs therefore when with increasing strain

$$\frac{\Delta\tau^*}{\tau} = \frac{\tau_{T_1} - \tau_{T_2}}{\tau_{T_1}} = 1 - \frac{\tau_{T_2}}{\tau_{T_1}} = \text{a constant} \dots (2)$$

Cottrell also recognized that when two identical specimens are deformed to the same strain at different temperatures, the total flow stress difference is made up of a reversible component due to the different amount of thermal energy available and an irreversible component due to the different dislocation configurations produced at the different temperatures (Fig. 53).

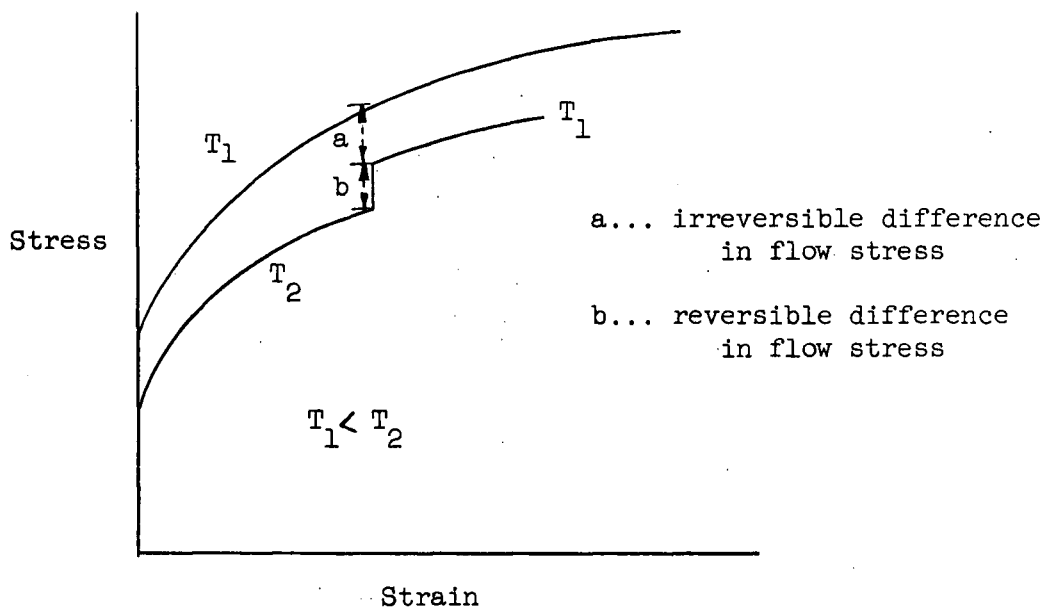


Fig. 53 Components of the difference in flow stress when two identical specimens are deformed at different temperatures.

Cottrell-Stokes obeyance has been interpreted<sup>69</sup> to mean that the type of dislocation configuration must remain constant during deformation with only the scale changing. Obeyance has also been shown to require that a constant proportionality exists between  $\tau_c$  and  $\tau^*$  during deformation.<sup>78</sup>

<sup>78</sup> Basinski showed that a Cottrell-Stokes test could be carried out at a constant temperature by periodically varying the strain rate and that such tests might be more accurate in that they eliminate some of the difficulties associated with temperature change tests ( the necessity of stopping the test to change temperature and the difficulty in defining flow stress due to yield point effects ).

The origin of  $\tau^*$  the thermal component may be due to a number of processes all of which can be thermally activated. Therefore rate theory has been used in an attempt to establish the rate controlling process for various systems. Since  $\tau^*$  is the stress associated with thermal activation, studies of the strain rate and temperature dependence of  $\tau^*$  can be carried out in order to determine such rate parameters as activation energy, activation volume and activation distance. By comparing experimental values with those theoretically predicted, it is sometimes possible to postulate the rate controlling mechanism. Mechanisms that can be thermally activated and therefore rate controlling include the following:

- 1) cross slip
- 2) forest intersection
- 3) the non conservative motion of jogs in screw dislocations
- 4) climb
- 5) overcoming of the Peierls stress

If a single activation process is rate controlling over a certain temperature range then the strain rate associated with deformation may be expressed as

$$\dot{\gamma} = \dot{\gamma}_0 e^{-\Delta G/kT} \dots\dots\dots (3)$$

$$\dot{\gamma} = N A b v e^{-\Delta G/kT} \dots\dots\dots (4)$$

where

- N = number of sites per unit volume where activation occurs
- A = area swept out per successful activation event
- b = Burgers vector
- v = frequency with which barrier is attempted
- G = Gibbs free energy of activation

The development of equation 3 to give useful mathematical expressions is outlined in Appendix I. The relationships to be used in the present work include the following:

Activation volume  $v = bdl \dots\dots\dots (5)$

$$= kT \left( \frac{\partial \ln \dot{\gamma}/\dot{\gamma}_0}{\partial \tau^*} \right)_T \dots\dots\dots (6)$$

$$= 2kT \left( \frac{\Delta \ln \dot{\epsilon}/\dot{\epsilon}_0}{\Delta \sigma^*} \right)_T \dots\dots\dots (7)$$

Activation enthalpy  $\Delta H = -kT^2 \left( \frac{\partial \ln \dot{\gamma}/\dot{\gamma}_0}{\partial \tau^*} \right)_T \left( \frac{\partial \tau^*}{\partial T} \right)_{\dot{\gamma}/\dot{\gamma}_0} \dots\dots (8)$

$$= -\frac{vT}{2} \left( \frac{\Delta \sigma^*}{\Delta T} \right)_{\dot{\epsilon}/\dot{\epsilon}_0} \dots\dots\dots (9)$$

Thermal component of the activation energy

$$= \Delta G = \Delta H - T \Delta S \dots\dots\dots(10)$$

$$= \frac{\Delta H + \frac{\gamma^*}{\mu \cdot l} \frac{\partial \mu}{\partial T} T v}{1 - \frac{T}{\mu} \frac{\partial \mu}{\partial T}} \dots\dots\dots(11)$$

$$\text{Apparent activation energy} = \Delta G_0 = \Delta G + v \gamma^* \dots\dots\dots(12)$$

where

- d = activation distance
- l = dislocation length involved in thermal activation
- $\dot{\gamma}$  = shear strain rate
- $\dot{\epsilon}$  = tensile strain rate
- $\gamma$  = shear stress
- $\sigma$  = tensile stress
- $\mu$  = shear modulus
- $\Delta S$  = entropy change during thermal activation

It has been assumed that the shear stress in polycrystals can be approximated by taking one-half of the tensile stress. Such an approximation will not affect the calculated values of  $\Delta H$ ,  $\Delta G$ , or  $\Delta G_0$  since the conversion must be made in both numerator and denominator. It will however affect the values of the activation volume in that  $\gamma^*$  appears in the denominator of expression 6. This will be discussed in more detail later.

## 2.2. TEMPERATURE CHANGE TESTS

Temperature change tests were undertaken not only to check the validity of the Cottrell-Stokes law but also to obtain a better knowledge of the effect of prestrain at elevated temperatures on the subsequent deformation behaviour at low temperatures.

### 2.2.1. Procedure

In cadmium  $-196^{\circ}\text{C}$  was used as a base temperature while the upper cycling temperature varied from  $-140^{\circ}\text{C}$  to  $-30^{\circ}\text{C}$ . Strain increments between 1.5% and 2.0% were used at each temperature. After deformation at the upper temperature, the specimens were cooled to  $-196^{\circ}\text{C}$  as rapidly as possible in order to minimize recovery effects. This cooling could usually be accomplished within 30 seconds. During the temperature change operation, the load was maintained at about 20% of the flow stress. Since static recovery is negligible at  $-196^{\circ}\text{C}$ , the specimens were held for 15 minutes prior to resumption of testing in order to equilibrate the testing device.  $\Delta\sigma^*$  values could not be obtained during an increase in temperature due to recovery during the time necessary for temperature equilibration.

Because of the limited ductility of zinc, the Cottrell-Stokes law for temperature change tests could not be investigated. Therefore tests were limited to prestraining 20 $\mu$  zinc to a given value of strain at some elevated temperature between  $+20^{\circ}\text{C}$  and  $-95^{\circ}\text{C}$  and subsequently deforming the specimen to fracture at  $-120^{\circ}\text{C}$ .

### 2.2.2. Cottrell-Stokes Tests

For the various temperature change tests on 25 $\mu$  and 400 $\mu$  cadmium, the  $\Delta\sigma^*$  values obtained were corrected to take into account the change in

$\Delta\sigma$  due to the temperature dependence of the shear modulus. Shear modulus values were obtained from the work of Koster<sup>57</sup>.

The  $\Delta\sigma^*$  values were then normalized to  $\frac{\Delta\sigma^*}{\Delta T}$  in order to give values of the reversible change in flow stress per °K. When these are examined in terms of the flow stress at the standard temperature of -196°C, Cottrell-Stokes plots as shown in Fig. 54 are obtained.

It is observed from Fig. 54 that the Cottrell-Stokes law is not strictly obeyed for temperature change tests.  $\frac{\Delta\sigma^*}{\sigma_{77} \Delta T}$  values decrease slightly during the early stages of deformation and increase again at higher values of  $\sigma_{77}$ . This is true for both grain sizes. The dotted lines indicate ideal Cottrell-Stokes obedience.

From Fig. 54 it is also noted that the experimental value of  $\frac{\Delta\sigma^*}{\Delta T}$  at a given value of flow stress at -196°C is independent of the upper cycling temperature. This is true for both grain sizes although the values of  $\frac{\Delta\sigma^*}{\sigma_{77} \Delta T}$  are considerably lower for 400 $\mu$  material.

The results of the temperature change tests are therefore very similar to those reported by Bullen et al for polycrystalline copper deformed between 173°K and 373°K and subsequently deformed at 77°K<sup>58,59,60</sup>. They noted a deviation from ideal Cottrell-Stokes behaviour at high values of stress which gave increased values of  $\frac{\Delta\sigma^*}{\sigma_{77} \Delta T}$ . They also found values of  $\frac{\Delta\sigma^*}{\Delta T}$  which at a given value of stress at 77°K were independent of the upper cycling temperature between 173°K and 373°K. They therefore concluded that the same sequence of "obstacle" formation occurs during deformation independent of the temperature but that the rate of obstacle production with increasing strain may be temperature dependent due to the removal of obstacles by some process of dynamic recovery. They made no attempt to identify the

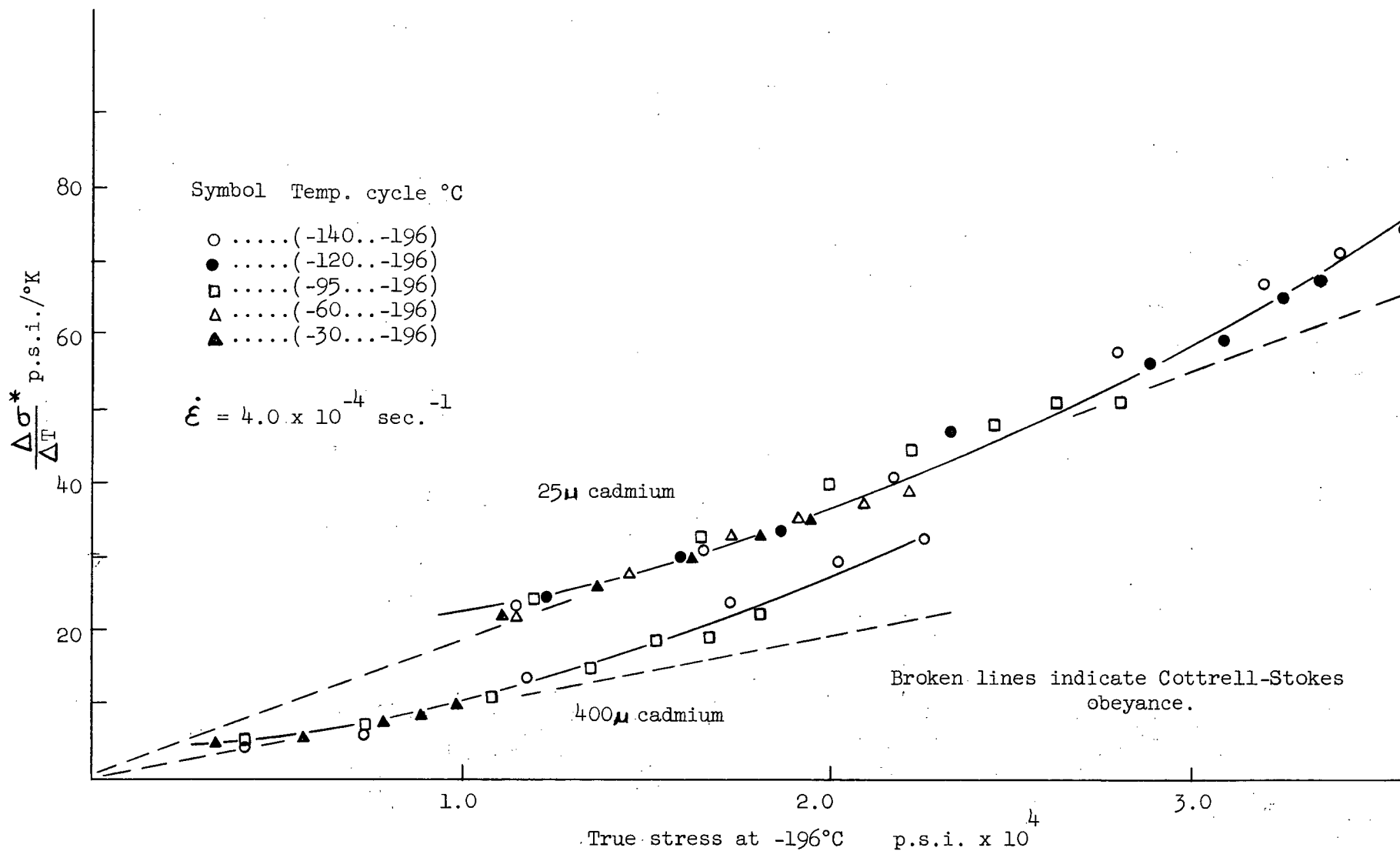


Fig. 54 The relationship between the change in flow stress per °K and the resultant stress at -196°C obtained during the temperature cycling of cadmium.

"obstacles" but postulated that recovery was associated with the annihilation and rearrangement of dislocations by the action of point defects.

Although Bullen found no grain size dependence of  $\frac{\Delta\sigma^*}{\sigma \Delta T}$ , only a rather narrow range of grain sizes was used. It also appeared that there was no effect of preferred orientation.

### 2.2.3. The Mechanical Equation of State

If the sequence of events occurring during deformation is the same at any two temperatures, then one would expect that the irreversible component of the flow stress difference as shown in Fig. 53 would be zero. The difference in flow stress at a given strain at two different temperatures is therefore due only to a difference in  $\sigma^*$ . Under such conditions it is expected that a mechanical equation of state might be valid. The flow stress can then be expressed as a unique function of the instantaneous value of the strain, strain rate and temperature and is independent of the prior strain history<sup>81</sup>. Therefore

$$\sigma = \sigma(\epsilon, \dot{\epsilon}, T)$$

Bullen in fact did observe that during temperature cycling below approximately 300°K there was always an "incubation strain" during which the irreversible component of the flow stress difference as shown in Fig. 53 was zero. His results for various temperature cycles are shown in Fig. 55. The incubation strains taken from his results are shown in Table 7. It is observed that the magnitude of the incubation strain increased as the upper cycling temperature decreased. In this region of strain therefore, the dislocation configuration at a given value of strain is independent of temperature which leads to temperature insensitive work hardening and the obedience

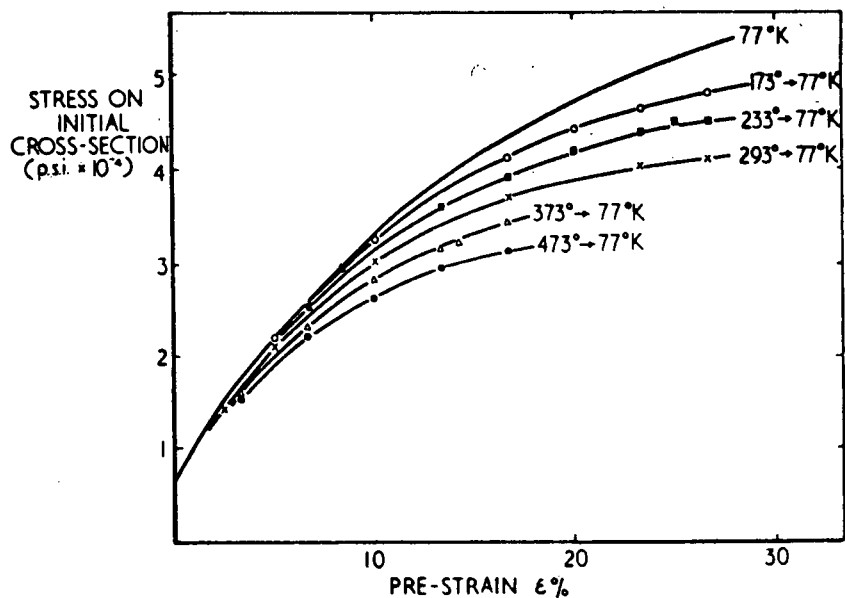


Fig. 55 The effect of elevated temperature prestraining on the stress-strain curve of polycrystalline copper at 77°K (after Bullen<sup>58</sup>).

TABLE 7

Incubation strain required in polycrystalline copper prior to the appearance of an irreversible component of the difference in flow stress

| Lower cycling temperature | Upper cycling temperature | Incubation strain |
|---------------------------|---------------------------|-------------------|
| 77°K                      | 173°K                     | 9%                |
| 77°K                      | 233°K                     | 5%                |
| 77°K                      | 293°K                     | 1%                |

of the mechanical equation of state. The insensitivity of the hardening rate to temperature and the increase in incubation strain with decreasing temperature are in qualitative agreement with the results of Russell although the temperature range of insensitivity as found by Russell extended to somewhat higher temperatures than those found by Bullen.

### 2.2.3. a) Cadmium

Fig. 56 illustrates the flow stress cycling obtained when 25 $\mu$  cadmium is deformed alternately at -140°C and -196°C. For comparison the normal stress-strain curves at the two temperatures are also indicated. It is seen that in the early regions of strain where dynamic recovery does not occur at either of the temperatures involved, the total flow stress difference is due entirely to the difference in  $\sigma^*$ . The slight yield points obtained on reloading at -196°C are due to an unloading effect as described in Appendix II and can be ignored.

As deformation proceeded into the region of dynamic recovery, the reversible flow stress difference could not account for the total difference in the stress at a given value of strain. As the upper cycling temperature was increased above -120°C, irreversible components of the flow stress difference were evident immediately after yielding.

### 2.2.3. b) Zinc

The results of the prestrain tests on 20 $\mu$  zinc are shown in Figs. 57 and 58. Fig. 57 illustrates the effect of prestraining at -95°C to five different strains on the subsequent deformation behaviour at -120°C. It is observed that in all cases the flow stress at -120°C after prestraining at -95°C, was exactly that found on straining exclusively at -120°C to that particular value of strain.

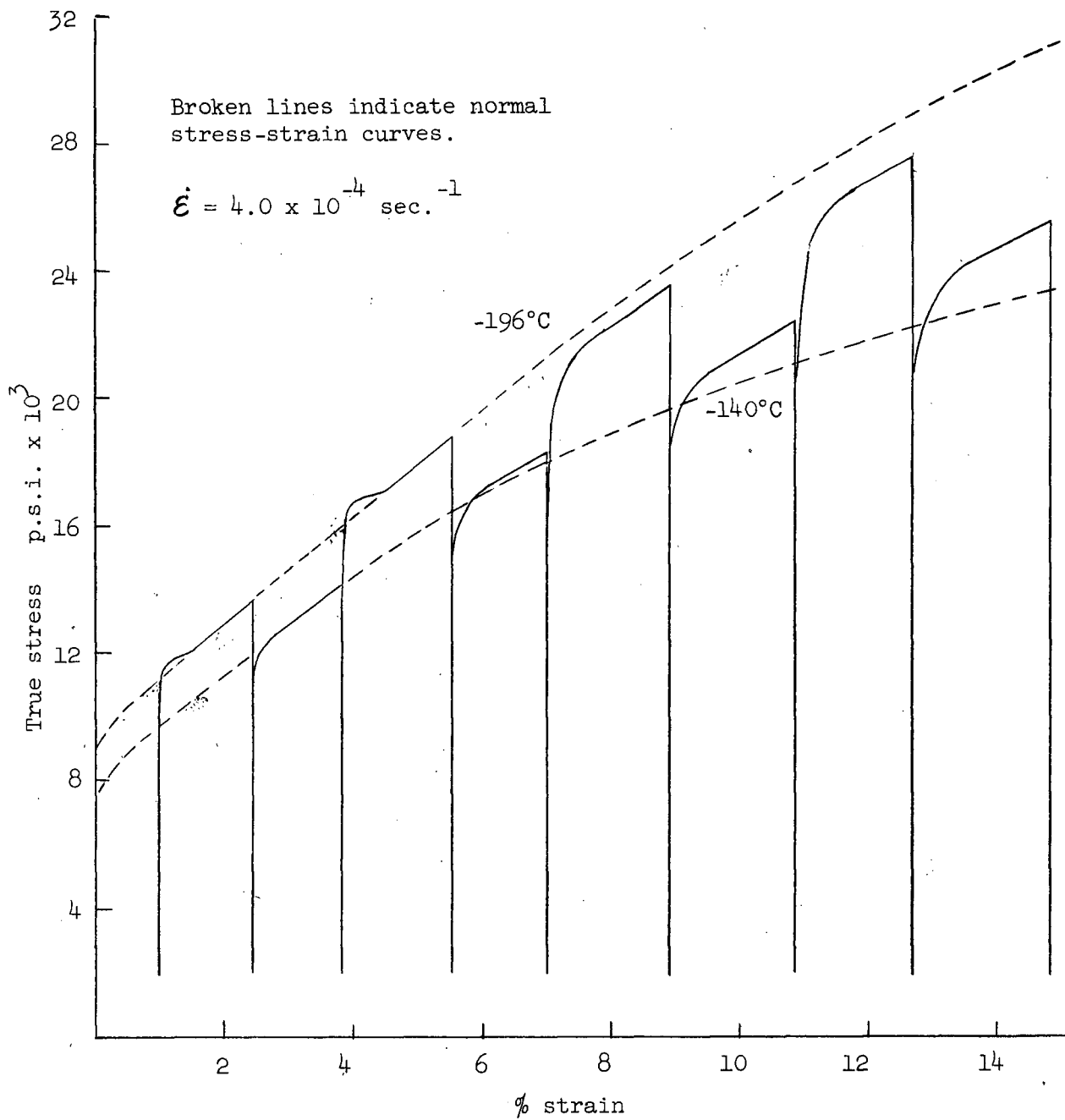


Fig. 56 Temperature cycling of 25 $\mu$  cadmium between -140°C and -196°C.

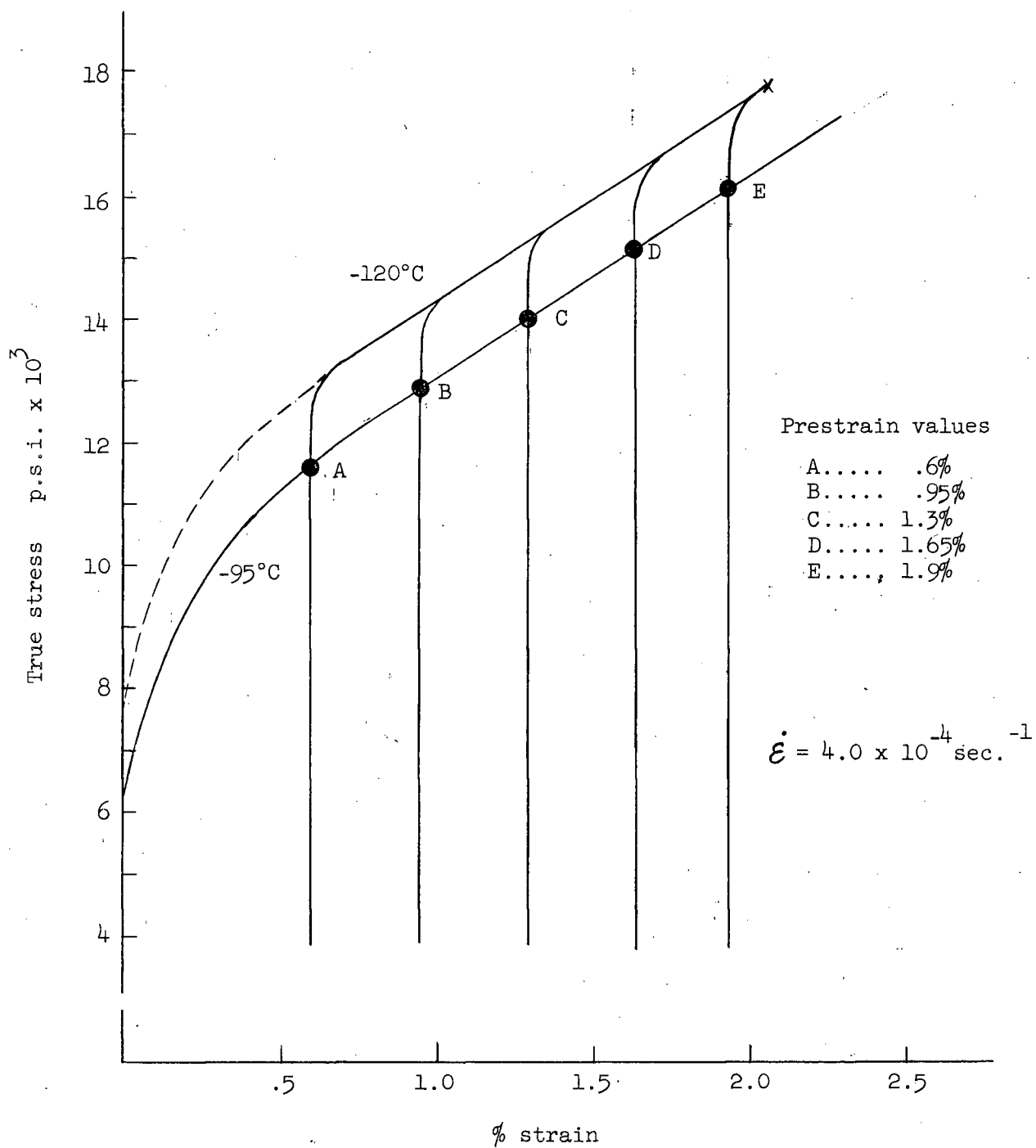


Fig. 57 The effect of prestraining at -95°C on the subsequent deformation behaviour at -120°C in 20μ zinc.

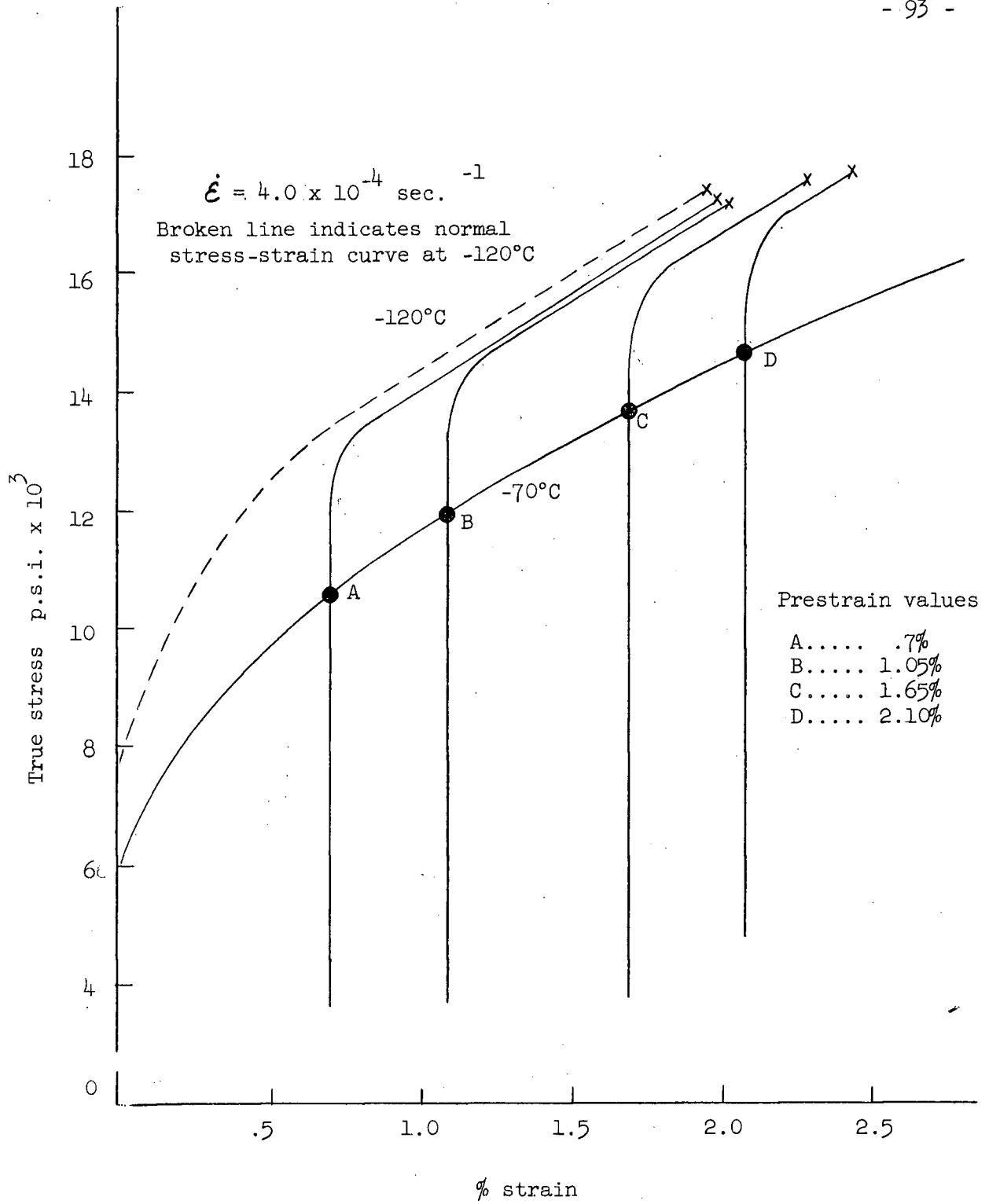


Fig. 58 The effect of prestraining at -70°C on the subsequent deformation behaviour at -120°C of 20μ zinc.

The results are therefore similar to cadmium in that the flow stress at a particular value of strain at temperatures below  $T_H = .26$  arises due to a common dislocation configuration and the change in stress with temperature merely reflects a change in the thermal component of stress  $\sigma^*$ . However in this temperature range for zinc, fracture occurs before an irreversible effect is obtained with increasing strain as is observed with cadmium.

Prestraining above  $T_H = .26$  as shown in Fig. 58, produced an irreversible component of the flow stress difference at all values of strain.

It would therefore appear that in the regions of strain below  $T_H = .26$  where linear hardening occurs in both zinc and cadmium, that "equivalent states" are obtained at equal strains. In this region therefore it is probable that a mechanical equation of state could be formulated. A mechanical equation of state for metals is rarely valid except during Stage I and Stage II hardening of f.c.c. single crystals at low temperatures. Once parabolic hardening associated with dynamic recovery begins, the mechanical equation of state becomes invalid.

Mitra and Dorn<sup>5</sup> have stated that equivalent states are obtained in polycrystals only when  $\sigma_G$  and "l" (the average dislocation length being thermally activated) are constant. Since the results below  $T_H = .26$  indicate that the flow stress difference is just due to a difference in  $\sigma^*$ , then  $\sigma_G \frac{\mu_0}{\mu_T}$  must be constant independent of temperature at a given value of strain. Tests were not comprehensive enough to establish the constancy of "l".

#### 2.2.4. Equivalent States above $T_H = .26$

It may be as suggested by Bullen that in a given system the

sequence of events occurring during deformation does not change with temperature but the rate at which the sequence proceeds might be temperature dependent. Under such a definition, the results of the previous section would be interpreted in terms of a constant rate of obstacle production below  $T_H = .26$  in the temperature insensitive hardening region. However above  $T_H = .26$  where dynamic recovery occurs at all values of strain, it is necessary to equate states at different values of strain at any two temperatures in order to satisfy Bullen's postulate. This condition is illustrated in Fig. 59.

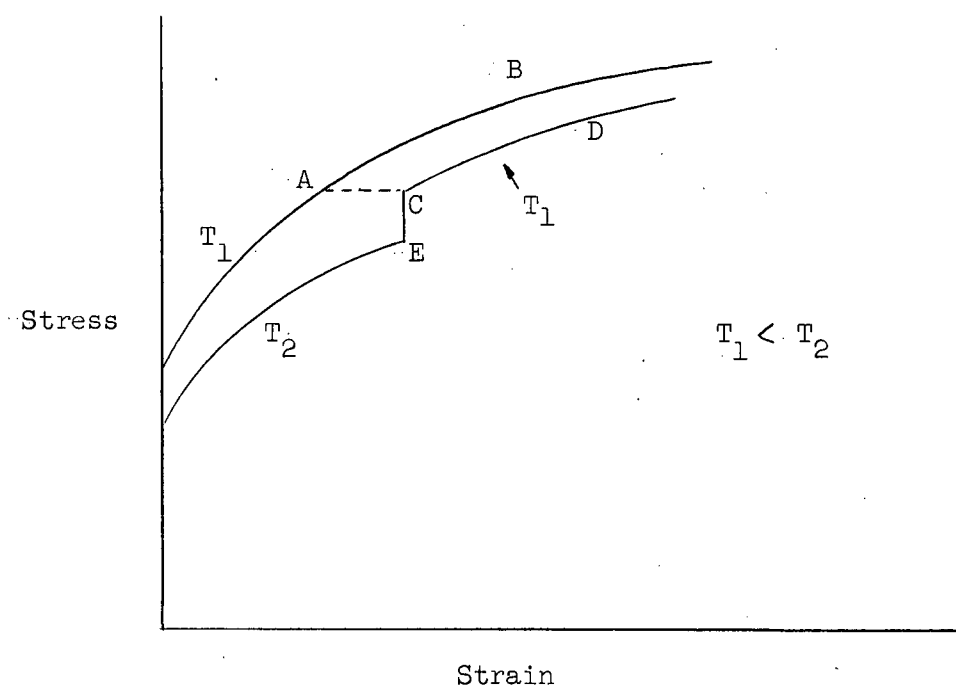
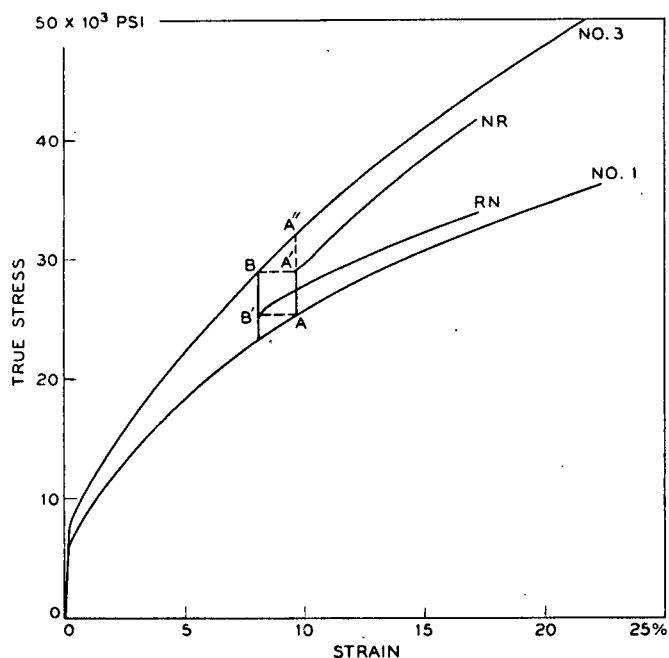


Fig. 59 Equivalent states at different strains.

The irreversible difference in flow stress then develops because of a different rate of obstacle production at different temperatures. The state of the crystal at "E" deformed at  $T_2$  is the same as the state obtained at "A" when deformed at  $T_1$ . CE represents the difference in the thermal component of stress and CD can be related directly to AB. The equivalent strain

values at  $T_1$  and  $T_2$  are then given by  $\epsilon_{T_1}$  and  $\epsilon_{T_2}$  respectively.

Using this above method of analysis, the amount of prestrain  $\epsilon_T$  at various elevated temperatures was related to an equivalent value of strain at  $-120^\circ\text{C}$  in 20 $\mu$  zinc. The results are shown in Fig. 61. With increasing temperature of prestrain, an increasing amount of strain is required to give a certain equivalent strain at  $-120^\circ\text{C}$ . When the sections CD and AB were superimposed, the hardening rates in all cases were the same. Tietz and Dorn<sup>82</sup> using aluminum found that the hardening rate CD was slightly greater than AB. On the other hand Sylwestrowicz<sup>83</sup> using polycrystalline copper and aluminum was able to qualitatively show that the  $\Delta\sigma$  value (AA') obtained on decreasing the test temperature from 300°K to 77°K was identical to the  $\Delta\sigma$  value (BB') obtained on increasing the temperature at a stress corresponding to A (Fig. 60). This suggests equivalence of states at A and B.



—Stress-strain curves of copper specimens, strained at different temperatures. Curve No. 1 — at 300°K; Curve No. 3 — at 76°K; Curve RN — at 300°K after pre-straining at 76°K; Curve NR — at 76°K after presenting at 300°K.

Fig. 60

Reversible temperature change tests at equivalent states in polycrystalline copper.

(after Sylwestrowicz<sup>83</sup>).

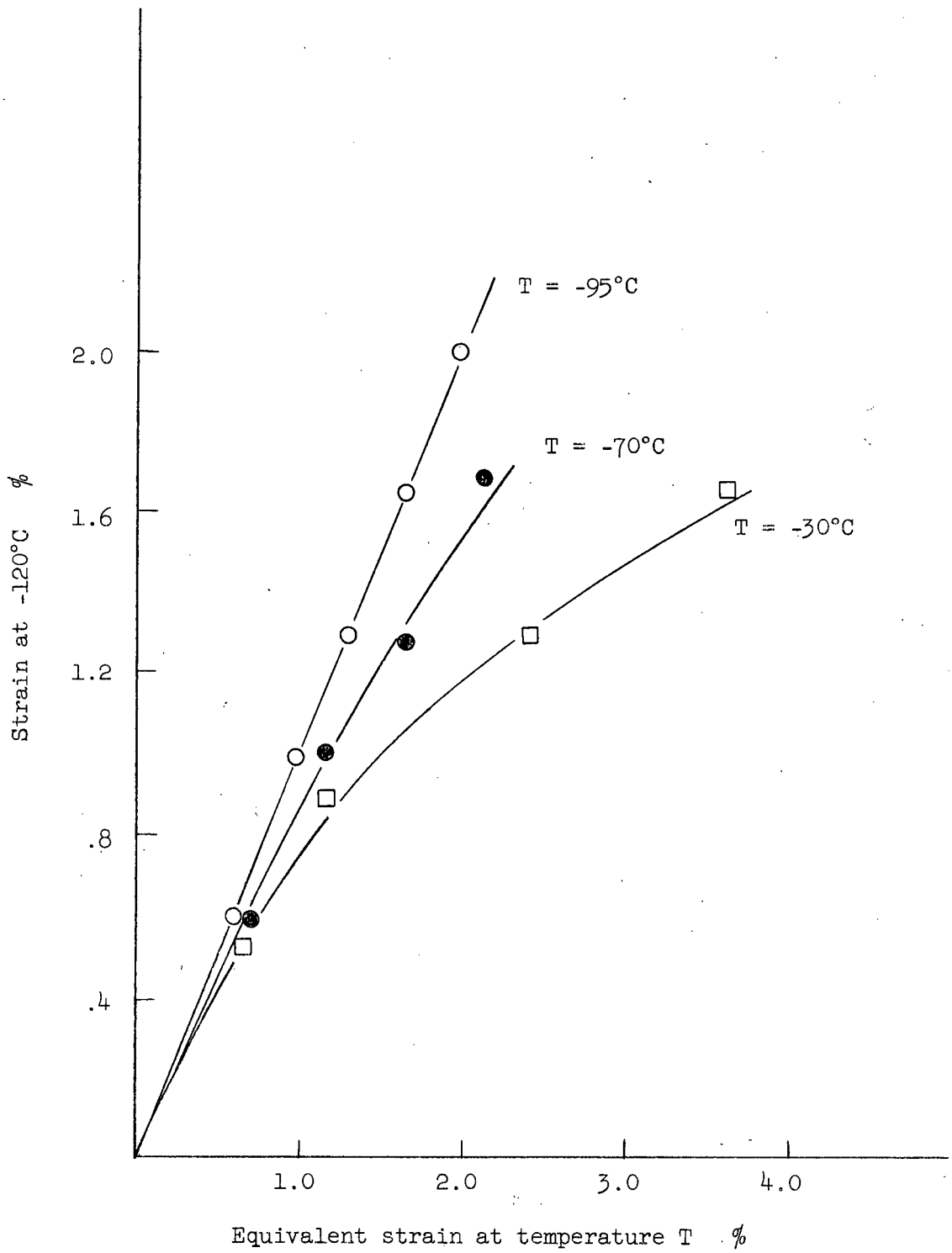


Fig. 61 The correlation of strains at different temperatures in 201 zinc.

Although such an analysis might appear unwarranted at this point because of the lack of detailed experimental data, it is thought that there is some merit in the idea of equivalent states at various strains at different temperatures in zinc and cadmium above  $T_H = .26$ . This is not to be construed as applying to all metal systems where dynamic recovery can affect the nature of the hardening. Much would depend on the exact nature of the recovery process. If it involved a process which caused a distinctive change in the nature and character of  $\sigma_G$  then it is doubtful if such an analysis can be made. However if recovery is linked to the observations of Price<sup>39</sup> concerning the rearrangement and gradual disappearance of debris then the above ideas may have some merit. Price observed that basal dislocations and debris interact strongly. Because of the rearrangement and removal of debris in a temperature region of recovery, larger values of strain are therefore required to arrive at an equivalent obstacle density to that produced at a given value of strain when recovery does not occur. Since the rate of rearrangement of debris as observed by Price increased with increasing temperature, it is expected that the "equivalent strain" as observed in Fig.61 will increase with increasing temperature.

### 2.3. STRAIN RATE CHANGE TESTS

The accurate determination of the reversible change in flow stress accompanying a change in strain rate is of prime importance since the experimental value of  $\Delta\sigma^*$  is used not only in determining the validity of the Cottrell-Stokes law but also to determine the experimental values of activation volume and activation energy. A discussion of the difficulties encountered in correctly determining  $\Delta\sigma^*$  is given in Appendix III.

2.3.1. Procedure

For the purpose of this work,  $\Delta\sigma^*$  was obtained during an increase in strain rate. For polycrystalline zinc and cadmium the strain rate was cycled between  $4.0 \times 10^{-5}$  and  $4.0 \times 10^{-4}$   $\text{sec}^{-1}$  corresponding to a crosshead speed change from .002 to .02 inches per minute. Cadmium single crystals were cycled using crosshead speeds of .02 and .2 inches per minute corresponding to initial shear strain rates of approximately  $3.8 \times 10^{-4}$   $\text{sec}^{-1}$  and  $3.8 \times 10^{-3}$   $\text{sec}^{-1}$ .

2.3.2. Cottrell-Stokes Behaviour in Cadmium at -196°C.

Single crystals ( $\chi_0 = 36^\circ$ ,  $\lambda_0 = 38^\circ$ ) and polycrystals of three different grain sizes (  $25\mu$ ,  $400\mu$ ,  $1250\mu$  ) were tested for Cottrell-Stokes behaviour at -196°C.

2.3.2. a) Single Crystals

Three single crystals of identical orientation were tested and all showed similar behaviour to that shown in Fig. 6. It is seen that during basal glide in Stage I, there is a gradual decrease in the value of  $\frac{\Delta\tau}{\tau}$  with increasing strain. However in Stage II the Cottrell-Stokes law is obeyed confirming the results of Davis<sup>61</sup>. With the beginning of Stage III it would appear that there is a slight but consistent increase in  $\frac{\Delta\tau}{\tau}$ . Although it may be argued that this apparent increase could just be a result of the experimental error in determining  $\Delta\tau$ , it will be shown in the ensuing results for polycrystals that dynamic recovery following linear hardening is associated with continually increasing values of  $\frac{\Delta\sigma}{\sigma}$ .

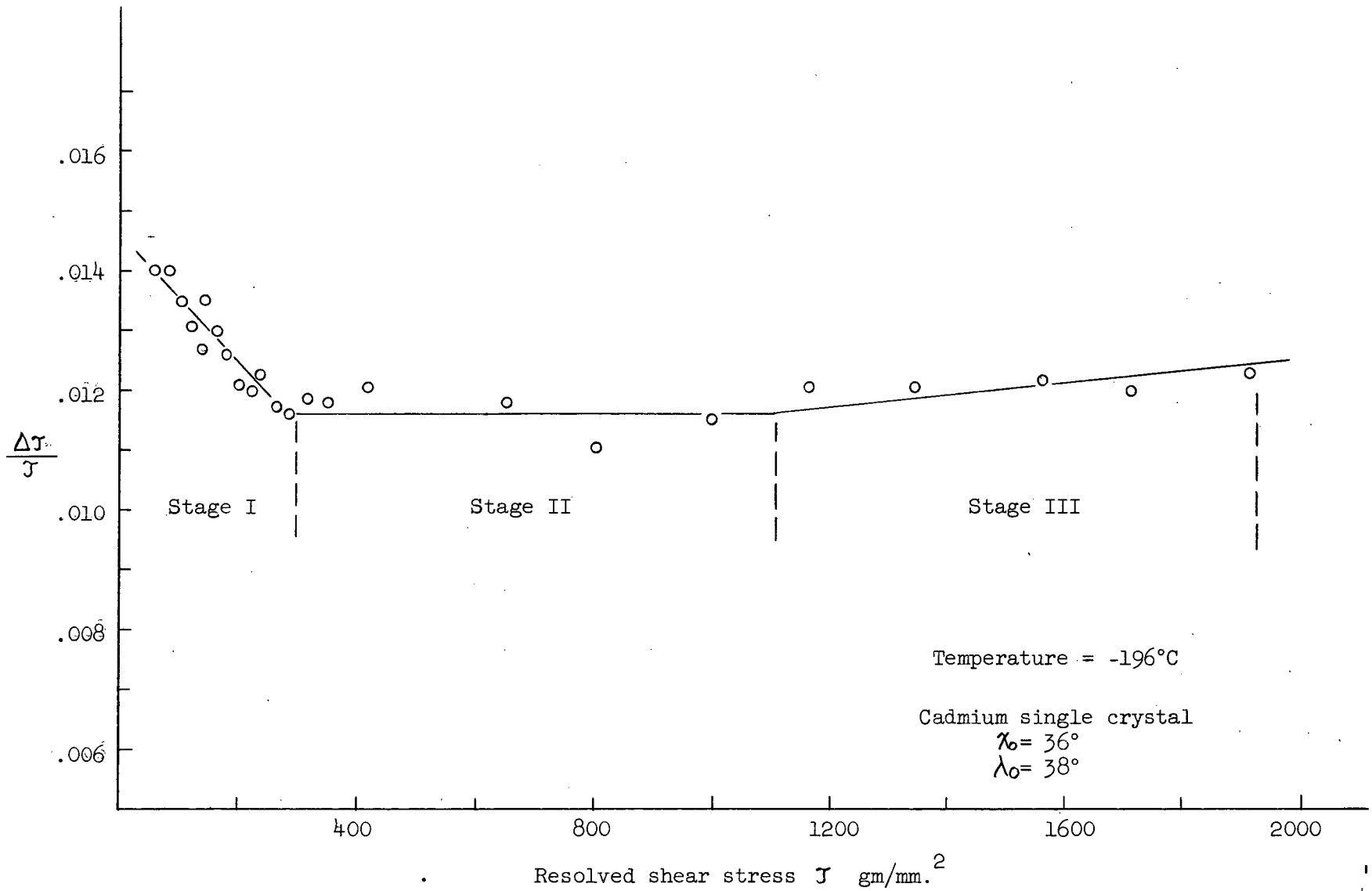


Fig.62 The variation of the Cottrell-Stokes parameter during the deformation of a cadmium single crystal at -196°C.

2.3.2. b) Polycrystals

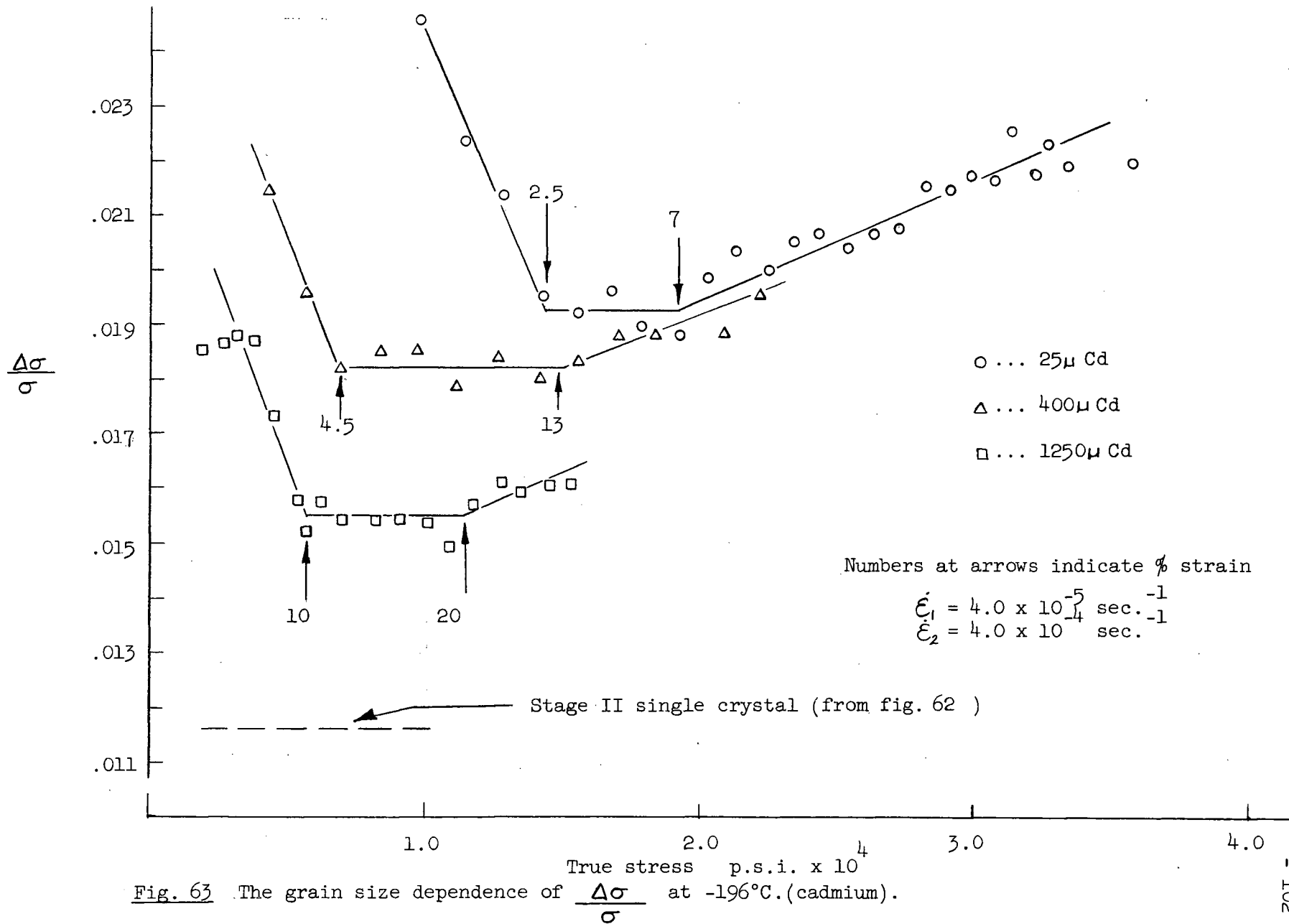
The three stage behaviour for single crystals is also observed during the deformation of polycrystals (Fig. 63). In all cases there is a region of strain in the first few percent of deformation during which  $\frac{\Delta\sigma}{\sigma}$  decreases. The extent of this initial region increases with increasing grain size and at 1250 $\mu$  corresponds rather well to the change in work hardening slopes observed in Fig. 49. This initial region in polycrystals may therefore be related in some manner to the basal glide region of single crystal deformation.

From Fig. 63 it is seen that the Cottrell-Stokes law is obeyed in intermediate strain regions similar to that observed for Stage II of single crystals. This region of obedience ends with a gradual increase in the value of  $\frac{\Delta\sigma}{\sigma}$ . The stress and strain values at which this occurs for each grain size are summarized in Table 8. They correspond very well to the beginning of parabolic hardening observed in Fig. 49. It would therefore appear that the initiation of dynamic recovery at -196°C in single crystals and polycrystals is associated with increasing values of the Cottrell-Stokes ratio.

TABLE 8

Grain size dependence of Cottrell-stokes behaviour (cadmium at -196°C)

| Grain Size     | Strain at beginning of C.S. obedience | Strain at beginning of recovery | Stress at beginning of recovery                      | Constant Cottrell-Stokes ratio |
|----------------|---------------------------------------|---------------------------------|--|--------------------------------|
| 25 $\mu$       | 2.5%                                  | 7%                              | 19,000<br>p.s.i.                                     | .0195                          |
| 400 $\mu$      | 4.5%                                  | 13%                             | 14,500   | .0180                          |
| 1250 $\mu$     | 10%                                   | 20%                             | 11,000   | .0155                          |
| Single crystal | 130% shear                            | 100% tensile<br>180% shear      | 5,500 p.s.i.<br>1,100 gm/mm. <sup>2</sup><br>(shear) | .0115                          |



The results of strain rate changes on polycrystals above  $-196^{\circ}\text{C}$  are shown in Figs. 64 and 65 for  $25\mu$  and  $400\mu$  cadmium respectively. Regardless of the temperature or grain size there is a decrease in  $\frac{\Delta\sigma}{\sigma}$  in the initial regions of deformation previously related to Stage I deformation of single crystals. Fig. 66 shows that  $\frac{\Delta\sigma}{\sigma}$  decreases during Stage I deformation of a single crystal deformed at  $-50^{\circ}\text{C}$  where recovery is known to affect hardening. Therefore whether dynamic recovery occurs or not, the Cottrell-Stokes ratio decreases during Stage I deformation.

As the temperature increases above  $-196^{\circ}\text{C}$ , there is a decrease in the amount of strain showing Cottrell-Stokes obedience until above  $-120^{\circ}\text{C}$  ( $T_H = .26$ ), this region disappears completely. Above  $T_H = .26$  for cadmium regardless of the grain size, the values of  $\frac{\Delta\sigma}{\sigma}$  increase immediately after the initial region associated with Stage I. Therefore the strain rate and temperature insensitive hardening regions below  $T_H = .26$  described in Part I would seem to be associated with Cottrell-Stokes law obedience.

Several strain rate change tests were performed on  $20\mu$  zinc at temperatures between  $-70^{\circ}\text{C}$  and  $-120^{\circ}\text{C}$ . The relationships shown in Fig. 67 indicate that the results are qualitatively the same as those for cadmium. However at  $-95^{\circ}\text{C}$  and  $-120^{\circ}\text{C}$  (below  $T_H = .26$ ) fracture occurs before any general increase in  $\frac{\Delta\sigma}{\sigma}$  indicating the absence of dynamic recovery. At  $-70^{\circ}\text{C}$  there was a slight increase in  $\frac{\Delta\sigma}{\sigma}$  similar to that observed during dynamic recovery above  $T_H = .26$  in cadmium.

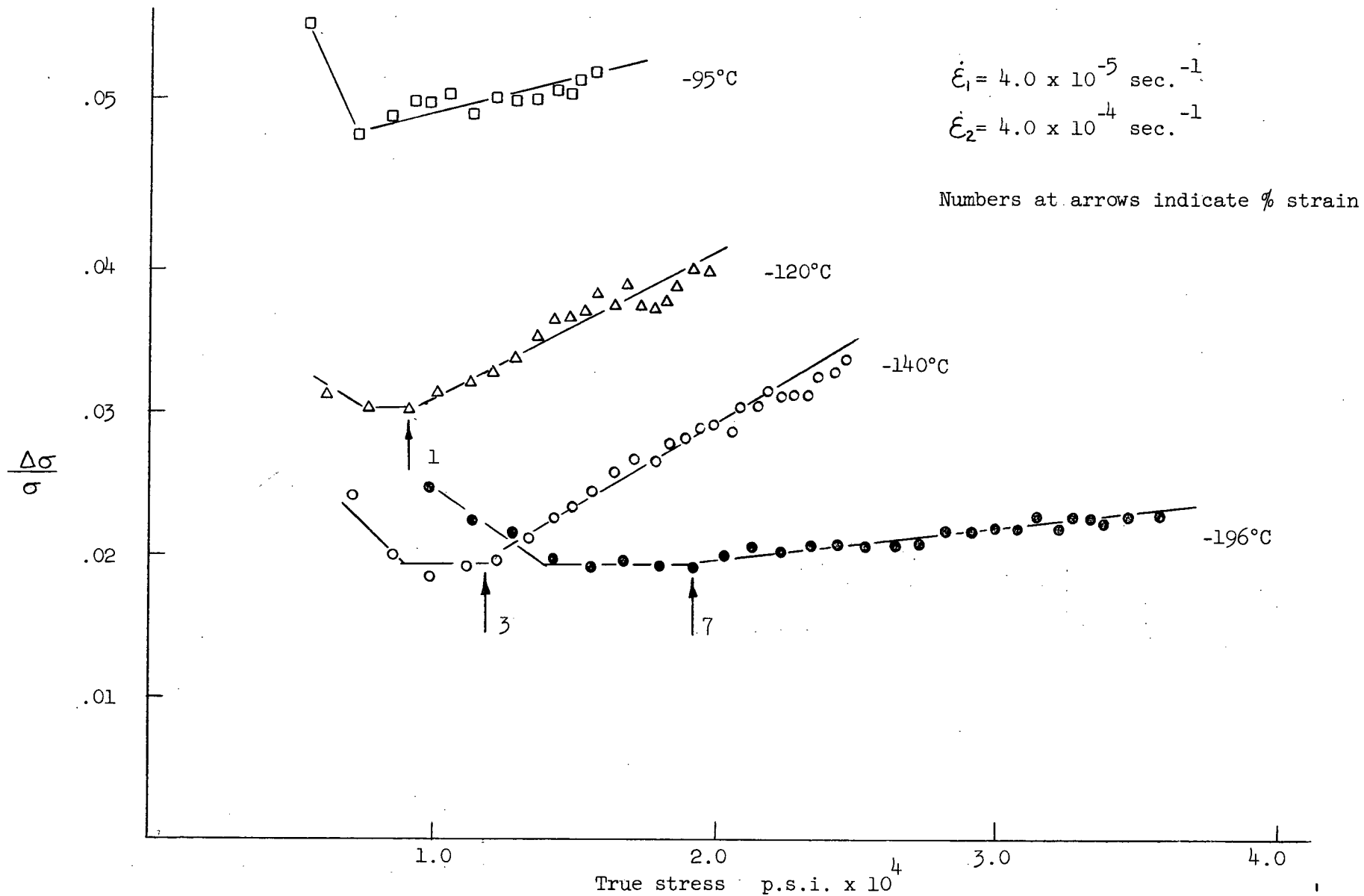


Fig.64 The variation with stress of  $\frac{\Delta\sigma}{\sigma}$  obtained from 25μ cadmium at different temperatures.

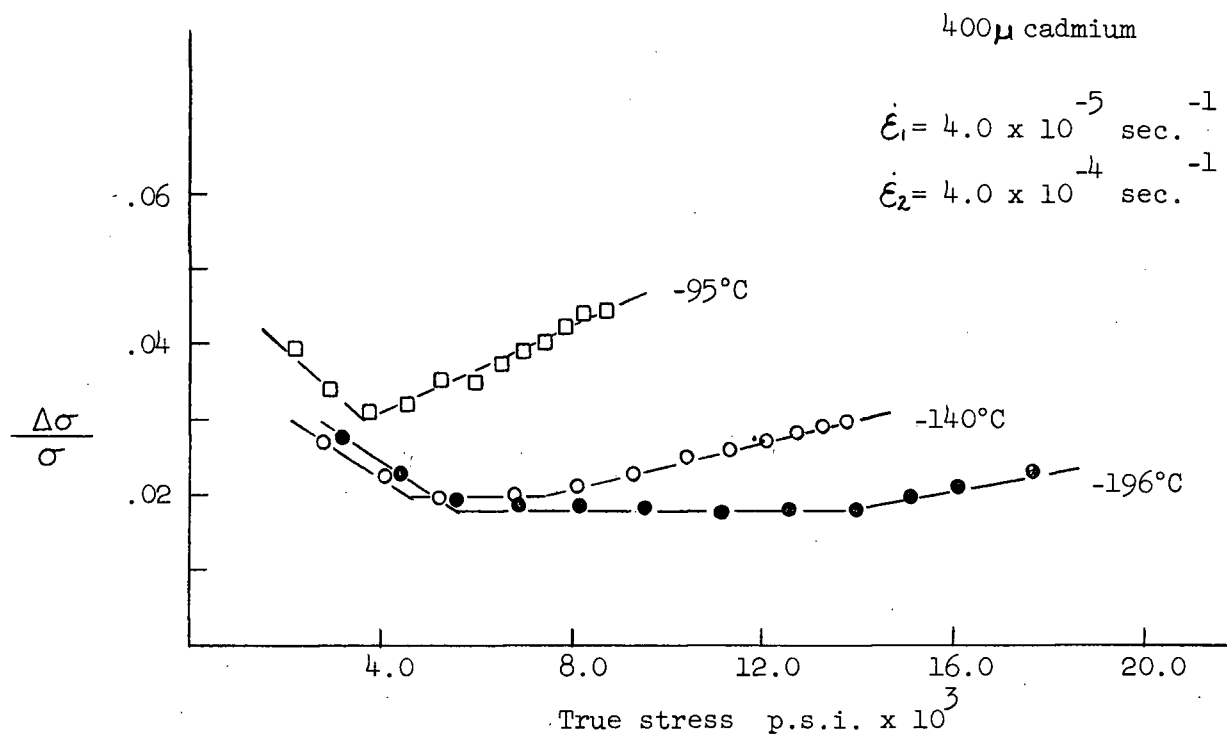


Fig. 65 The stress dependence of  $\frac{\Delta\sigma}{\sigma}$  (400 $\mu$  cadmium).

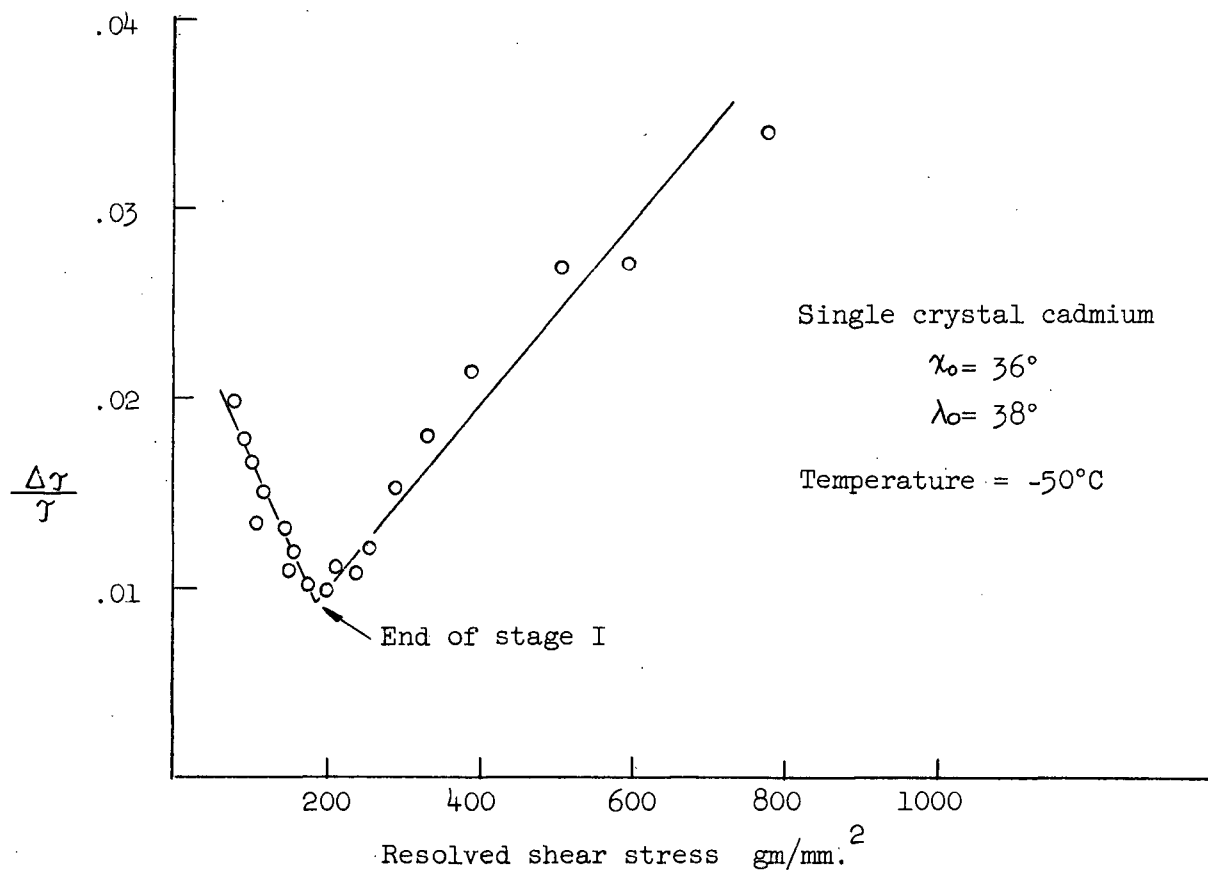


Fig. 66 The failure of the Cottrell-Stokes law at  $-50^\circ\text{C}$ .

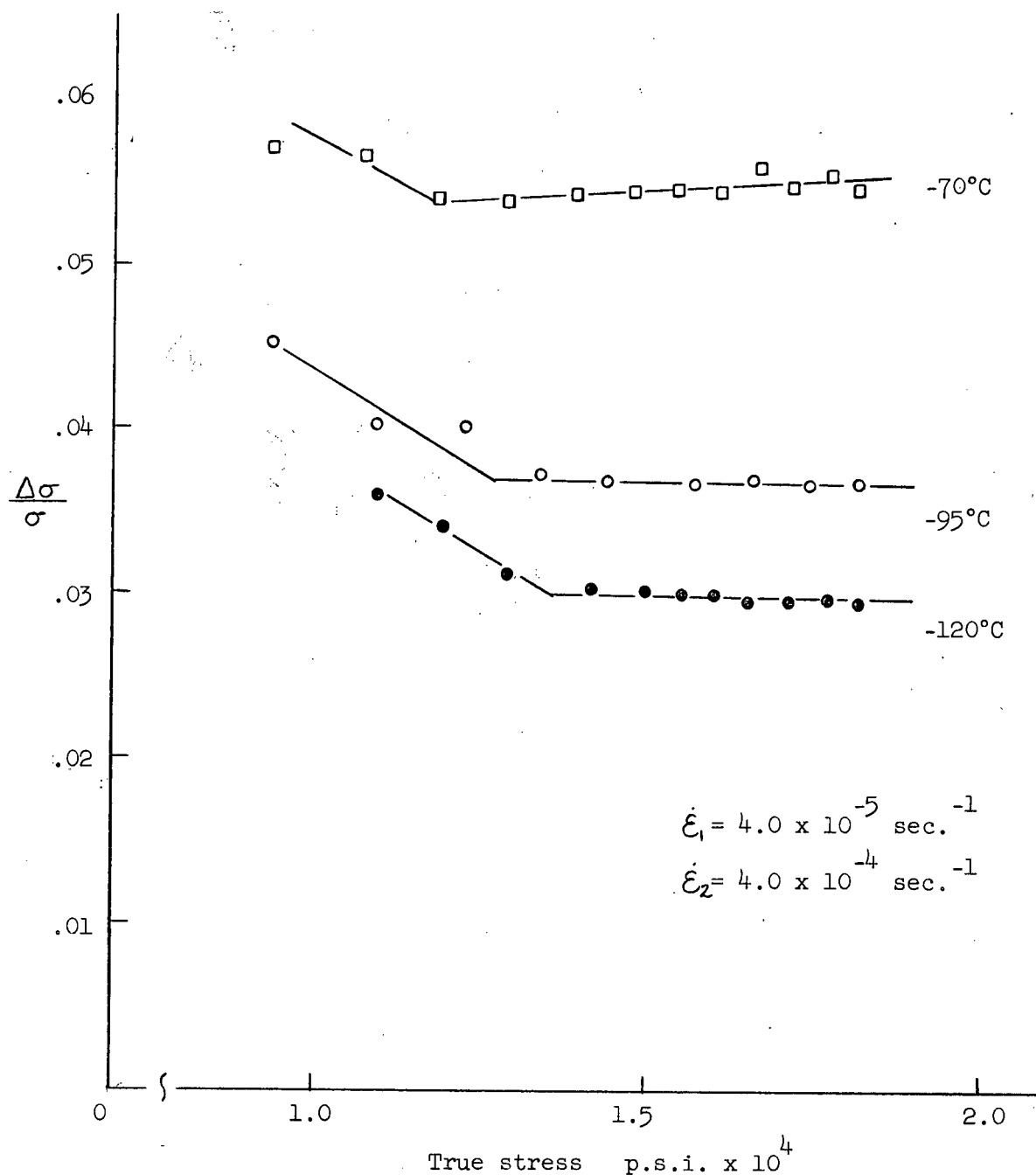


Fig. 67 The variation with stress of the Cottrell-Stokes parameter  $\frac{\Delta\sigma}{\sigma}$  obtained from strain rate change tests on 20 $\mu$  zinc.

Since linear hardening in polycrystals at -196°C is not affected by dynamic recovery, the experimental determination of activation volume and activation energy is simplified and more accurate than at higher temperatures.

#### 2.4.1. Activation Volume

In order to calculate the activation volume it is assumed that the shear stress in polycrystals is equal to one-half of the tensile stress  $\gamma = \frac{\sigma}{2}$ . The correct factor for the conversion is controlled by the degree of preferred orientation and therefore can vary with grain size<sup>84</sup>. However it will have a value somewhere between 1/2 and 1/4<sup>85</sup>. Since the activation volume is experimentally determined from the expression

$$v = kT \left( \frac{\Delta \ln \dot{\epsilon} / \dot{\epsilon}_0}{\Delta J^*} \right)_T$$

the values of "v" obtained represent the lowest possible values if the conversion factor of 1/2 is used.

The manner in which the activation volume varies with the applied stress for polycrystals is shown in Fig. 68. To a first approximation, v is a function of the stress, decreasing in an almost exponential manner with increasing stress. At any constant value of stress, v increases with increasing grain size, an observation expected due to the decreasing values of  $\frac{\Delta \sigma}{\sigma}$  with an increase in grain size (Fig. 63).

The grain size (stress) dependence of the activation volume at yield is shown in Table 9. If a simple assumption is now made that the activation distance "d" can be approximated by the Burgers vector b, then

$$v = lb^2$$

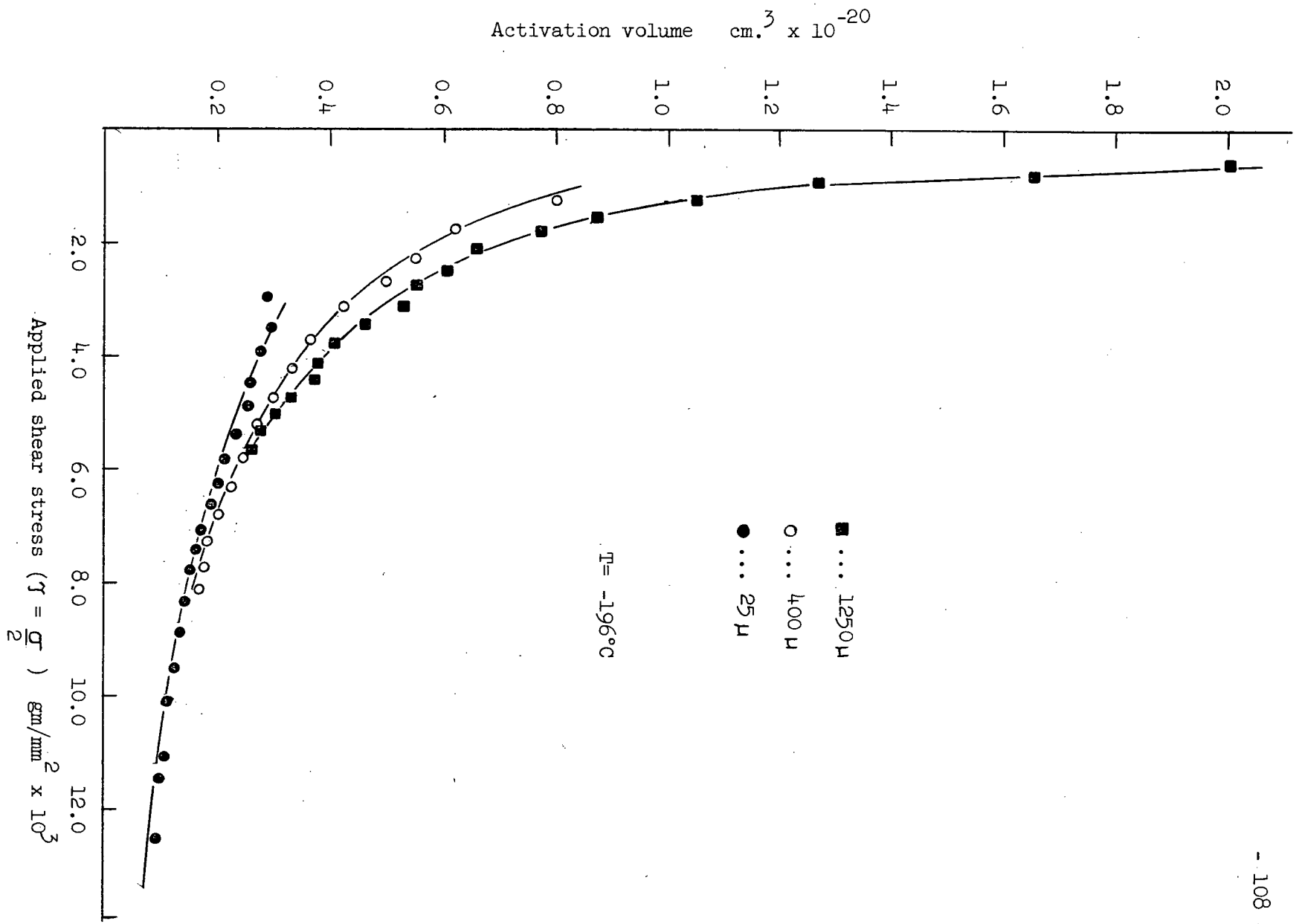


Fig. 68 The stress dependence of the activation volume (cadmium)

TABLE 9

Grain size dependence of the activation volume at yield in cadmium at  $-196^{\circ}\text{C}$ .

| Grain Size   | Activation volume at yield<br>( $\text{cm}^3$ ) | Activation volume at yield<br>( $b^3$ ) | Forest density at yield<br>lines/ $\text{cm}^2$ | Average activated length "l" at yield<br>( $\text{cm}$ ) | Activation volume at start of dyn. recovery<br>( $\text{cm}^3$ ) |
|--|---|---|---|--|--|
| 25 $\mu$   | $.30 \times 10^{-20}$                           | 110                                     | $9.0 \times 10^{10}$                            | $3.3 \times 10^{-6}$                                     | $.20 \times 10^{-20}$  |
| 400 $\mu$  | $1.20 \times 10^{-20}$                          | 450                                     | $5.5 \times 10^9$                               | $1.3 \times 10^{-5}$                                     | $.26 \times 10^{-20}$  |
| 1250 $\mu$   | $2.70 \times 10^{-20}$                          | 1000                                    | $1.1 \times 10^9$                               | $3.0 \times 10^{-5}$                                     | $.38 \times 10^{-20}$  |
| Single crystal<br>$\lambda_0 = 36^{\circ}, \lambda_0 = 38^{\circ}$ | $30.0 \times 10^{-20}$                          | 11,000                                  | $1.0 \times 10^7$                               | $3.3 \times 10^{-4}$                                     | $1.75 \times 10^{-20}$   |

From this an estimate of some smeared average of dislocation length being activated per event at yield can be obtained. These values along with single crystal data are shown in Table 9. It is seen that there is a consistent increase in "l" from  $3.3 \times 10^{-6}$  cm. to  $3.3 \times 10^{-4}$  cm. as the grain size increases from  $25\mu$  to single crystal dimensions.

If it is further assumed that the rate controlling mechanism is one of forest intersection, then an estimate of the forest density at yield may be obtained since  $\rho = \frac{1}{l^2}$  is a good approximation of the forest density. From Table 9 it is seen that  $\rho$  varies from  $9.0 \times 10^{10}$  lines/cm<sup>2</sup> for  $25\mu$  cadmium to approximately  $10^7$  lines/cm<sup>2</sup> for single crystals. These values are realistic for the initial forest density. Mitra and Dorn found that intersection is the rate controlling process during the deformation of aluminum and copper single crystals at 77°K. For crystals initially oriented for easy glide, they calculated a forest density at yield of the order of  $10^9$  lines/cm<sup>2</sup>. For aluminum polycrystals they found an initial density of about  $10^{10}$  lines/cm<sup>2</sup>.

The activation volume at the end of Stage I deformation in cadmium was found to be  $5.0 \times 10^{-20}$  cm<sup>3</sup>. On the basis of the previous assumptions this would indicate a forest density of approximately  $3 \times 10^8$  lines per cm<sup>2</sup>. This represents an increase in the forest density during Stage I of slightly more than an order of magnitude.

By assuming an activation distance of  $d = b$  the density values calculated for cadmium may be slightly low in that "d" may be somewhat larger. Price found that the stacking fault energy for cadmium is probably between 15 and 30 ergs/cm<sup>2</sup>. This is considerably lower than previously believed. Therefore before intersection can occur there must be a recombination of the basal partials. This tends to give a more gradual slope to the force-

distance curve than would be expected if the stacking fault energy was high. This in turn effectively increases the possible activation distance. However at 77°K, a significant proportion of the energy required for intersection is supplied by the effective stress since the thermal component of the activation energy  $\Delta G$  should be quite small. This therefore limits the value of the activation distance during thermal activation and the assumption that  $d = b$  is not unrealistic.

It has been assumed up to this point that intersection is the rate controlling process governing yield and linear hardening at -196°C. This will be discussed more fully in subsequent sections with regard to possible alternative mechanisms.

#### 2.4.2. Activation Energy

With the known values of the activation volume it is now possible to calculate a value of the apparent activation energy  $\Delta G_0$  at yield for 25 $\mu$  and 400 $\mu$  cadmium. The  $\frac{\Delta\sigma^*}{\Delta T}$  values required for the calculation were obtained from the yield stress-temperature relationships of Fig. 32. They agreed very well with the extrapolated values at yield of  $\frac{\Delta\sigma^*}{\Delta T}$  obtained from Cottrell-Stokes temperature change tests.

The values obtained for the various rate parameters are shown in Table 10 and were calculated using equations 9, 11 and 12.

TABLE 10

Energy values at yield for cadmium deformed at -196°C.

| Grain size | $\Delta H$ e.v. | $\Delta G$ e.v. | $v\dot{\gamma}^*$ e.v. | $\Delta G_0$ e.v. |
|------------|-----------------|-----------------|------------------------|-------------------|
| 25 $\mu$   | .10             | .08             | .28                    | .36               |
| 400 $\mu$  | .08             | .06             | .33                    | .39               |

The values shown in Table 10 can be considered accurate to at best  $\pm 10\%$ . Within experimental error the apparent activation energy  $\Delta G_0$  appears to be independent of grain size. This suggests that the force-distance curve does not change significantly with grain size and therefore that the mechanism of yield is independent of grain size. The change in activation volume with grain size therefore merely reflects the variation of the forest spacing "l" as previously assumed. The significance of  $\Delta G_0$  will be discussed later. However it is noted that the thermal component  $\Delta G$  is much smaller than the  $v\gamma^*$  term. This is to be expected since with decreasing temperature an increasing proportion of the energy  $\Delta G_0$  will be associated with the work done by the effective stress.

## 2.5. HARDENING ABOVE $-196^\circ\text{C}$ IN ZINC AND CADMIUM

### 2.5.1. Yield Behaviour in Cadmium

The values of  $v$ ,  $\Delta H$ ,  $\Delta G$ ,  $\Delta G_0$  and  $v\gamma^*$  at yield in  $25\mu$  cadmium at temperatures above  $-196^\circ\text{C}$  are shown in Table 11. Values are quoted to two significant figures which is unjustified because of experimental limitations. This procedure was followed only to provide a method of comparison between values calculated in the same manner using consistent techniques of analysing experimental data.

It is seen that below  $-120^\circ\text{C}$  there is a steady increase in  $\Delta G_0$  and  $v\gamma^*$  with increasing temperature. This increase is consistent with an energy barrier as shown in Fig. 69a in which there is a fairly gradual slope of the force distance relationship. With this type of barrier it is expected that both  $\Delta G_0$  and  $v\gamma^*$  will increase with increasing temperature as indicated

TABLE 11

Energy values at yield in 25 $\mu$  cadmium.

| Temperature<br>(°C) | $\Delta H$<br>(e.v.) | $\Delta G$<br>(e.v.) | $vT^*$<br>(e.v.) | $\Delta G_0$<br>(e.v.) | Activation<br>volume $v_3$<br>(cm.) |
|---------------------|----------------------|----------------------|------------------|------------------------|-------------------------------------|
| -196                | .10                  | .08                  | .28              | .36                    | $.30 \times 10^{-20}$               |
| -140                | .40                  | .35                  | .42              | .77                    | $.60 \times 10^{-20}$               |
| -120                | .47                  | .41                  | .41              | .82                    | $.70 \times 10^{-20}$               |
| -95                 | .42                  | .37                  | .26              | .63                    | $.55 \times 10^{-20}$               |
| -60                 | .50                  | .43                  | .20              | .63                    | $.55 \times 10^{-20}$               |
| -30                 | .57                  | .50                  | .12              | .62                    | $.50 \times 10^{-20}$               |

by the two random temperatures  $T_1$  and  $T_2$ .

Under such conditions it is therefore impossible to predict a rate controlling mechanism strictly from the values of  $\Delta G_0$ . It was for this reason that  $\Delta G_0$  was labelled "apparent". It does not include the work done by the effective stress before thermal activation. In order to calculate  $\Delta G_0^*$ , the total activation energy, it is necessary to know the critical temperature  $T_c$  where  $\Upsilon^* = 0$ . Under such conditions

$$\Delta G = \Delta G_0 = \Delta G_0^*$$

Alternatively  $\Delta G_0^*$  may be calculated simply by knowing the strain rate dependence of the critical temperature<sup>86</sup>. Therefore all that can be said about  $\Delta G_0^*$  below  $-120^\circ\text{C}$  is that it is something in excess of .8 e.v. (the value of  $\Delta G_0^*$  at  $-120^\circ\text{C}$ ).

Above  $-120^\circ\text{C}$   $\Delta G_0$  tends to remain constant at approximately .6 e.v. This temperature independence might suggest a rate controlling process above  $-120^\circ\text{C}$  which is associated with an energy barrier as shown in Fig. 69b for which neither  $\Delta G_0$  nor "d" changes appreciably with temperature. Under such conditions  $\Delta G_0^*$  may be approximated by  $\Delta G_0$  and is therefore equal to .6 e.v.  $\pm$  .1 e.v.

This proposed change in the rate controlling mechanism at  $-120^\circ\text{C}$  in 25 $\mu$  cadmium is illustrated quite clearly by the dependence of  $\Delta G$  at yield on temperature as shown in Fig. 70.

Before such a proposed interpretation can become acceptable two major inconsistencies with theory must be explained.

First of all the rate theory results indicate a change in the rate controlling mechanism of yield at a temperature of  $-120^\circ\text{C}$ . However the

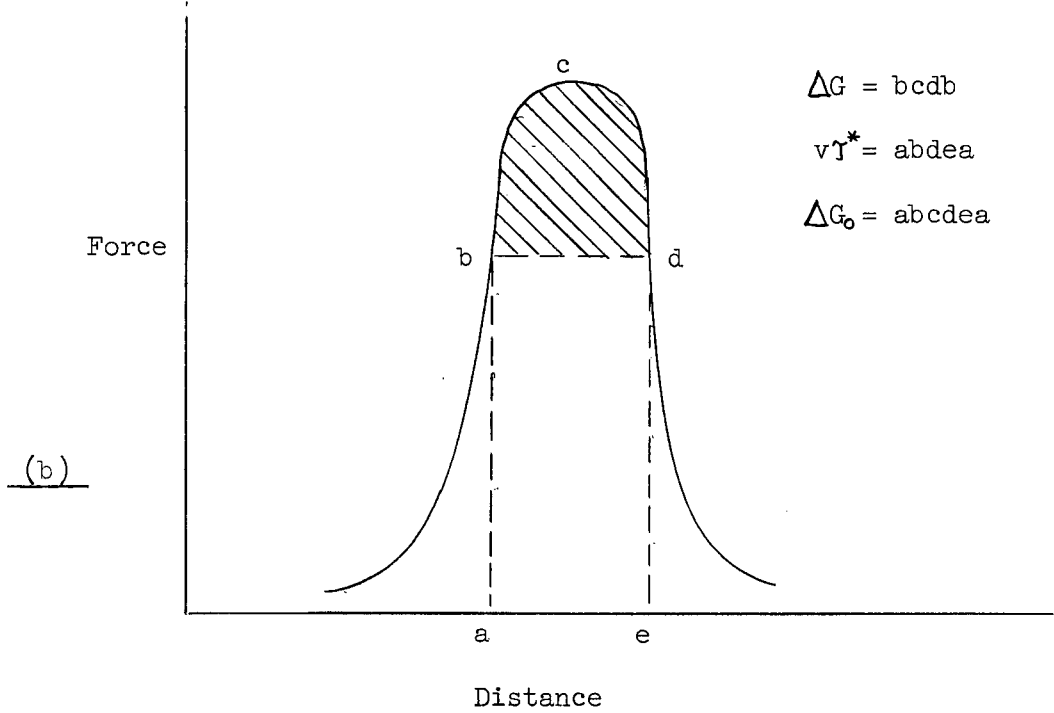
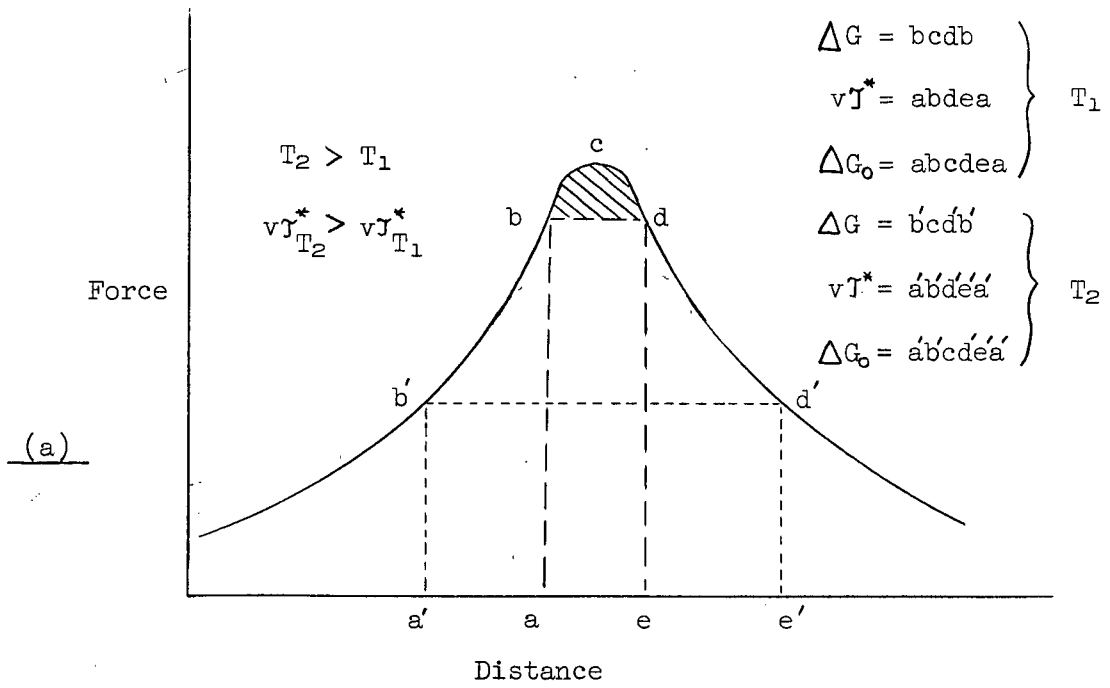


Fig. 69 Force-Distance curves

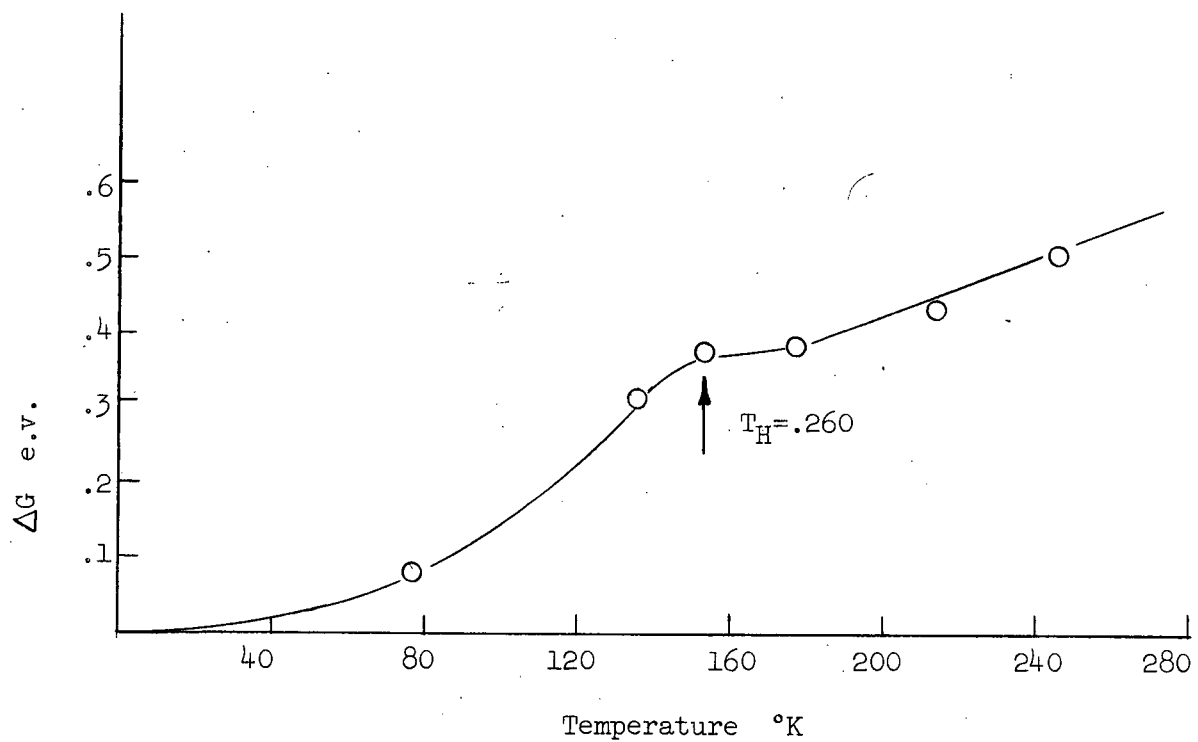


Fig. 70 The variation of  $\Delta G$  with temperature for  $25\mu$  cadmium.

yield stress has been found to vary linearly with temperature (Fig. 32). This linearity suggests a common mechanism controlling yield. It may be however that the change at  $-120^{\circ}\text{C}$  causes only a slight change in the yield stress-temperature slope which falls within the experimental scatter of the linear relationship shown in Fig. 32. Further tests below  $-196^{\circ}\text{C}$  should provide a more complete understanding of the temperature dependence of yield. Stoloff actually did observe a change in slope at approximately  $-120^{\circ}\text{C}$  but his experimental scatter was too great to accurately establish the change in  $\frac{\Delta\sigma^*}{\Delta T}$ .

The second inconsistency concerns the nature of the temperature dependence of  $\Delta G$  below  $-120^{\circ}\text{C}$ . From the relationship

$$\Delta G = -kT \ln \frac{\dot{\gamma}}{\dot{\gamma}_0}$$

if  $\dot{\gamma}_0$  is not a function of temperature, then  $\Delta G$  should vary in a linear manner with temperature. However from Fig. 72 it is seen that a linear relationship does not exist below  $-120^{\circ}\text{C}$ . Either deformation is not controlled by a single mechanism which would place in doubt any calculation based on rate theory or the nature of the force-distance curve changes with temperature. This latter possibility could occur without a change in the basic rate process if for instance the stacking fault energy changes with temperature<sup>15</sup>. At this point there is considerable doubt as to the magnitude of the stacking fault energy in cadmium let alone any possible temperature dependence.

Thornton and Hirsch<sup>68</sup> have proposed that the activation distance will vary with temperature due to a change in the stacking fault energy. This would alter the shape of the force-distance curve without affecting the basic rate mechanism.

Conrad<sup>14, 15</sup> using an intersection model for magnesium single crystals has shown that the nature of the force-distance curve may vary slightly with temperature (stress) due to the influence of stress on the amount gliding dislocations bow out in the slip plane thereby changing the effective forest spacing "l".

Another possibility is that the pre-exponential term  $\dot{\gamma}_0 = NAbv$  varies with temperature. However in the development of rate theory expressions,  $\dot{\gamma}_0$  must be assumed temperature independent in order to arrive at useful mathematical expressions. If in fact  $\dot{\gamma}_0$  does vary, then the derived formulations must be modified.

At this time not enough experimental data are available because of the limited test temperatures available below  $-120^\circ\text{C}$  in order to distinguish between the above possible causes. A liquid helium cryostat is now nearing completion which will allow for a more extensive testing program.

At this point no attempt has been made to discuss the significance of the experimental value of  $\Delta G_0 = .6 \pm .1$  e.v. at temperatures above  $T_H = .26$ . This discussion will follow in section 3.2. which includes a comprehensive survey of the possible mechanisms of dynamic recovery.

#### 2.5.2. The Variation of $\Delta H$ with Strain in $25\mu$ Cadmium.

The manner in which  $\Delta H$  varies with strain at different temperatures is shown in Fig. 71. Because of the unknown variation of  $\gamma^*$  with strain the values of  $\Delta G$  and  $\Delta G_0$  cannot be obtained. However the strain dependence of  $\Delta G$  will be similar to that of  $\Delta H$  in that the entropy factor is not expected to lower  $\Delta H$  by more than about 20%.

From Fig. 71 it is observed that the linear hardening regions below  $-120^{\circ}\text{C}$  are associated with strain independent values of  $\Delta H$ . This is as expected when the Cottrell-Stokes law is obeyed. When dynamic recovery occurs  $\Delta H$  decreases substantially.

### 2.5.3. Yield Behavior in Zinc.

The experimental values of the various components of the activation energy at yield in 20% zinc are given in Table 12. It is observed that the results for zinc are similar to those for cadmium. Both indicate a temperature independent value of  $\Delta G_0$  of about .6 e.v. in the recovery range above  $T_H = .26$ . The values of  $\Delta G$  for zinc are slightly lower than those for cadmium but do show a similar temperature relationship as shown in Fig. 72. The break in the  $\Delta G$  - temperature relationship for zinc at  $T_H = .26$  is not as obvious because of the limited data below this temperature. The activation volume values for zinc are comparable to those of cadmium with the zinc values being about 25% smaller.

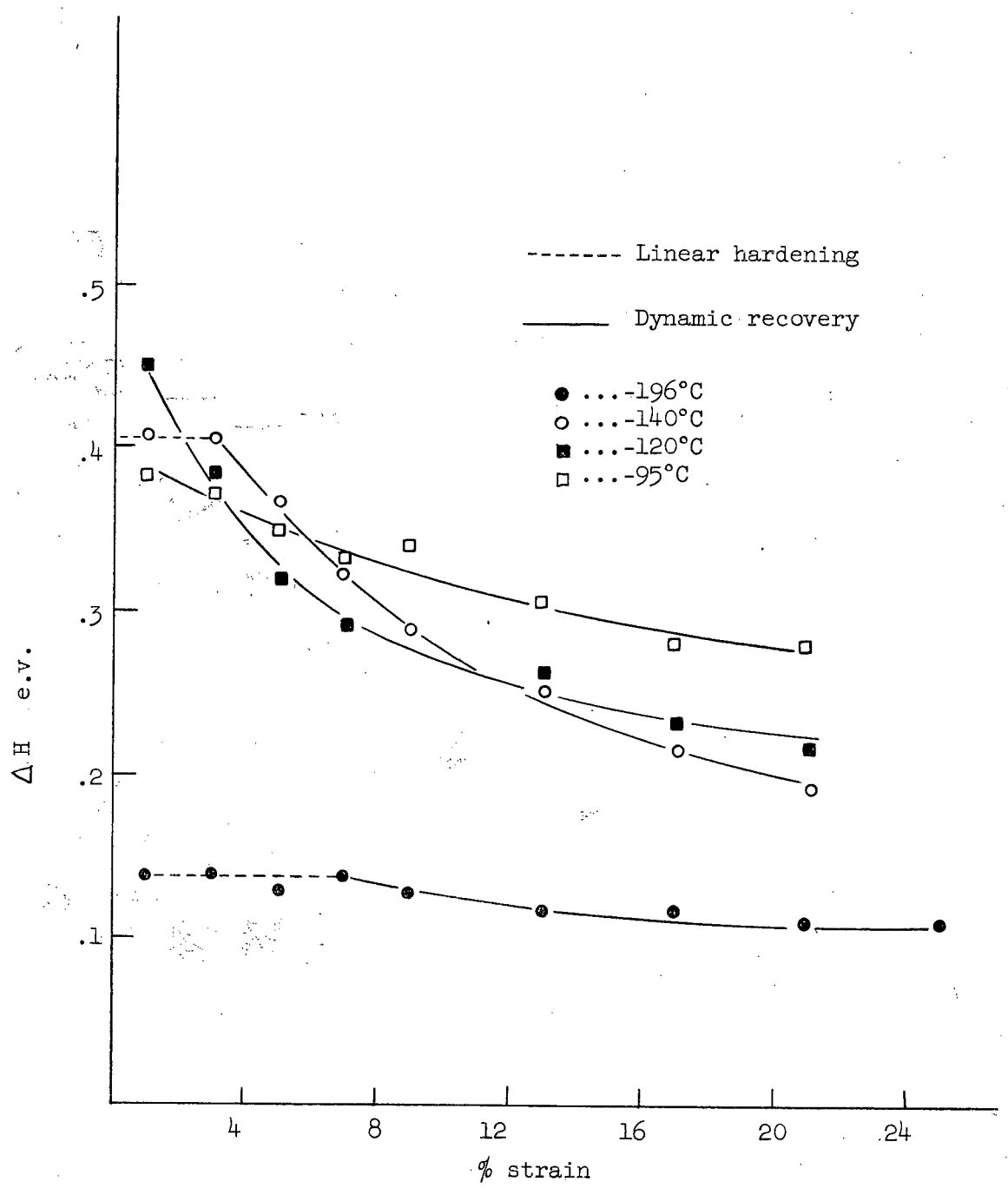


Fig. 71 The variation of  $\Delta H$  with strain and temperature in  $25\mu$  cadmium.

TABLE 12

Rate parameters at yield in 20 $\mu$  zinc.

| Temperature<br>°C | $T_H$ | $\Delta H$<br>e.v. | $\Delta G$<br>e.v. | $v_T^*$<br>e.v. | $\Delta G_0$<br>e.v. | $v$<br>cm. <sup>3</sup> |
|-------------------|-------|--------------------|--------------------|-----------------|----------------------|-------------------------|
| -120              | .26   | .21                | .17                | .40             | .57                  | $.36 \times 10^{-20}$   |
| -105              | .28   | .27                | .23                | .42             | .65                  | $.41 \times 10^{-20}$   |
| -95               | .30   | .29                | .24                | .40             | .64                  | $.43 \times 10^{-20}$   |
| -70               | .34   | .33                | .27                | .34             | .61                  | $.40 \times 10^{-20}$   |
| -30               | .41   | .42                | .36                | .24             | .60                  | $.40 \times 10^{-20}$   |

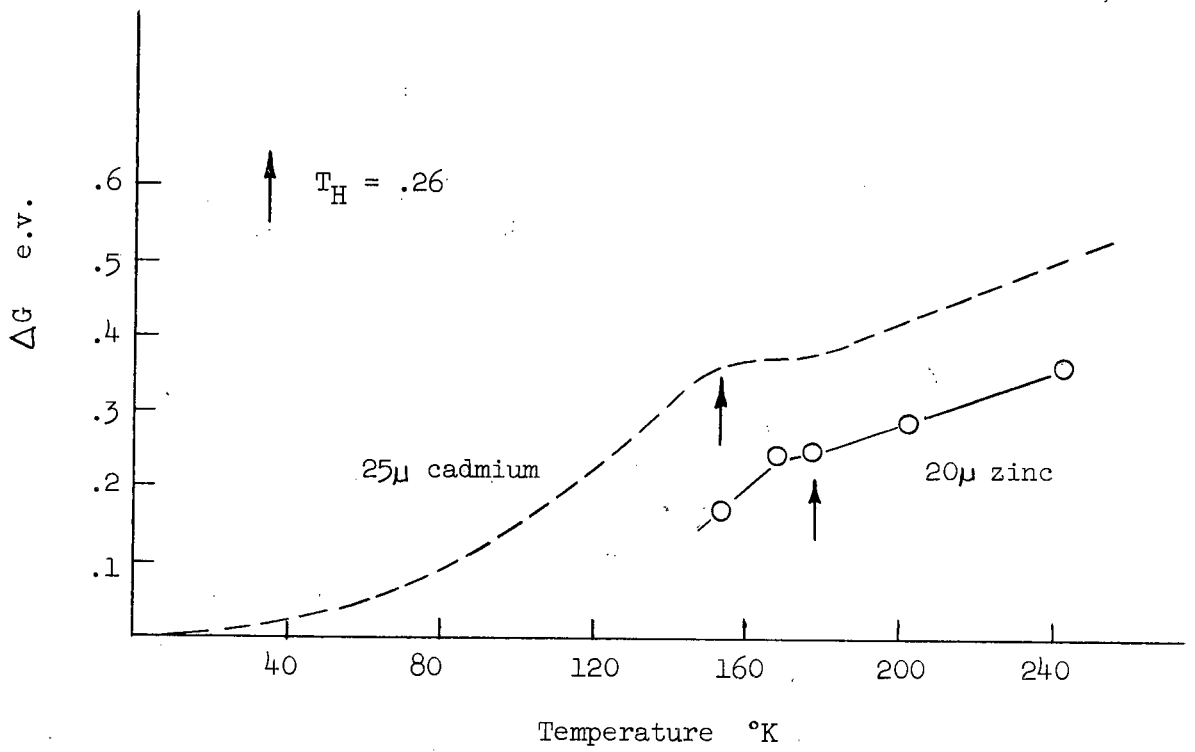


Fig. 72 The variation of  $\Delta G$  with temperature for 20 $\mu$  zinc.

### 3. DISCUSSION

Before any discussion of the present results is attempted, it is desirable to review the electron transmission observations of Price on dislocation structure and motion in platelets of zinc and cadmium. Since the flow stress is generally thought to arise from some combination of long and short range elastic interactions between dislocations and from a short range thermal component of stress, Price's observations on the formation and behaviour of dislocation loops and their subsequent interaction with dislocations are thought to be significant with regard to the mechanisms of hardening in zinc and cadmium.

#### 3.1 Loop Formation and Annealing

Dislocation loops can form on specific atomic planes by a variety of processes.

(i) Price observed that prismatic loops can form behind moving basal edge dislocations by a process illustrated in Fig. 73 .

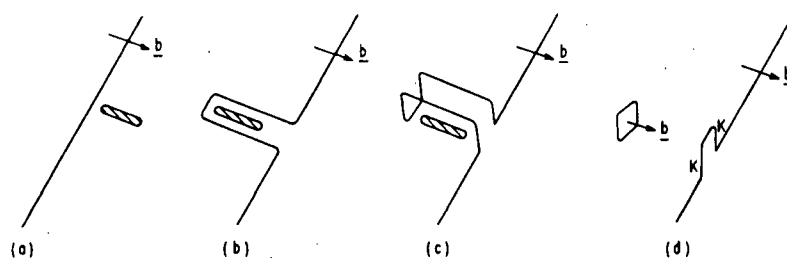


Fig. 73

The formation of a prismatic dislocation loop by an edge dislocation which is held up at an obstacle.

This loop formation is thought to be associated with the cross glide of the screw components (c) and the subsequent annihilation of these components by glide on a parallel glide plane. This type of loop will be sessile because of its edge components on non basal planes. The kinks on the original dislocation (d) are expected to retard its further motion. Loops thought to be formed by this type of mechanism have been observed by Lally<sup>89</sup> during the Stage I deformation of magnesium at 20°C.

(ii) Price also observed loop formation behind moving basal screw dislocations. A jog on a screw may affect the motion of the screw depending on the size of the jog as shown in Fig. 74 .

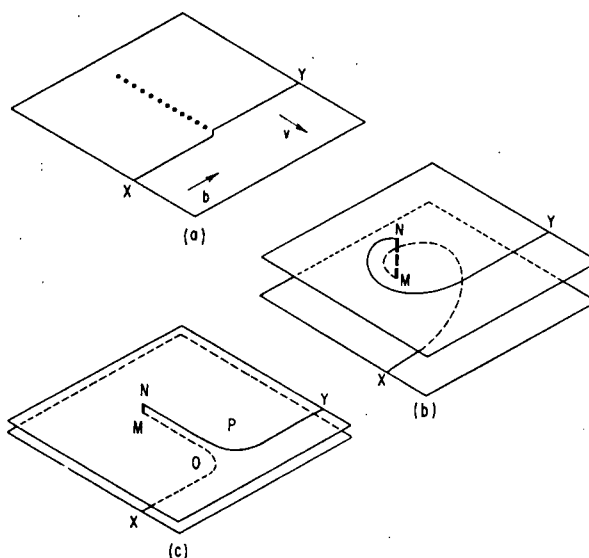


Fig. 74 The effect of jogs of various heights on screw dislocation motion.

Small jogs (1b-2b) can move non conservatively along with the dislocation leaving a row of point defects behind (a). This process may be thermally activated and therefore rate controlling. Very large jogs do not move and can act as pinning points for single ended Frank-Read sources.(b). Intermediate jogs (3b-300b) however can lead to the formation of an edge

dislocation dipole (c) and after pinching off, to the formation of an elongated loop on a non basal plane. Such dipoles and loops have been observed in a variety of metal systems.

(iii) Sessile dislocation loops which contain a stacking fault and have a Burgers vector  $\frac{1}{2}c + p$ , may be produced by the collapse of vacancy discs as postulated by Seeger<sup>25</sup>. Berghezan<sup>63</sup> has observed such loops on basal planes in zinc foils which were heavily deformed at +20°C. Similar loops were observed to form by Price<sup>93</sup> due to ion damage in the electron microscope. The temperature range studied by Price extended down to -100°C. Whether such loops will contribute to work hardening will depend on the rate of loop production compared to the strain rate imposed on the system. The rate of loop production in turn will depend on the supersaturation of vacancies in a given area and the thermal energy available for vacancy migration.

(iv) A fourth type of loop formation was observed in considerable detail by Price. Elongated sessile loops with Burgers vectors  $c + a$  were observed to form on the basal planes by the multiple cross glide of  $\{11\bar{2}2\}$   $\langle 11\bar{2}3 \rangle$  dislocations. The stages in the formation of these loops are illustrated in Fig. 75. It was observed that the loops acted as strong barriers to the motion of basal dislocations on the same glide plane and also produced a strong elastic interaction with other basal dislocations on parallel glide planes as long as the distance between the plane of the dislocation and the loop plane was not greater than the loop width.

A summary of the various types of loops is given in Table 13. The different types of dislocations possible in the hexagonal system are illustrated for clarity in Fig. 76.

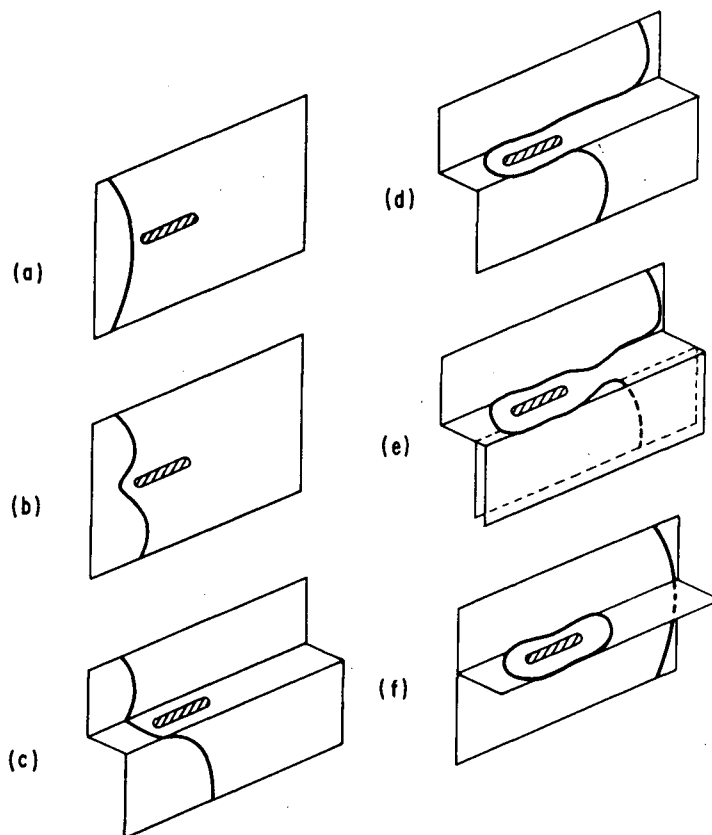


Fig. 75 Stages in the formation of an elongated loop on the basal plane by the cross glide of a  $\{11\bar{2}2\} \langle 11\bar{2}3 \rangle$  screw dislocation

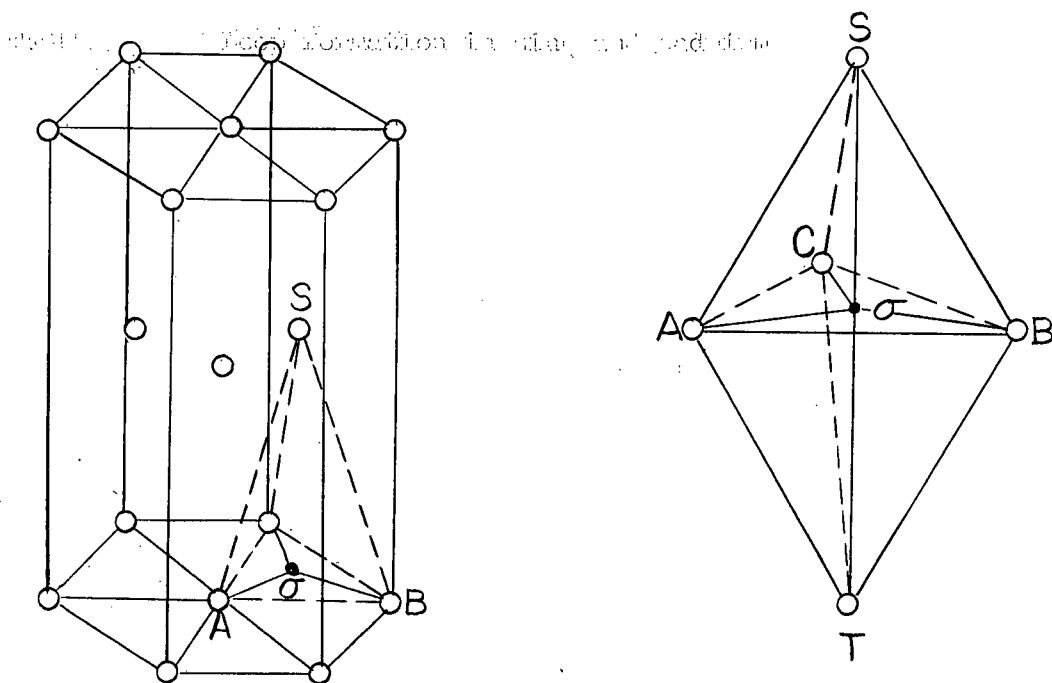
The various types of loop formation have been described in detail because it is thought that this debris may be a principal source of obstacles leading to hardening due to the lack in the hexagonal system of strong Cottrell-Lomer barriers.

Comprehensive studies concerning the annealing behaviour of loops during deformation have only been carried out for those formed as a result of  $\{11\bar{2}2\} \langle 11\bar{2}3 \rangle$  dislocation motion. Price has come to the following conclusions regarding the behavior of these loops in zinc and cadmium.

(i) At temperatures below  $T_H = .27$ , the loops are completely stable and can act as strong barriers to the motion of basal dislocations.

TABLE 13 Loop formation in zinc and cadmium.

| Method of Formation  | Plane of Loop | Burgers Vector   |
|--|---------------|--|
| (i) Behind moving basal edges as in Fig.73                               | Non basal     | a  |
| (ii) Cross glide of basal screws   | Non basal     | a  |
| (iii) Condensation of vacancies  | Basal         | $\frac{1}{2}c + p$                                     |
| (iv) Cross glide of $\{11\bar{2}2\}$ $\langle 11\bar{2}3 \rangle$ screws | Basal         | $c + a$<br>can decompose to<br>c or $\frac{1}{2}c + p$ |



| <u>Kind</u> | <u>Type</u>     | <u>Number</u> |
|-------------|-----------------|---------------|
| Perfect     | AB = a          | 6             |
|             | ST = c          | 1             |
|             | SA + BT = c + a | 6             |
| Imperfect   | Aσ = p          | 3             |
|             | σS = 1/2 c      | 2             |
|             | AS = 1/2 c + p  | 3             |

Fig. 76 Dislocations in hexagonal close packed crystals (after Dorn<sup>86</sup>).

(ii) At temperatures between  $T_H = .27$  and  $T_H = .40$  the elongated loops break up into rows of circular loops by a process of pipe diffusion. The driving force for splitting is supplied by the potential decrease in line energy. The area within the elongated loops is conserved during the splitting operation and the rate at which splitting occurs increases with increasing temperature. Price envisaged that the activation energy for such a process will be equal to  $U_j + U_p$  where  $U_j$  is associated with the required jog formation and  $U_p$  is the pipe diffusion energy. Implicit in the concept of loop splitting as opposed to loop shrinkage is that  $U_j + U_p$  must be less than the self diffusion energy  $U_D$ .

(iii) At temperatures above  $T_H = .40$  the circular loops gradually disappeared by a process of climb. The measured activation energy for the shrinkage of loops was found to be equal to the self diffusion energy.

The observations of Price are of particular significance with regard to the present work in that the temperature region above which loop splitting occurs (.27), is similar to that above which temperature and strain rate independent linear work hardening disappear in polycrystalline zinc and cadmium and above which there is a decrease in the hardening rate associated with both Stage I and Stage II deformation of single crystals.

### 3.2. DYNAMIC RECOVERY

In a very broad sense dynamic recovery may be related to either of the following processes:

- i) cross slip
- ii) diffusion controlled processes

### 3.2.1. Cross Slip

Cross slip is known to be a dynamic recovery mechanism in f.c.c. metals. In hexagonal metals, cross slip must be looked at from a slightly different point of view. It may be a required mechanism to permit basal dislocations to move readily onto non basal planes and thereby allow for the operation of additional slip systems. On the other hand it may operate as an adjunct to the operating systems in order to allow dislocations to move around barriers and therefore relieve points of stress concentration. Only under the latter condition would cross slip be classified as a dynamic recovery process.

Cross slip has not been observed under normal light microscopy in either zinc cadmium or magnesium. However Lally using replicas has observed it during the stage I deformation of magnesium at +20°C. Therefore replica studies on polycrystalline zinc and cadmium are currently in progress to establish whether cross slip occurs to a significant degree. It must occur on a limited scale in order to account for the loop formation behind moving basal dislocations described in the previous section. However such isolated instances are not expected to materially affect the flow stress. Although it is true that such cross slip does allow for the circumvention of obstacles the net result of the overall process is the production of sessile loops which will act as strong barriers to further dislocation motion.

89

The observations of Lally and Hirsch indicate that during the Stage I deformation of magnesium, the dislocation structure consists of a high density of elongated edge dipoles. Very few screws were observed. It was postulated that the edge dipoles were formed by the trapping of edge components from different sources on nearby glide planes. Screws of opposite

sign on the other hand can annihilate leading to a low screw density. Under such conditions, it could be postulated that dynamic recovery in magnesium is associated with the temperature at which cross slip can occur leading to a lower overall dislocation density and a different dislocation configuration.

Similar observations to those of Lally cannot be made on zinc or cadmium because of the higher effective temperature at +20°C which will give rise to a considerable dislocation rearrangement during the time necessary for foil preparation. The observations on magnesium however are of importance in that it is tempting to invoke cross slip as the mechanism of dynamic recovery. However on a more macroscopic scale the interpretation becomes more complex. Conrad<sup>16, 18</sup> has observed a similar temperature dependence of  $\theta_1/G$  in magnesium to that observed in zinc and cadmium. Specifically  $\theta/G$  remains constant below approximately  $T_H = .23$  and decreases above this temperature. Therefore the effective temperature above which the hardening rate decreases in all three metal systems is approximately the same. However the ease of cross slip is related to the stacking fault energy in that the partials must recombine before the process can occur. Although there is considerable controversy with regard to the magnitude of the stacking fault energies in the three systems, it is generally thought that the stacking fault energy of magnesium is appreciably higher than that of either zinc or cadmium.

Because of the association between the stacking fault energy and cross slip it would not be expected that all three metals will undergo dynamic recovery at the same effective temperature. Therefore it is not possible to link dynamic recovery to cross slip.

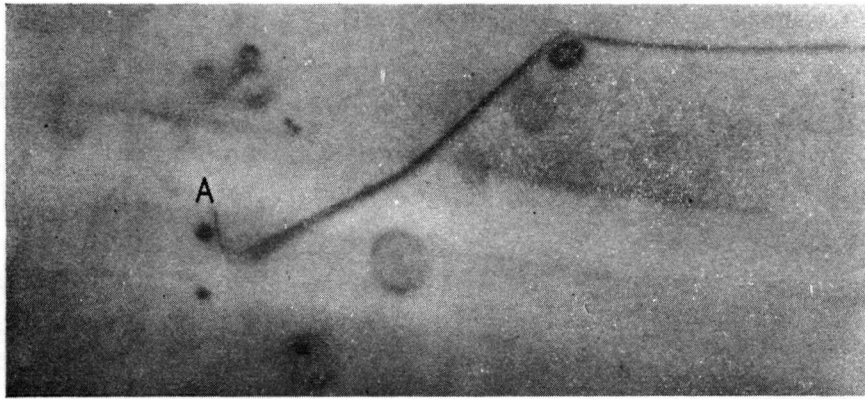
### 3.2.2. Diffusion Controlled Processes

Dislocation climb when governed by the self diffusion energy  $U_D$  was not observed by Price at temperatures below  $T_H = .4$ . Therefore it cannot be considered as a dynamic recovery mechanism in the region of  $T_H = .26$ .

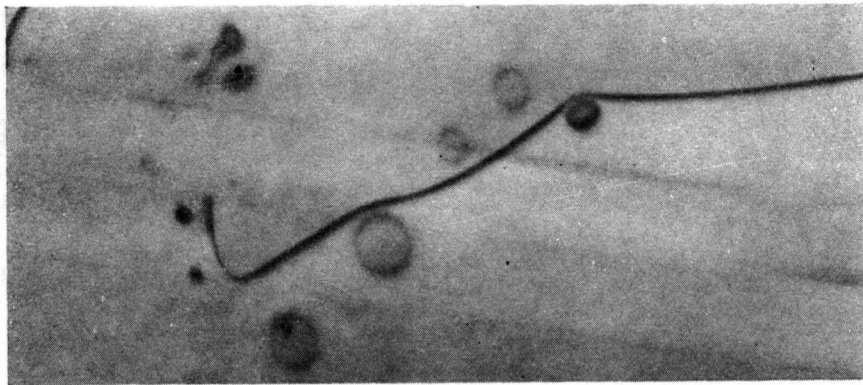
Kroupa and Price<sup>88</sup> have observed that above  $T_H = .26$  in zinc circular  $c + a$  or  $c$  loops produced behind  $\{11\bar{2}2\}\langle 11\bar{2}3 \rangle$  screws can move under the stress associated with the interaction of the loops with approaching basal dislocations (Fig. 78). This motion was termed conservative climb since it did not involve self diffusion but rather the generation of vacancies on one side of the loop and their subsequent motion along the loop to the other side. The activation energy for conservative climb will therefore be the pipe diffusion energy  $U_p$ .

Such loop instability is a mechanism of dynamic recovery since, as observed by Price, the normally sessile loops act as strong barriers to basal dislocation motion. Loop motion by conservative climb should therefore result in a considerable relief of the back stress associated with pile-ups behind the loops.

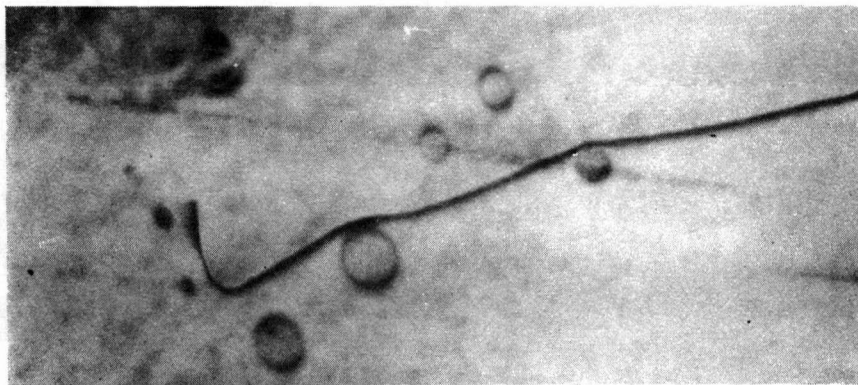
In the present work, extensive  $\{11\bar{2}2\}\langle 11\bar{2}3 \rangle$  slip was observed in polycrystalline zinc and cadmium. Therefore a significant concentration of basal loops should be formed. The value of  $\Delta G_0$  at yield for polycrystals at temperatures above  $T_H = .26$  was determined to be almost identical for both zinc and cadmium at  $.6 \pm .1$  e.v.<sup>96</sup> Friedel has stated that the expected values of the pipe diffusion energy in zinc and cadmium are .62 e.v. and .57 e.v. respectively. From an energetic point of view it is therefore



(a)



(b)



(c)

0.1 $\mu$

Fig. 77

Sequence of transmission electron micrographs showing the 'conservative climb' motion of a dislocation loop with a  $[0001]$  Burgers vector due to its interaction with a moving edge dislocation with a  $\frac{1}{3}[1120]$  Burgers vector. The plane of the micrograph is parallel to the basal plane of the zinc platelet.

(after Price ).

possible to postulate that dynamic recovery is associated with the conservative climb of basal loops. Since the energy required for elongated loop breakup ( $U_p + U_j$ ) is greater than that of conservative climb ( $U_p$ ), it may be argued that the rate controlling process is actually that of loop breakup. However because of the higher dislocation density in real crystals as opposed to Price's specimens, it is probable that the edge dipole will tend to pinch off earlier in the sequence of loop formation. Therefore the process of loop splitting is not as important a process.

In order for such a conservative climb interpretation to be valid for single crystals, it is necessary to postulate that some  $\{11\bar{2}2\}$   $\langle 11\bar{2}3 \rangle$  slip can occur during both Stage I and Stage II single crystal deformation.

<sup>13</sup>  
Basinski has shown that the Cottrell-Stokes law is only strictly obeyed in magnesium at temperatures below 46°K. However the deviations that occur at higher temperatures are not particularly severe. In any case there is a considerable increase in  $\gamma^*$  during both stages of deformation which was interpreted by Basinski in terms of an increasing forest concentration.

Essentially similar results were obtained during this work on cadmium single crystals. Although the Cottrell-Stokes law was not obeyed during Stage I, there was a considerable decrease in the activation volume at all temperatures studied. At -196°C "v" decreased from  $30 \times 10^{-20}$  cm.<sup>3</sup> to  $5 \times 10^{-20}$  cm.<sup>3</sup> Based on an intersection mechanism this corresponds to approximately a 30 fold increase in the forest density during Stage I. It would appear therefore that there is some non basal activity during Stage I and this could lead to a significant concentration of basal loops.

Dynamic recovery to this point has been associated only with the conservative climb of basal loops produced behind 2<sup>nd</sup> order pyramidal screws. However the pipe diffusion process may also have a significant effect on the nature and mobility of the other types of loop debris mentioned in the previous section. Since this debris is produced only as a result of basal dislocation motion, if similar processes involving conservative climb can occur, then it is not necessary to postulate a change in the forest density during single crystal deformation in order to explain dynamic recovery. Before this interpretation can proceed it will be necessary to know more about the annealing characteristics of debris.

As an alternative to a pipe diffusion mechanism, there is a distinct possibility that recovery may be associated with the annealing characteristics of excess vacancies produced during deformation. Resistivity studies made by Sharp, Mitchell and Christian<sup>90</sup> on cadmium single crystals and polycrystals deformed 12%, indicated the existence of an annealing peak in the vicinity of  $T_H = .25$ . They determined the activation energy to be  $.25 \pm .2$  e.v. and associated the peak with single vacancy migration.

Peiffer and Stevenson<sup>91 92</sup> in a similar study observed two annealing peaks, one at  $T_H = .23$  and another at  $T_H = .28$ . The activation energies were .24 and .30 e.v. respectively. They believed that one of the peaks was associated with single vacancy migration although they were not sure which one. The expected value for the energy associated with vacancy motion in cadmium is .41 e.v.<sup>97</sup> This is somewhat lower than the  $.6 \pm .1$  e.v. activation energy found to control the dynamic recovery of zinc and cadmium. However due to the approximations involved in the rate theory expressions when applied to deformation, it is not outside the realm of probability that vacancy migration and dynamic recovery are somehow linked.

The exact nature of such a relationship is rather vague. If the net result of migration is the production of basal dislocation loops by vacancy condensation, then it would be expected that such loops will contribute to hardening and will not lead to a recovery effect. On the other hand by annealing out at edge dislocations excess vacancies can cause climb allowing for the circumvention of obstacles. Climb therefore can occur at lower temperatures than  $T_H = .4$  and under such conditions is controlled only by the vacancy migration energy. Although Price did not observe climb below  $T_H = .4$ , it is probable that the excess vacancy concentration in the platelets used for study was quite low due to the low dislocation density and the availability of the specimen surface.

In summary it must be concluded that the exact cause of the dynamic recovery occurring in the vicinity of  $T_H = .26$  cannot be definitely established at this time. However because of the better correlation of energies, it is thought that the most likely process is one involving pipe diffusion leading to the conservative climb of normally sessile basal dislocation loops.

### 3.3. THE MECHANICAL EQUATION OF STATE

It was shown in section 2.2.3. that a mechanical equation of state could be formulated for polycrystals in the regions of linear hardening below  $T_H = .26$ . Only under these conditions is it possible to obtain equivalent states at an equal value of strain when deformation occurs at different temperatures.

The concept of dynamic recovery being associated with the conservative climb of loops is consistent with the above observations. Basal loops should remain stable in the linear hardening regions. The

overall dislocation configuration at a given value of strain will therefore be independent of temperature.

However once conservative climb can occur, it is not expected that equivalent states will be found at equal strains because of the temperature dependence of the rate of loop annealing as observed by Price.

### 3.4. THE COTTRELL-STOKES LAW

It was observed that at all temperatures the Cottrell-Stokes law was not strictly obeyed during the Stage I deformation of cadmium single crystals or during the early strain regions of polycrystals. In both cases the  $\frac{\Delta\sigma}{\sigma}$  ratio decreased with increasing strain. In effect this means that the rate of increase of  $\sigma^*$  was somewhat less than the rate of increase of  $\sigma_G$ . In polycrystals this may be related to grain boundary effects. This early region of strain is associated with the gradual build up of a stable dislocation configuration at the grain boundaries (pile ups). This contribution to stress will be athermal, contributing only to  $\sigma_G$ . It is therefore expected that the increase in  $\sigma_G$  will be somewhat in excess of  $\sigma^*$  which is associated with intragranular processes.

Although  $\frac{\Delta\gamma}{\gamma}$  decreases during Stage I hardening there is a significant decrease in the activation volume. This implies that there is an increase in the value of  $\gamma^*$  with increasing strain although not as great as the increase in  $\gamma_G$ . This observation is not consistent with the theory of Seeger<sup>24</sup> regarding Stage I hexagonal metal deformation. He assumes that  $\Theta_I/G$  can be calculated by only considering the elastic interactions between individual parallel dislocations and that the contribution to  $\Theta_I/G$  from  $\gamma^*$  is negligible. For such a theory to be correct, the activation volume must remain constant during Stage I. Because of the marked change

in "v" in cadmium, it must be concluded that  $\Theta_I/G$  represents an important contribution to the observed rate of hardening and cannot be neglected.

### 3.4.1. Obeysance

The Cottrell-Stokes law is obeyed only during the linear hardening regions of polycrystals and during the Stage II hardening of single crystals below  $T_H = .26$ . In order to postulate the origin and relationship between  $\sigma^*$  and  $\sigma_G$  it is necessary to know how twinning may affect the two stress components. As observed in single crystals the formation of a twin does not affect the flow stress required for further deformation. Basal slip within a twinned region therefore must represent an important contribution to deformation only immediately after the twin formation before the macroscopic observed stress returns to its previous value. Therefore although twinning may affect the work hardening rate, it does not change the instantaneous relative values of the two stress components.

This "status quo" condition during deformation may also be applied to the nature of the dislocation configuration in the neighbourhood of grain boundaries. Once a stable configuration is obtained it will be assumed that hardening becomes intragranular and the component of  $\sigma_G$  associated with boundaries need not be considered with regard to the Cottrell-Stokes law.

The athermal component of stress is therefore associated with some combination of the following components:

- i) the interaction of forest and glide dislocations
- ii) the interaction of loops and glide dislocations

It will be assumed that  $\sigma^*$  arises due to an intersection mechanism. The Cottrell-Stokes obeyance can therefore be interpreted in terms of an increasing forest density with increasing strain.  $\sigma^*$  remains proportional to both athermal stress components because the basal loop density will be a function of the forest density.

### 3.4.2. Dynamic Recovery

It has been shown that in both single crystals and polycrystals, dynamic recovery is associated with increasing values of  $\frac{\Delta\sigma}{\sigma}$ . This means that the rate of increase of  $\sigma_G$  is somewhat less than that of  $\sigma^*$ . If recovery is related to loop instability and if a significant proportion of  $\sigma_G$  is derived from the nature of loop-dislocation interactions, then it is expected that  $\sigma_G$  will increase at a lower rate because of the relief of back stress which occurs because of obstacle motion.

### 3.5. RATE CONTROLLING PROCESSES BELOW $T_H = .26$

It was proposed that forest intersection is the rate controlling process governing yield in single crystals and polycrystals below  $T_H = .26$ . This was done without any consideration of possible alternate mechanisms. These will now be discussed.

#### 3.5.1. Peierls Stress

The Peierls stress for the motion of basal dislocations is very low because of the close-packed nature of the basal plane. It cannot therefore be considered as a rate controlling process. However during polycrystalline deformation when non basal slip must occur, the Peierls

stress associated with movement on the corrugated pyramidal planes may be significant and rate controlling.

The activation volume at yield in 25 $\mu$  cadmium at -196°C based on a shear stress conversion of  $\gamma = \frac{\sigma}{2}$ , was  $.30 \times 10^{-20}$  cm.<sup>3</sup>. In terms of a basal dislocation where  $a = 2.97 \text{ \AA}$ , this gave a value of  $110b^3$ . However in terms of a c+a pyramidal dislocation this reduces to about  $17b^3$  a much more acceptable value for the Peierls mechanism.

However it was also observed (Table 9) that the activation volume increased with increasing grain size, a trend not expected for the Peierls mechanism. From Fig. 68 it was observed that for a given grain size "v" decreased substantially with increasing strain. If the Peierls mechanism is rate controlling the activation volume should not vary with strain.

Since the Peierls mechanism is not compatible with all of the experimental observations, it can be rejected as a possible controlling mechanism.

### 3.5.2. Cross Slip

Cross slip has been considered in section 3.3. as a possible mechanism of dynamic recovery. It may also be argued that cross slip could control yield at temperatures below  $T_H = .26$  if it is required in order for basal dislocations to move onto non basal planes and thereby control the extent of non basal slip. However this argument cannot be validated in that the only non basal traces that are observed in zinc and cadmium arise from  $\{11\bar{2}2\} \langle 11\bar{2}3 \rangle$  slip. This is not a cross slip system. Also as pointed out in section 1.4.1., when  $\{11\bar{2}2\} \langle 11\bar{2}3 \rangle$  slip occurs, the number of independent systems that can operate is sufficient to promote extensive polycrystalline

deformation. Therefore cross slip is not a necessary process in order for deformation to proceed.

### 3.5.3. The Non Conservative Motion of Jogs

<sup>98</sup> Frank first postulated that a jogged screw dislocation can move only if the jog leaves behind it either a row of vacancies or interstitials depending on its sign and direction of motion. The conservative motion of vacancy jogs is thought to be associated with a relatively high activation energy and therefore need not be considered.

It is usually not possible to distinguish between a jog or an intersection mechanism merely from the values of rate theory parameters. Both processes are expected to have similar values of activation volume in the range from  $10^2 b^3$  to  $10^4 b^3$ .

The concept of a jog mechanism being rate controlling is not strongly supported by experimental observations. It was advanced by Mott<sup>99</sup> mainly to explain the nature of the flow stress variations in copper single crystals. In copper it has been observed that the flow stress is almost temperature independent between  $T_H = .2$  and  $T_H = .5$ . At higher temperatures there is a significant drop in stress. Mott therefore proposed that at temperatures below  $T_H = .5$ , the self diffusion process required for the mechanism to proceed cannot occur at an appropriate rate in terms of the applied strain rate. The vacancy nucleation at the jog is therefore completely athermal leading to a temperature independent flow stress. It was also assumed by Mott that energy is not available for vacancy migration away from the region of the jog. Under such conditions any thermal fluctuation will tend to move the jog forward a single atomic spacing, but if the vacancy

produced is not mobile, the jog can be pulled back by the interaction with the vacancy produced. Therefore the flow stress should not be temperature dependent below  $T_H = .5$ . Above this temperature however where the energy for self diffusion is available, the vacancies produced should be mobile and a temperature dependent flow stress should result.

There are some questionable features of this theory. First of all it is not clear why the nucleation of a vacancy at a jog should be a completely athermal process. The thermal energy available in this temperature range should be sufficient to provide a portion of the energy needed for vacancy nucleation.

Secondly, even if vacancy nucleation is an athermal process, the temperature at which a temperature dependent flow stress occurs should be associated only with the energy for vacancy migration. This should occur at temperatures well below  $T_H = .5$ .

In zinc and cadmium it is believed that single vacancy motion can occur at appreciable rates above  $T_H = .25$ . Therefore below this temperature according to the jog mechanism, the flow stress of zinc and cadmium will be governed by the athermal process of vacancy nucleation. This should lead to a temperature independent flow stress. This was not observed. There is a considerable increase in the flow stress in both systems below  $T_H = .26$ . It is therefore unlikely that the non conservative motion of jogs is the rate controlling process at low temperatures in zinc and cadmium.

#### 3.5.4. Intersection

The postulate of forest intersection was not made merely

because other mechanisms could not explain all of the experimental observations. There are no major inconsistencies with the forest mechanism. The estimate of forest spacings of Table 9 made from activation volume data are reasonable for the systems involved. The variation of activation volumes at  $-196^{\circ}\text{C}$  from  $1.1 \times 10^{23}$  b for  $25\mu$  cadmium to  $1.1 \times 10^{24}$  b<sup>3</sup> for single crystals is within the expected range for intersection. The variation has been shown to arise from the expected difference in the forest spacing as the grain size changes and is not due to a change in the force distance curve. The non linear variation of  $\Delta G$  with temperature can be interpreted from the forest mechanism to be due either to a change in the stacking fault energy with temperature or to a change in the effective value of the forest spacing due to the manner in which a dislocation bows out under the influence of a stress.

#### 4. SUMMARY AND CONCLUSIONS

The observations and interpretations of the deformation characteristics of zinc and cadmium may be summarized as follows:

- 1) Negative work hardening beyond the point of maximum stress in polycrystalline zinc and cadmium at temperatures above  $T_H = .4$  is associated with recrystallization. However at temperatures up to at least  $T_H = .5$  recrystallization does not go to completion during deformation. At least 50% of the structure outside the necked area remains unrecrystallized.
- 2) Grain boundary migration can occur in the initial hardening regions and is particularly important as a recovery mechanism above  $T_H = .4$ . Slight boundary corrugations were observed in cadmium at temperatures down to  $-95^\circ\text{C}$  suggesting that the change in fracture mode from ductile shear to intergranular fracture which occurs at  $-120^\circ\text{C}$  is associated with the cessation of recovery by boundary migration.
- 3)  $\{11\bar{2}2\}\langle 11\bar{2}3\rangle$  is the only non basal slip system observed during polycrystalline deformation. It is more prevalent as the temperature decreases. At  $+20^\circ\text{C}$  it is more extensive in zinc than in cadmium at an equivalent temperature. The non basal traces are wavy and discontinuous at elevated temperatures. At low temperatures they are straight and tend to concentrate into bands. Qualitatively it appears that the amount of non basal slip increases as the grain size decreases.
- 4) The formation of low angle boundaries during deformation is similar in both systems and does not vary in nature or extent with temperature.

- 5) In cadmium single crystals the resolved basal shear stress at which Stage I ends is independent of temperature in the range from  $-50^{\circ}\text{C}$  to  $-196^{\circ}\text{C}$ .
- 6) Twinning is a general feature of Stage II cadmium deformation at temperatures below  $-50^{\circ}\text{C}$ .
- 7) A region of temperature and strain rate independent linear work hardening develops below  $T_H = .26$  in both polycrystalline zinc and cadmium. The amount of strain associated with linear hardening increases as the temperature decreases. The rate of hardening is similar in both systems.
- 8) Cadmium single crystals also show constant Stage I and Stage II hardening rates below  $T_H = .26$  and continuously decreasing hardening rates above this temperature. This is similar to the behaviour of zinc and magnesium.
- 9) The maximum linear hardening rate of polycrystalline cadmium at  $-196^{\circ}\text{C}$  varies linearly with  $d^{-\frac{1}{2}}$ . The extrapolated value of  $\theta$  to  $d^{-\frac{1}{2}} = 0$  corresponds to the tensile Stage II hardening rate of single crystals. This change in hardening rate can be explained in terms of a change in the frequency of  $\{11\bar{2}\}\langle 11\bar{2}\rangle$  slip.
- 10) The Cottrell-Stokes law is not strictly obeyed for either temperature or strain rate change tests. Obedience is only observed during the linear hardening of polycrystals and during Stage II single crystal hardening below  $T_H = .26$ . Dynamic recovery is associated with increasing values of  $\frac{\Delta\sigma}{\sigma}$ .
- 11) In polycrystalline zinc and cadmium equivalent states at equal strains

are only obtained during linear hardening. Therefore only in these regions can a mechanical equation of state be formulated.

- 12) Yield at temperatures below  $T_H = .26$  can be interpreted in terms of a forest intersection mechanism. The total activation cannot be estimated but is somewhat in excess of .8 e.v. in cadmium .
- 13) It is probable that dynamic recovery above  $T_H = .26$  is associated with a diffusion controlled process. The most likely mechanism involves the conservative climb of normally sessile basal loops by a process of pipe diffusion. The experimental activation energy for yield in polycrystalline zinc and cadmium is  $.6 \pm .1$  e.v.

5. SUGGESTIONS FOR FUTURE WORK

Several lines of investigation are immediately recognized from the results of this work. These include:

- 1) An extension of testing to temperatures below  $-196^{\circ}\text{C}$  in order to completely establish the flow stress-temperature relationships.
- 2) A thorough electron microscopy replica study on slip traces in order to establish the significance of cross slip in polycrystalline zinc and cadmium.
- 3) An extensive resistivity study of various deformed states in order to establish the relevance of single vacancy motion to dynamic recovery.

Rate Theory

As mentioned in section 2.1. when deformation is governed by a single rate controlling process, the shear strain rate may be expressed by

$$\dot{\gamma} = \dot{\gamma}_0 e^{-\Delta G/kT} \dots\dots\dots(1)$$

A more general expression as indicated by Dorn<sup>81</sup>, is given by

$$\dot{\gamma}_i = \dot{\gamma}_{0_i} e^{-\Delta G_i/kT} \dots\dots\dots(2)$$

where "i" refers to the i<sup>th</sup> kind of mechanism.

Several different thermally activated processes can operate at the same time. If they occur sequentially then the steady state strain rate observed during creep will be associated with the slowest process, i.e. the process with the highest activation energy. If the strain rate is fixed as is usual in a tensile test, then the magnitude of the stress will reflect the particular controlling process in that any activation process occurs under the combined influence of thermal energy and the effective stress.

An example of sequential processes would be the movement of a jogged screw dislocation during pyramidal glide in a hexagonal metal. Energy must be supplied for the non-conservative motion of the jog, for forest intersection, to overcome the Peierls stress and for possible cross slip around obstacles. If this sequence of processes must occur before deformation can proceed, then one of the processes will be rate controlling. Which one will depend on the nature of the effective stress on the dislocation at any stage of the process. The stress will increase to a value at which the thermal energy available at that temperature is sufficient to continue deformation

at the required strain rate. Under such a sequential system it is quite possible that the rate controlling process can change during deformation from one of the aforementioned processes to another.

If however two or more independent processes control the strain rate, then the total strain rate is given by  $\dot{\gamma} = \sum_i \dot{\gamma}_i$  and the application of simple rate theory to deformation is not possible.

If it is assumed that a single process is rate controlling then from (1)

$$\Delta G = -kT \ln \dot{\gamma} / \dot{\gamma}_0 \dots\dots\dots(3)$$

If it is now assumed that at a constant dislocation configuration the strain rate is given by

$$\dot{\gamma} = \dot{\gamma}(T, \gamma^*) \dots\dots\dots(4)$$

then by differentiating (4) with respect to temperature at constant effective stress and recombining

$$\Delta G = -kT^2 \left( \frac{\partial \ln \dot{\gamma} / \dot{\gamma}_0}{\partial \gamma^*} \right)_T \left( \frac{\partial \gamma^*}{\partial T} \right)_{\dot{\gamma} / \dot{\gamma}_0} + T \left( \frac{\partial \Delta G}{\partial T} \right)_{\gamma^*} \dots\dots\dots(5)$$

Since in general the activation entropy is given by

$$\Delta S = - \left( \frac{\partial \Delta G}{\partial T} \right) \dots\dots\dots(6)$$

then the activation enthalpy is given by

$$\Delta H = -kT^2 \left( \frac{\partial \ln \dot{\gamma} / \dot{\gamma}_0}{\partial \gamma^*} \right)_T \left( \frac{\partial \gamma^*}{\partial T} \right)_{\dot{\gamma} / \dot{\gamma}_0} \dots\dots\dots(7)$$

The activation volume defined as

$$v = bdl \dots\dots\dots(8)$$

where

- b = Burgers vector
- d = activation distance
- l = length of dislocation  
undergoing activation.

is given by the stress dependence of  $\Delta G$  such that

$$v = -\left(\frac{\partial \Delta G}{\partial \tau^*}\right)_T = kT \left(\frac{\partial \ln \dot{\gamma} / \dot{\gamma}_0}{\partial \tau^*}\right)_T \dots\dots\dots(9)$$

Therefore activation energy and activation volume can be determined from reversible temperature and strain rate changes during deformation. Probably the largest source of error in this type of calculation can be traced to the lack of reversibility in some systems. If  $\dot{\gamma}_0$ , which is a function of the active dislocation density, changes during the strain rate change, then the measured value of  $\Delta \tau^*$  and subsequent calculated values of  $v$ ,  $\Delta G$ , and  $\Delta H$  will be in error.

In order to calculate  $\Delta G$ , it is necessary to develop an expression whereby the entropy term  $\left(\frac{\partial \Delta G}{\partial T}\right)_{\tau^*}$  can be readily evaluated from experimental data. Mitra and Dorn using a graphical technique have attempted such a calculation but in the process appear to have interchanged free energy and enthalpy. Schoeck<sup>74</sup> in a consistent thermodynamic treatment has arrived at the following expression for the free energy change (thermal component).

$$\Delta G = \frac{\Delta H + T \frac{\partial \mu}{\partial T} \frac{\gamma_a}{\mu} v}{1 - \frac{T}{\mu} \frac{\partial \mu}{\partial T}} \dots\dots\dots(10)$$

This he claims makes possible a simple calculation of  $\Delta G$  since it only contains terms that can be easily determined from experimental data. However his formulation is based on the questionable relationship

$$\dot{\gamma} = \dot{\gamma} ( T, \gamma_a ) \dots\dots\dots(11)$$

This differs from (4) in the use of the applied stress  $\gamma_a$  instead of the effective stress  $\gamma^*$ . The strain rate for a given system under certain conditions of temperature and applied stress is associated with a certain rate controlling mechanism. This mechanism operates under the combined influence of the thermal energy available and the effective stress  $\gamma^*$ . Ultimately therefore the strain rate and the effective stress are dependent variables and the dependence of  $\dot{\gamma}$  on the macroscopic flow stress  $\gamma_a$  is unjustified.

If  $\gamma^*$  is substituted for  $\gamma_a$  in Schoeck's expression (10), a relationship similar to (10) but containing  $\gamma^*$  instead of  $\gamma_a$  is obtained. Because of the unknown nature of  $\gamma^*$  during deformation, it is difficult to make any reasonable estimate of  $\Delta G$ .

Much of the confusion in the literature concerning rate expressions involves the statement of the basic rate equation (1). It has been common to substitute  $\Delta H$ , the enthalpy change for  $\Delta G$  in (1). When this is done, it is assumed that the entropy term  $e^{-S/k}$  is incorporated into the pre-exponential term  $\dot{\gamma}_0$ . This approximation of the rate equation is valid only if the entropy change does not represent a significant contribution to the overall free energy change and if it does not vary appreciably with temperature or stress.

73

As outlined by Conrad, attempts have been made to calculate the energy of activation including the work done by the effective stress during thermal activation. In this case this "total" activation energy is usually

expressed as

$$\Delta H_o = \Delta H + Fd \dots\dots\dots(12)$$

where

F= the force on the dislocation segment

Since  $Fd = lbd\gamma^* = v\gamma^*$ , therefore

$$\Delta H_o = \Delta H + v\gamma^* \dots\dots\dots(13)$$

where  $v\gamma^*$  represents the work done by the applied stress during thermal activation.

However the energies represented in (13) should be free energies so that

$$\Delta G_o = \Delta G + v\gamma^* \dots\dots\dots(14)$$

A typical force distance diagram is shown in Fig.78 to illustrate the various energy terms. The term  $\Delta G_o$  must be labelled only as the "apparent" activation energy since it does not include the work done by the effective stress before the activated event. The true activation energy is given by the total area under the force distance curve ( $\Delta G_o^*$ ). This can be ascertained only if the conditions under which  $\gamma^* = 0$  are known. When  $\gamma^* = 0$ ,  $\Delta G = \Delta G_o = \Delta G_o^*$ . However even if the critical temperature where  $\gamma^* = 0$  can be accurately established, it must be assumed that the force distance curve does not change with temperature if the value of  $\Delta G_o^*$  found at  $T_c$  is applied to other temperatures where the same rate controlling process is thought to occur. Even if the same process is thought to occur over a range of temperatures, if the stacking fault energy changes with temperature then for some processes the shape of the force-distance diagram can change with temperature.

The calculation of  $\Delta G_o$  is therefore restricted to conditions

of yield when  $\tilde{\gamma}^*$  can be estimated from the yield stress-temperature relationship.

Gregory<sup>11</sup> developed a similar relationship to expression (13) in order to calculate the "total" activation energy. However he used the applied stress  $\tilde{\gamma}_a$  instead of  $\tilde{\gamma}^*$  in the last term. This is unjustified and can lead to serious errors especially when  $\tilde{\gamma}_a \gg \tilde{\gamma}^*$ .

$$\Delta G = ABCA$$

$$vJ^* = ACx_2x_1A$$

$$\Delta G_o = x_1ABCx_2x_1$$

$$\Delta G_o^* = x_oABCx_3x_o$$

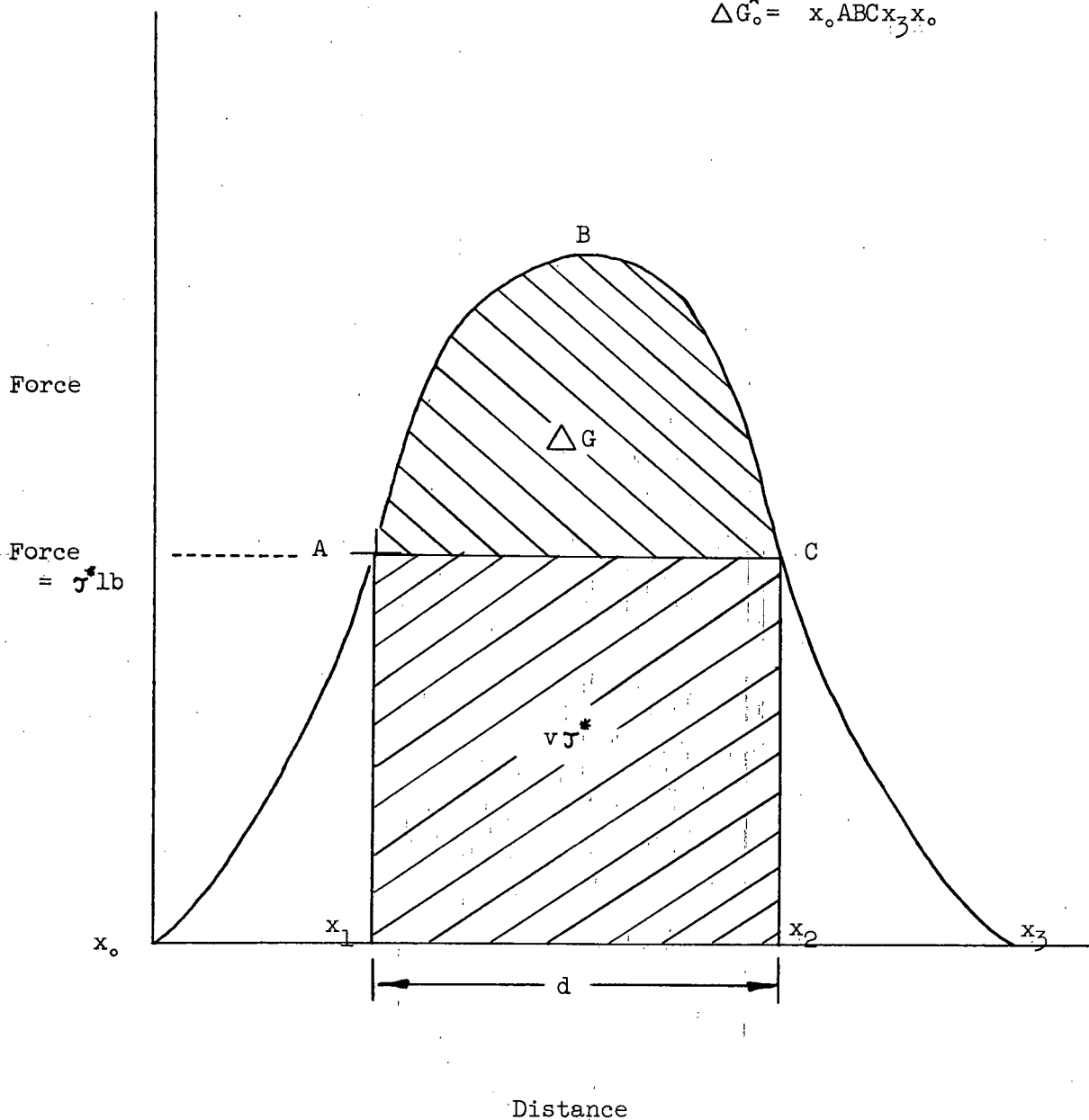


Fig. 78 Typical Force-Distance curve for a thermally activated deformation process.

APPENDIX 2Unloading Yield Points in Cadmium.

During the early stages of deformation when cycling  $25\mu$  and  $400\mu$  cadmium between  $-140^\circ\text{C}$  and  $-196^\circ\text{C}$ , slight yield points as shown in Fig. 79 were observed on reloading at  $-196^\circ\text{C}$ .

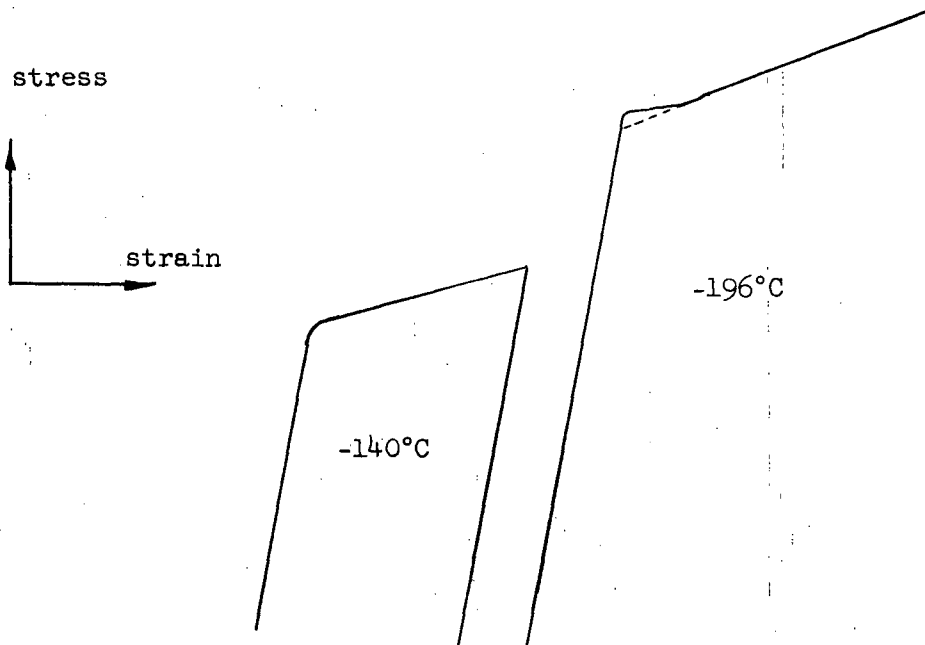


Fig. 79 Unloading yield point in polycrystalline cadmium

These made the determination of  $\Delta\sigma^*$  difficult because of the ambiguity of the yield stress at  $-196^\circ\text{C}$ .

Several authors have observed unloading yield points in f.c.c. metals. Haasen and Kelly<sup>100</sup> and Makin<sup>101</sup> observed yield points in single crystals of aluminum, copper and nickel produced by unloading and reloading. They postulated that Cottrell-Lomer sessiles are produced during unloading causing a higher yield stress on reloading.

Bolling<sup>102</sup> using polycrystalline Ag, Al, Cu, Ni and Pb, found that

unloading yield point phenomena is a common occurrence in f.c.c. metals. He further observed that the magnitude of the stress increase was dependent on the amount of unloading and independent of time. Yield points were only observed however when recovery during the unloading cycle was negligible.

<sup>103</sup>  
Birnbbaum, testing zinc and magnesium single crystals between 77°C and 293°K found no yield points after reloading. Further he observed that in copper single crystals, the magnitude of the stress increase was orientation independent, an observation not consistent with the concept of Cottrell-Lomer sessile production. He therefore postulated that a change occurs during unloading in the nature of glide-forest dislocation interactions.

In order to obtain a better understanding of the yield phenomena in cadmium, 25 $\mu$  and 400 $\mu$  specimens were examined at -196°C. They were deformed using 2% strain increments followed by unloading to a given percentage of the flow stress. Specimens were then held for various periods of time before reloading.

It was found that the holding time up to five minutes had no effect on the magnitude of the flow stress on reloading. However the occurrence of yield points was a function of the amount of unloading as previously observed by Bolling. No yield phenomena was observed until at least 40% of the load was removed.

At low values of strain  $\sigma_a = \sigma_c$  (Fig. 80). However with increasing deformation,  $\sigma_a$  became somewhat greater than  $\sigma_c$ . Bolling observed similar behaviour and explained it in terms of creep during the unloading cycle.

Fig. 81 illustrates the variation of  $\sigma_b/\sigma_a$  with increasing strain. In all cases specimens were unloaded to 10% of the flow stress and held for five minutes before reloading. The unloading operation was continuous and took about ten seconds.

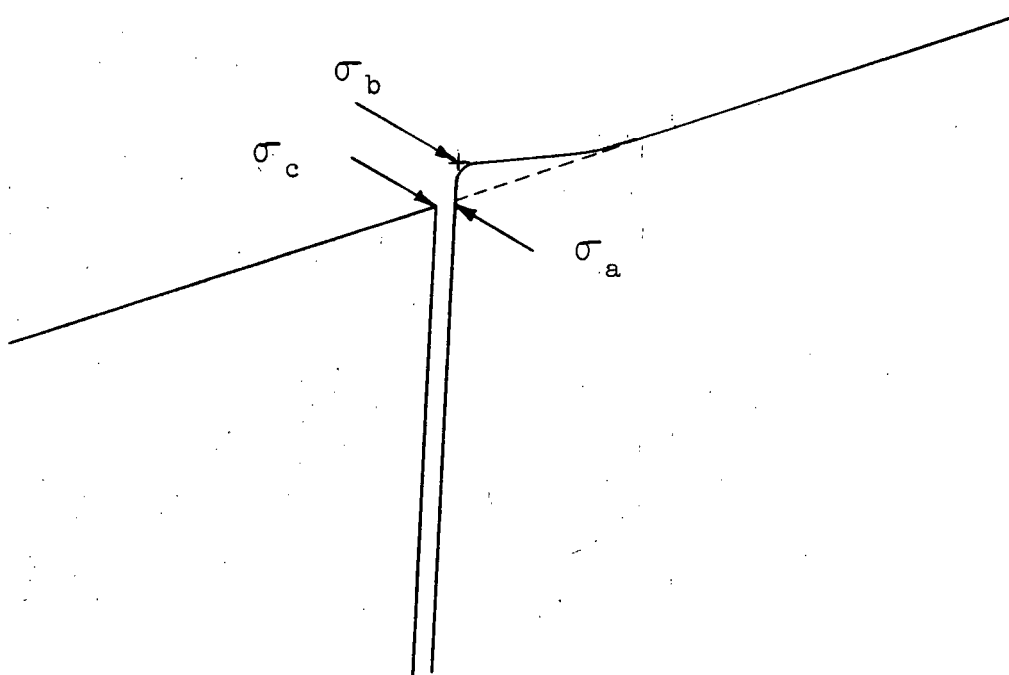


Fig.80 Unloading yield point terminology

It is observed from Fig. 81 that the yield effect is considerably greater in 400 $\mu$  cadmium than in 25 $\mu$ . The values of  $\sigma_b/\sigma_a$  remain approximately constant up to a value of strain which has been previously identified with the start of dynamic recovery at -196°C. Beyond this value of strain,  $\sigma_b/\sigma_a$  decreased and the yield effect gradually disappeared.

Specimens were also tested at -95°C and no yield effects were observed. In fact slight static recovery occurred. The drop in stress associated with unloading and thirty second holding at 10% of the flow stress, is shown as a function of the flow stress in Fig. 82. Therefore during Cottrell-Stokes tests, appropriate corrections were made to  $\frac{\Delta\sigma}{\Delta T}$  to take into account the static recovery occurring during the operation of changing temperatures.

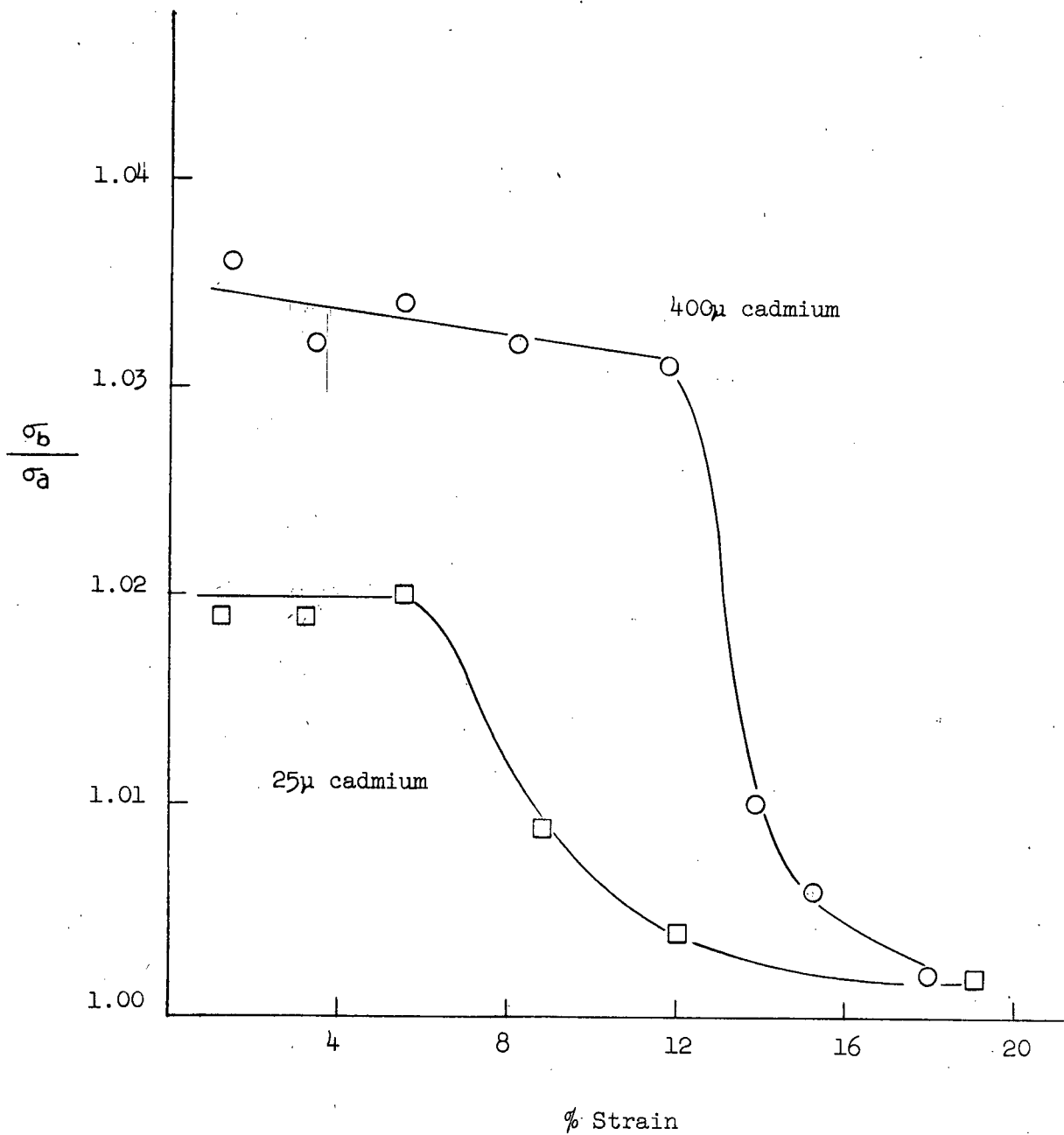


Fig. 81 The variation of  $\frac{\sigma_b}{\sigma_a}$  with strain at  $-196^\circ\text{C}$ .

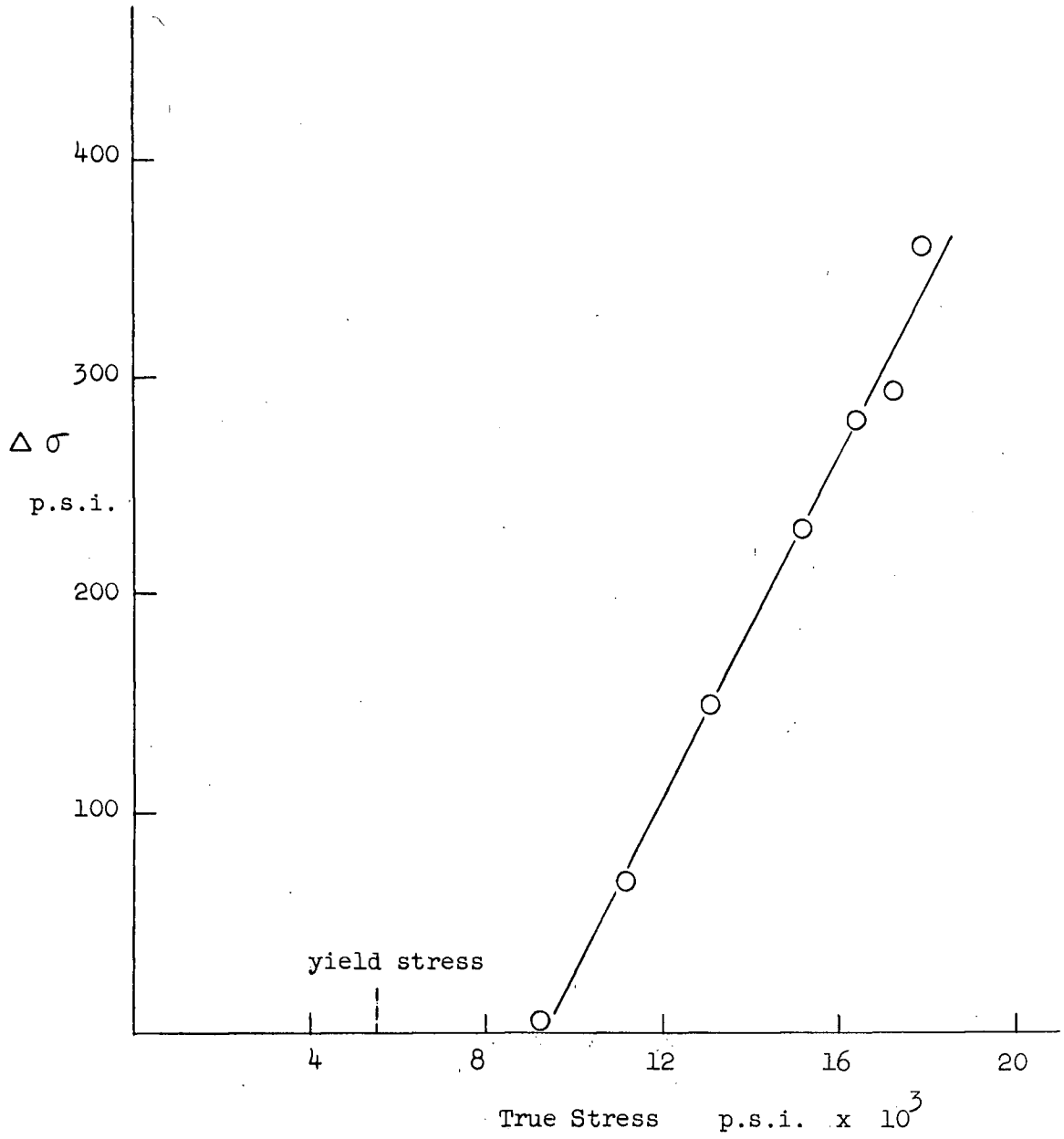


Fig. 82 The decrease in flow stress due to static recovery during interrupted testing of 25 $\mu$  cadmium at  $-95^\circ\text{C}$ . ( 30 second holding at 10% of the flow stress ).

APPENDIX 3

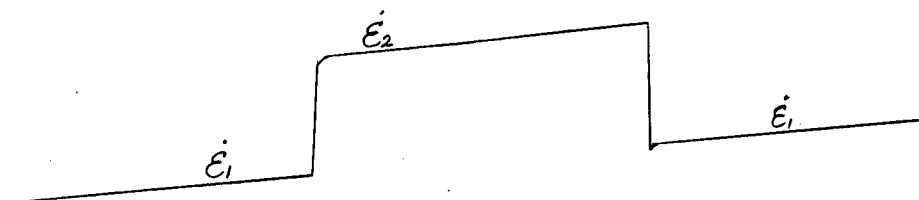
The Determination of  $\Delta\sigma$  from Strain Rate Change Tests

An ideal strain rate change should occur in an instantaneous fashion without an intermediate drop in load or a measurable time lag during the change. These factors become of extreme importance if one is attempting to analyze materials at high effective temperatures where recovery can occur.

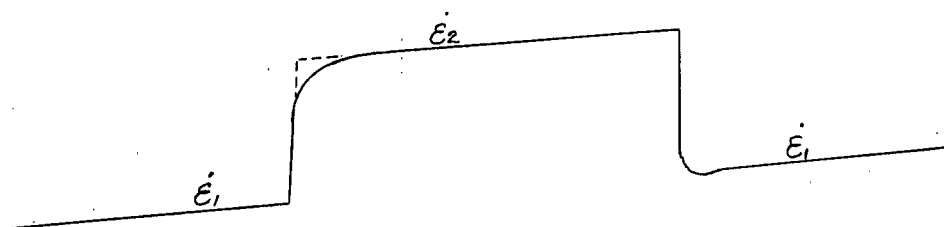
When using an Instron, mechanical difficulties are sometimes responsible for a considerable error in the determination of  $\Delta\sigma$ . Although the Instron used during this work was equipped with an automatic push button crosshead speed change, a considerable time lag was observed during a decrease in strain rate. When the crosshead speed was changed from .02"/min. to .002"/min. there was a delay time of 1.6 seconds during which time the machine stopped. When changing from .2"/min. to .02"/min. the delay time was .8 seconds. However at these higher speeds there was also a slight reversal of the screws during the change which caused a drop in load on the specimen.

There was no measurable delay time associated with a change to an increased crosshead speed. Therefore all  $\Delta\sigma$  values were obtained during an increase in strain rate. In many materials it is necessary to obtain  $\Delta\sigma$  from a decrease in strain rate because of the appearance of distinct yield points on increasing the strain rate. For this work it was decided that any error arising from any slight yield phenomenon would be much less than that resulting from the time delay during a decrease in strain rate.

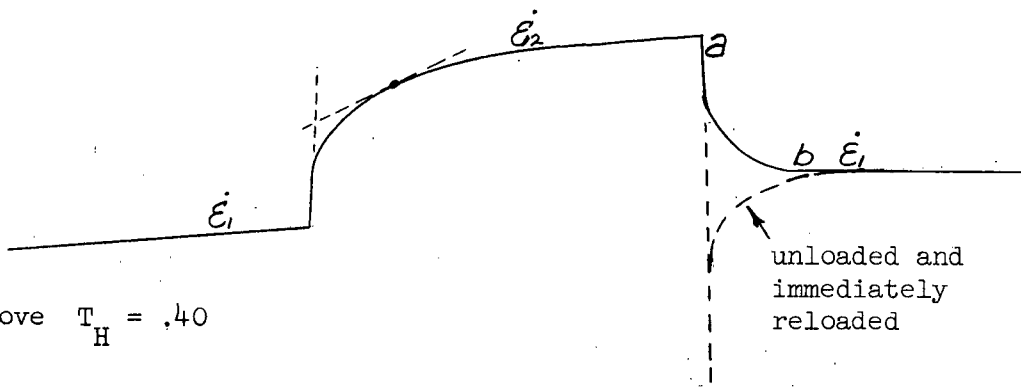
Fig.83 illustrates the nature of the change in flow stress during strain rate change tests under various conditions.



(a) below  $T_H = .26$  in linear hardening regions .



(b) between  $T_H = .26$  and  $T_H = .40$  and in dynamic recovery regions below  $T_H = .26$  .



(c) above  $T_H = .40$

Fig.83 The nature of the flow stress obtained during strain rate change tests in polycrystals

Obtaining  $\Delta\sigma$  values at low temperatures was relatively easy because of the abrupt nature of yield after a change in strain rate (Fig. 83 a) . With increasing strain however yield became more gradual similar to that obtained at all values of strain at temperatures above  $T_H = .26$  . Under these conditions  $\Delta\sigma$  was obtained by extrapolating the elastic and work hardening regions. (Fig. 83 b) .

As the temperature increased to the region of  $T_H = .40$  it became extremely difficult to obtain reliable values of  $\Delta\sigma$  because of the almost completely parabolic nature of yield after an increase in strain rate (Fig. 83 c) . For this reason rate theory calculations were not attempted above  $T_H = .40$  .

Some work softening occurred on decreasing the strain rate at all temperatures above  $T_H = .26$  . This gave rise to a more gradual decrease in the observed flow stress after the strain rate change had been made. This became more pronounced with increasing temperature (Fig. 83 c) . If the load was removed and immediately reapplied there was no evidence of any yield point which is usually associated with work softening. However yield points were observed during strain rate changes on cadmium single crystals similar to those reported by Langenecker<sup>94</sup> in aluminum and zinc. It would therefore appear that in polycrystals at elevated temperatures considerable dislocation rearrangement can occur in the time necessary for a decrease in strain rate. One is faced with the difficulty of establishing the flow stress along a-b (Fig. 83 c) at which yield is occurring at the reduced strain rate. Since this region usually involves up to at least .5% strain there is considerable doubt if any such determination really reflects a reversible change.

Some ambiguity is also associated with an increase in strain rate. However it should be somewhat less due to the absence of the delay times observed during a decrease in strain rate. At temperatures above  $T_H = .40$  the work hardening rate after an increase in strain rate is not sufficiently linear to allow for an extrapolation as in Fig.83 b . Under such conditions  $\Delta\sigma$  should be obtained by extrapolating the work hardening rate at a certain constant value of strain (Fig.83 c).

BIBLIOGRAPHY

- 1) E. Macherauch, Z. Metallkunde, 55, 91, (1964).
- 2) L.M. Clarebrough and M.E. Hargreaves, Progress in Metal Physics 8, 1, (1959).
- 3) P.B. Feltham and J.D. Meakin, Phil. Mag., 2, 103, (1957).
- 4) B. Russell and D. Jaffrey, Acta Met., 13, 1, (1965).
- 5) S.K. Mitra and J.E. Dorn, Trans. A.I.M.E. 227, 1015, (1963).
- 6) H. Conrad and S. Frederick, Acta Met., 10, 1013, (1962).
- 7) H. Conrad and L. Hayes, Trans. A.S.M., 56, 249, (1963).
- 8) H. Conrad, J. Iron and Steel Inst., 198, 364, (1961).
- 9) H. Conrad and G. Schoeck, Acta Met., 8, 791, (1960).
- 10) H. Conrad, Phil. Mag., 5, 745, (1960).
- 11) D.P. Gregory, A.N. Stroh and G.H. Rowe, Trans. A.I.M.E., 227, 678, (1963).
- 12) Z.S. Basinski and J.W. Christian, Aust. J. Physics, 13, 299, (1960).
- 13) Z.S. Basinski, Aust. J. Physics, 13, 284, (1960).
- 14) H. Conrad, R. Armstrong, H. Wiedersich and G. Schoeck, Phil. Mag. 6, 177, (1961).
- 15) H. Conrad, L. Hays, G. Schoeck and H. Wiedersich, Acta Met., 9, 367, (1961).
- 16) H. Conrad and W.D. Robertson, Trans. A.I.M.E., 209, 503, (1957).
- 17) H. Conrad, Trans. A.I.M.E., 215, 58, (1959).
- 18) H. Conrad and W.D. Robertson, Trans. A.I.M.E., 212, 536, (1958).
- 19) P. Ward, J. Mote and J. Dorn, Trans. A.I.M.E., 221, 1148, (1961).
- 20) J.D. Mote and J.E. Dorn, Trans. A.I.M.E., 218, 491, (1960).
- 21) F.E. Hauser, P.R. Landon and J.E. Dorn, Trans. A.S.M., 48, 986, (1956).
- 22) F.E. Hauser, C.D. Starr, L. Tietz and J.E. Dorn, Trans. A.S.M., 47, 102, (1955).
- 23) E. Schmid and W. Boas, "Plasticity of Crystals", Hughes, London, (1950).
- 24) A. Seeger, W. Kronmüller, S. Mader and H. Träuble, Phil. Mag. 6, 639, (1961).

- 25) A. Seeger and H. Träuble, Z. Metallkunde, 51, 441, (1960).
- 26) A. Deruyttere and G.B. Greenough, J. Inst. Metals, 84, 337, (1955).
- 27) G.W. Greenwood and A.G. Quarell, J. Inst. Metals, 82, 551, (1953).
- 28) N.S. Stoloff and M. Gensamer, Trans. A.I.M.E., 227, 70, (1963).
- 29) A.W. Magnusson and W.M. Baldwin, J. Mech. Phys. Sol., 5, 172, (1957).
- 30) J.J. Gilman and V.J. DeCarlo, J. Metals, 8, 511, (1956).
- 31) H.C. Chang and N.J. Grant, Trans. A.I.M.E., 4, 619, (1952).
- 32) R. von Mises, Z. angew. Math. Mech., 8, 161, (1928).
- 33) A. Seeger, Phil. Mag., 46, 1194, (1955).
- 34) N.S. Stoloff and R.G. Davies, J. Inst. Metals, 93, 127, (1965).
- 35) H.S. Rosenbaum, Acta Met., 9, 742, (1961).
- 36) R.L. Bell and R.W. Cahn, Proc. Roy. Soc., (London), A239, 994, (1957).
- 37) P.B. Price, Phil. Mag., 5, 873, (1960).
- 38) P.B. Price, Phil. Mag., 6, 449, (1961).
- 39) P.B. Price, "Electron Microscopy and Strength of Crystals", Wiley, 41, (1963).
- 40) P.B. Price, J. Applied Physics, 32, 1746, (1961).
- 41) P.B. Price, J. Applied Physics, 32, 1750, (1961).
- 42) Predvoditelev et al, Phys. Metals Metallog., 14, 44, (1962).
- 43) J.J. Gilman, Trans. A.I.M.E., 206, 1326, (1956).
- 44) E.J. Stofel et al, Sixth Interim Technical Report, U.S. Army Research Office, Contract No. DA-04-495-ORD-171, Cal. Inst. Tech. (1961).
- 45) T.H. Alden, Acta Met., 10, 653, (1962).
- 46) T.H. Alden, Acta Met., 11, 65, (1963).
- 47) N.S. Stoloff and M. Gensamer, Trans. A.I.M.E. 224, 732, (1962).
- 48) J.J. Gilman, Trans. A.I.M.E., 221, 456, (1961).
- 49) J.H. Wernick and E. E. Thomas, Trans. A.I.M.E., 218, 769, (1960).
- 50) R.C. Gifkins and J.W. Kelly, Acta Met., 1, 320, (1953).
- 51) C.H. Li, E.H. Edwards, J. Washburn and E.R. Parker, Acta Met., 1, 223, (1953).

- 52) J.B. Hess and C.S. Barrett, Trans. A.I.M.E., 185, 599, (1949).
- 53) J. Washburn and E.R. Parker, Trans. A.I.M.E., 194, 1076, (1952).
- 54) E. Crowan, Nature, 149, 643, (1942).
- 55) J.J. Gilman and T.H. Read, Trans. A.I.M.E., 197, 49, (1953).
- 56) J.J. Gilman, J. Metals, 6, 621, (1954).
- 57) W. Koster, Z. Metallkunde, 39, 4, (1948).
- 58) F.P. Bullen and M.M. Hutchinson, Phil. Mag., 7, 557, (1962).
- 59) F.P. Bullen and C. B. Rogers, Phil. Mag. 9, 401, (1964).
- 60) F.P. Bullen and M.M. Hutchinson, Phil. Mag., 8, 461, (1963).
- 61) K.G. Davis, Can. J. Physics, 41, 1454, (1963).
- 62) W. Fahrenhorst and E. Schmid, Z. Phys., 64, 845, (1930).
- 63) A. Berghezan, A. Fourdeux and S Amelinckx, Acta Met., 9, 464, (1961).
- 64) A. Seeger, "Dislocations and Mechanical Properties of Crystals",  
Wiley, (1956).
- 65) R.E. Reed-Hill and D.H. Baldwin, Trans. A.I.M.E., 233, 842, (1965).
- 66) A. Seeger, "The Relation between the Structure and the Mechanical  
Properties of Solids", London, (1963).
- 67) P.B. Hirsch, "The Relation between the Structure and the Mechanical  
Properties of Solids", London, (1963).
- 68) P.R. Thornton, T.E. Mitchell, P.B. Hirsch, Phil. Mag., 7, 337, (1962).
- 69) M.A. Adams and A.H. Cottrell, Phil. Mag., 46, 1187, (1955).
- 70) A.H. Cottrell and R.J. Stokes, Proc. Roy. Soc., 233, 17, (1955).
- 71) P. Haasen, Phil. Mag., 3, 384, (1958).
- 72) B.L. Mordike and P. Haasen, Phil. Mag., 7, 459, (1962).
- 73) H. Conrad, J. Metals, 16, 582, (1964).
- 74) G. Schoeck, Phys. Stat. Sol., 8, 499, (1965).
- 75) J.W. Christian and B.C. Masters, Proc. Roy. Soc., 281, 240, (1964).
- 76) H. Conrad and H. Wiedersich, Acta Met. 8, 128, (1960).
- 77) G.B. Gibbs, Phys. Stat. Sol. 2, 693, (1964).

- 78) Z.S. Basinski, Phil. Mag., 4, 393, (1959).
- 79) A. Seeger, "Conference on Defects in Crystalline Solids", Phys. Soc. London, (1954).
- 80) S.k. Mitra and J.E. Dorn, Trans. A.I.M.E., 224, 1062, (1962).
- 81) J.E. Dorn, "Energetics in Dislocation Mechanics", National Research Council Seminar on Energetics in Metallurgical Phenomena, Denver, (1962).
- 82) L. Tietz and J.E. Dorn, Trans. A.S.M., 41A, 163, (1949).
- 83) W.D. Sylwestrowicz, Trans. A.I.M.E., 212, 617, (1958).
- 84) D.V. Wilson and J.A. Chapman, Phil. Mag., 8, 1543, (1963).
- 85) R. Armstrong et al, Phil. Mag., 7, 45, (1962).
- 86) J.E. Dorn and J.B. Mitchell, "Proceedings of the Second International Symposium on Materials", Berkeley, (1964).
- 87) N.F. Mott Trans. A.I.M.E., 218, 962, (1960).
- 88) F. Kroupa and P.B. Price, Phil. Mag., 6, 243, (1960).
- 89) P.B. Hirsch and J.S. Lally, Phil. Mag. 12, Sept. (1965).
- 90) J.V. Sharp, A. Mitchell and J.W. Christian, Acta Met. 13, 965, (1965).
- 91) H. R. Peiffer and F.R. Stevenson, J. Applied Physics, 34, 2804, (1963).
- 92) H. R. Peiffer and F.R. Stevenson, Office of Naval Research, Technical Report No. 6, RIAS, Baltimore Maryland. (1963)
- 93) P.B. Price, Phys. Rev. Letters, 6, 615, (1961).
- 94) B. Langenecker, Acta Met., 9, 937, (1961).
- 95) P. Niessen, E. L. Holmes and W. C. Winegard, Can. Met. Quart., 2, 177, (1963).
- 96) J. Friedel, "Dislocations", Oxford, New York, Pergamon Press, (1964).
- 97) S.D. Gertsriken and B.F. Slyusar, Phys. Metals Metallog. (USSR), 6, 103, (1958).
- 98) H.G. Van Bueren, Acta Met., 3, 519, (1955).
- 99) N.F. Mott, Trans. A.I.M.E., 218, 962, (1960).
- 100) P. Haasen and A. Kelly, Acta Met. 5, 193, (1957).
- 101) M.J. Makin, Phil. Mag., 3, 287, (1958).

- 102) G.F. Bolling, Phil. Mag., 4, 537, (1959).
- 103) H.K. Birnbaum, Acta Met., 9, 320, (1961).
- 104) K. Lücke et al, Z. Metallkunde, 46, 792, (1955).